THESE DE DOCTORAT
DE l'UNIVERSITE PARIS SUD XI

pour obtenir le grade de
DOCTEUR DE L'UNIVERSITE PARIS SUD XI
Mention: Physique

ÉCOLE DOCTORALE:
Ecole Doctorale de Physique de la Région Parisienne - ED 107

Présentée par

Yunfei He

Titre:

STUDY ON THE INTERFACIAL PROPERTIES OF SURFACTANTS AND THEIR INTERACTIONS WITH DNA

Thèse soutenue au Laboratoire de Physique des Solides le 1 Juillet 2013 devant le jury composé de:

Michèle Adler	Rapporteur
Xueqin An	Rapporteur
Dominique Langevin	Directrice de thèse
Honglai Liu	Directeur de thèse
Brigitte Pansu	Président
Anniina Salonen	Co-encadrant

Study on the interfacial properties of surfactants and their interactions with DNA

Abstract

Bearing a hydrophilic part and a hydrophobic part, surfactants can adsorb onto interfaces and lower the tension (γ) of the interfaces, thereby enhancing the interfacial properties and leading to the applications of surfactants in cleaning, surface functionalization, foaming and emulsification. To understand how they work in these applications it is important to know the time-scales of the surfactant adsorption and desorption. This means that it is necessary to investigate the adsorption and desorption kinetics of surfactants, which have already been widely studied. However, traditional studies tend to make many assumptions, for example, extending the applicability of the equilibrium relations to the non-equilibrium cases. In this dissertation, using a bubble compression method, we first measured the equation of state $\gamma(\Gamma)$, followed the time-dependent surface concentration $\Gamma(t)$ and clarified the adsorption/desorption process without using many assumptions.

Cationic surfactants are receiving much interest for biological applications. The DNA/cationic surfactant system is of use in DNA extraction, DNA purification and gene delivery. Although the interaction between cationic surfactant and anionic polyelectrolyte has been extensively studied, there still remains need to further understand the complex system, especially to rationalize the choice of surfactants to reach controllable DNA binding ability and low toxicity to the organism. In this dissertation, we introduced the systematic investigation on the micellization processes of two novel cationic surfactants (gemini surfactants and ionic liquid surfactant) and their interactions with DNA.

Chapter 1 and Chapter 2 include a general introduction to surfactants, their micellization, interfacial properties, and interactions with DNA. One of the key themes is the complex interplay of surfactant molecules between the interface and the bulk. The adsorption and desorption kinetics of surfactants are included in the interfacial properties of surfactants, consisting the first important component of the thesis. The interaction between cationic surfactant and DNA will be discussed in detail, as it is the second essential part of this thesis.

Chapter 3 describes the experimental and numerical methods utilized in this

thesis.

Chapter 4 deals with the equation of state measurement and adsorption kinetics for two systems, including non-ionic surfactant $C_{12}E_6$ and ionic surfactant CTAB with a high concentration of salt. The rising bubble tensiometer is used like a Langmuir trough. A single bubble compression measurement combined with a known equilibrium surface tension (γ_{eq}) value allows the determination of the equation of state $\gamma(\Gamma)$, which is more accurate than the results from the traditional methods. Using the bubble compression method, the time-dependent surface concentrations $\Gamma(t)$ for both systems are measured, showing that the adsorption is diffusion controlled at short times. The derived diffusion constants compare well with literature values.

The desorption and adsorption processes are interrelated. In Chapter 5, we report the desorption of surfactants from the air/water interface for different systems ($C_{12}E_6$, CTAB or TTAB with sufficient salt, anionic surfactant AOT with different counterions). For the systems studied, the desorption processes are confirmed not to be purely diffusion-limited, showing the presence of an energy barrier in the desorption of surfactants from the interface. The energy barrier is influenced by the alkyl chain length, but not the counterion type.

In Chapter 6, we focus on the equilibrium and kinetic behaviors of the cationic gemini surfactant 12-2-12·2Br at the air/water interface. In the absence of electrolyte, an electrostatic barrier exists during the surfactant adsorption at longer times. The effect of NaBr concentration on the dynamic surface tensions of the 12-2-12·2Br solutions is also investigated. Addition of NaBr hardly affects the adsorption kinetics at times shorter than a given lag time, during which the adsorption is diffusive. Comparing the systems at equilibrium, salt has a stronger influence on 12-2-12·2Br than on CTAB in terms of surface concentration and *CMC*. For the 12-2-12·2Br system in the presence of 100 mM NaBr, the adsorption and desorption kinetics of surfactant molecules have also been studied.

Chapter 7 presents the micellization of cationic gemini surfactant 12-3-12·2Br and its interactions with DNA. Micellization of 12-3-12·2Br is entropically driven and thermodynamically favored above the Critical micelle concentration (*CMC*). The *CMC* increases slightly with temperature and decreases with ionic strength. 12-3-12·2Br interacts strongly with DNA, because of the electrostatic attraction between 12-3-12·2Br and DNA, and the hydrophobic interactions between the alkyl chains lead to a modulation of the DNA conformation. Salt screens the electrostatic attraction between 12-3-12·2Br and DNA, while promoting the aggregation of

12-3-12·2Br. With increasing DNA concentration, the critical aggregation concentration (*CAC*) remains constant, while the saturation concentration (C_2) increases. The effects of spacer length on the micellization of 12-O-12·2Br, where O is the carbon number in the spacer, and the interactions of 12-O-12·2Br with DNA are also investigated. Micellization of 12-3-12·2Br has the highest thermodynamic favorability. Increasing the spacer length of the gemini surfactant leads to a weakening of the interaction with DNA.

In Chapter 8, we present a systematic study on the interactions between the cationic ionic liquid surfactant [C_{12}mim]Br and DNA, using both experimental techniques and Molecular Dynamics (MD) simulation. The strong complexation occurs owing to the electrostatic attraction and the hydrophobic interactions. The aggregation of [C_{12}mim]Br is thermodynamically favored driven by enthalpy and entropy change. Upon the addition of [C_{12}mim]Br, the DNA chain undergoes compaction, conformational changes, accompanied by the change of net charges carried by the DNA/surfactant complex. MD simulation confirms the experimental results.

Keywords: surfactant; adsorption; desorption; DNA; interactions; ionic liquid

Contents

Chapter 1 Introduction

1.1 Interfacial properties of surfactants

Surfactants play important roles in many practical applications and products, such as cleaning, wetting, dispersing, emulsifying, foaming and anti-foaming agents, and some surfactants are of use in biological areas [1-4]. Surfactants are generally organic compounds which are amphiphilic, meaning that the surfactant molecules contain both hydrophobic groups (known as surfactant tails) and hydrophilic groups (known as surfactant headgroups), the typical representation of the surfactant structure is shown in Scheme 2.1. Due to its amphiphilic structure, the surfactant can adsorb onto interfaces and lower the tension (γ) of the interfaces.

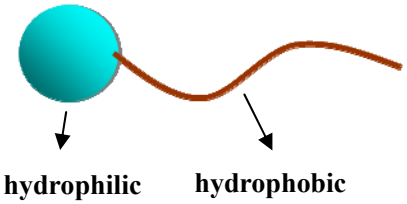

Scheme 1.1 Typical surfactant structure

The adsorption dynamics, i.e. the time-dependent adsorption process of surfactant molecules onto interfaces,, is of significant importance in lots of applications including foaming, emulsifying and coating processes, in which the bubbles, drops or films are rapidly formed [5-7]. The surfactant adsorption process from the bulk to the air/water interface can be divided into two: the motion of the surfactant molecules from the bulk to the sub-surface and the transfer of molecules from the sub-surface to the air/water interface [3, 8-10]. The details can be found in Scheme 1.2. In the absence of convection, the surfactant adsorption dynamics is dependent on the diffusion constants of the surfactant molecules. In some cases, the adsorption is limited only by the diffusion of the surfactant molecules to the interface [10-13]. In some other cases, there exists an energy barrier for the adsorption or desorption of the surfactant molecules, in other words, the adsorption dynamics is considered to be solely kinetically limited [14-17]. This energy barrier could be due to either steric or electrostatic repulsions. It is also possible, and true in most practical cases, that the adsorption process is controlled by both diffusion and the energy barrier [3, 18].

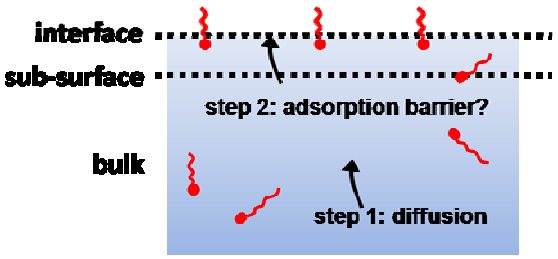

Scheme 1.2 Adsorption process of surfactants from the bulk onto the air/water interface

Although the adsorption and desorption kinetics of surfactants have been widely studied, most studies require the use of approximate relationships between the surface tension γ, the bulk concentration C and the surface concentration Γ. In this dissertation, by using a simple bubble compression method, we determined the equation of state $\gamma(\Gamma)$, which was used to obtain the time-dependent surface concentration $\Gamma(t)$ during the adsorption/desorption processes. This allowed for the comparison with existing models without the need for many free parameters.

1.1.1 Adsorption process of surfactants onto the air/water interface

The main difficulty for the study of the adsorption process of surfactant molecules is the determination of the surface concentration as the surface tension data are most often measured. From these data, one has to derive the surface concentration as a function of time in order to understand the controlling steps for the adsorption process. In Chapter 4 and Chapter 6, we have directly measured the equations of state for various surfactant systems and have shown the applicability of the interfacial equilibrium for the systems studied. We have also been able to obtain the time-dependent surface concentration $\Gamma(t)$ by performing series of successive measurements using a bubble compression method. Using the methods proposed, we successfully showed that the diffusion is the controlling step for the adsorption process in the systems studied.

1.1.2 Desorption process of surfactants onto the air/water interface

To investigate the desorption process of surfactants from the air/water interface, it is also necessary to obtain the surface concentration out of the surface tension data. Following on from the experiments presented in Chapter 4 we have studied the desorption process. In Chapter 5, we have chosen several types of surfactant systems,

including non-ionic surfactants and ionic surfactants in the presence of sufficient electrolyte. We have successfully proved that the desorption is not diffusion-limited by comparing the change in the surface concentration with the time-dependent surface concentration calculated using a model for diffusion-limited adsorption. We also show that desorption for the studied systems is kinetically limited by introducing kinetically-limited adsorption models.

1.2 Interactions between cationic surfactant and DNA

The oppositely charged system of cationic surfactant and DNA is of use in DNA extraction, DNA purification and gene delivery. Electrostatic attraction between cationic surfactant and DNA, as well as the hydrophobic interactions between the alkyl chains of surfactants lead to the complexation between cationic surfactant and DNA. The interactions between DNA and cationic surfactant have been widely investigated, however there still remains need to further understand this complex system, especially the influences of surfactant architecture, electrolyte, temperature *etc*. on the interaction process. In this dissertation, we present a systematic investigation of the micellization processes of two novel cationic surfactants (gemini surfactants and ionic liquid surfactant) and their interactions with DNA.

1.2.1 Interactions between cationic gemini surfactant and DNA

In Chapter 7, the micellization of cationic gemini surfactant 12-3-12·2Br and its interaction with salmon sperm DNA have been systematically investigated using a range of techniques. We focus on the 12-3-12·2Br/DNA system for two main reasons. First, the 12-O-12·2Br series are typical gemini cationic surfactants presenting excellent surfactant properties [19]. Furthermore, it has been found that surfactants with smaller spacers (O=2, 3) present superior DNA compaction efficiency in this series according to Karlsson *et al*. [20]. The highest transfection efficiency was reported to be shown with O=3 [21]. Second, the complexation process, microstructures, phase behavior in the 12-3-12·2Br/DNA system have been investigated with a variety of methods [22-24], however, there remains need to further explore the interaction mechanism of this complicated system. We have demonstrated the binding mechanism and thermodynamics in the 12-3-12·2Br/DNA system with microcalorimetry, UV-Vis spectroscopy, conductivity, light scattering and microscopic observation, among which the microcalorimetry was mostly utilized to

quantitatively monitor the extent of the stepwise interaction in 12-3-12·2Br/DNA system.

1.2.2 Interactions between ionic liquid surfactant and DNA

Ionic liquid (IL) surfactants can possess several advantages including excellent physicochemical properties and environmental friendliness. However, the investigation of its application in gene delivery systems is still very limited. In Chapter 8, the imidazolium-based IL surfactant 1-dodecyl-3-methylimidazolium bromide [C_{12}mim]Br was selected for its good surface activity, low *CMC* (compared with DTAB) and the potential applications in various areas [25-27]. We have systematically studied the interactions between [C_{12}mim]Br and DNA using various experimental methods and molecular dynamics simulations, and finally propose an interaction mechanism for the studied system.

Chapter 2 Background and theories

2.1 General introduction of surfactants

The surfactant molecule contains both a water insoluble (oil soluble) component and a water soluble (oil insoluble) component, which gives rise to the unique properties of surfactants. Due to their structure, surfactant molecules can adsorb at surfaces (e.g. air/water or oil/water). An aqueous solution with an interface with air, the molecules can position themselves such that the water insoluble hydrophobic tails extend out of the water phase into the air phase; however the water soluble hydrophilic head groups still remain in the water phase. At a water/oil interface, the water insoluble hydrophobic tails can extend out of the water phase and direct themselves into the oil phase, while the water soluble hydrophilic head groups still remain in the water phase. The organization of surfactants at the water/air interface and at the water/oil interface is shown in Scheme 2.1. The self assembly of surfactants at the surface can modify the surface properties and thus leads to their many applications.

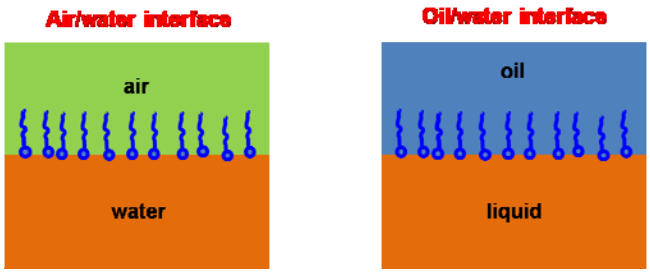

Scheme 2.1 Assembly of surfactants at the air/water interface and oil/water interface

The dual nature of the surfactants also controls their assembly in the bulk. Surfactant molecules can form aggregates including micelles, in which the hydrophobic tails compose the core of the aggregates and the hydrophilic headgroups are in contact with the aqueous phase. Various types of aggregates including spherical, or cylindrical micelles and bilayers can be found according to the spontaneous curvature (C_0) of the surfactant monolayer [28, 29], as seen in Scheme 2.2. Surfactants with large spontaneous curvature (e.g. charged surfactants) form spherical micelles, and a decrease of the spontaneous curvature leads to changes in the micellar structure. Surfactants with very large tails and small headgroups have a very low aqueous solubility and would prefer to form inverse micelles.

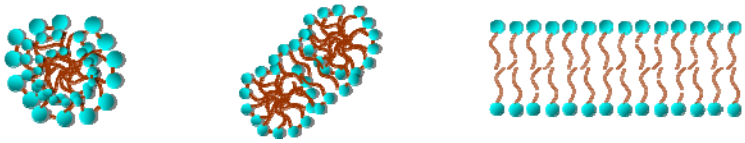

spherical micelle cylindrical micelle bilayer

Scheme 2.2 Various types of micelles

In addition to the micelles, surfactant molecules can also form other types of organized surfactant assemblies in solutions and on solids. Surfactant molecules can aggregate in nonpolar solvents to form inverse or reverse micelles. These types of micellar structures can even be found in polar solvents in which the surfactant has very low solubility. This occurs when the preferred curvature C_0 has a sign opposite to that found for a surfactant forming micelles in water with surfactant tails directing towards the nonpolar solvent and headgroups interacting with water in the core [30-32]. The structure for the inverse/reverse micelle can be seen in Scheme 2.3.

Mixtures of polar and non-polar solvents can be thermodynamically stabilised by surfactants into microemulsion phases. Microemulsions are homogeneous solutions composed of water, oil and surfactant, sometimes with the addition of cosurfactant [33, 34]. The oil in water microemulsion can be considered as oil-swollen micelles, while the water in oil microemulsion can be thought as water-swollen inverse/reverse micelles. This happens when C_0 is smaller than that of the oil-free surfactant micelles (or larger than the water-free reverse micelles, C_0 being by convention negative in this case). Both structures are shown in Scheme 2.3.

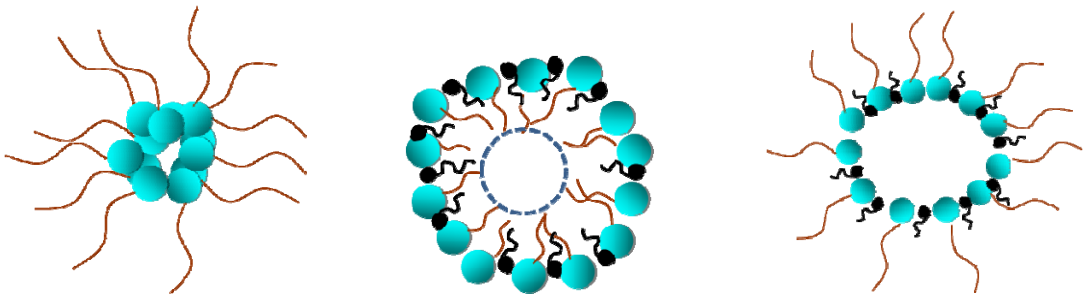

inverse/reverse micelle **oil in water microemulsion** **water in oil microemulsion**

Scheme 2.3 Types of surfactant self assemblies

As mentioned previously, in a typical surfactant solution, the surfactant molecules can be found dispersed as monomers in the bulk, adsorbed at the air/solution interface and at the solid/liquid interface of the container and as micelles

in the aqueous phase (provided the concentration is high enough). The energies of adsorption of surfactants in micelles and at interfaces is typically a few kT. This means that molecules adsorb and desorb continuously to and from the interfaces leading to a dynamic equilibrium between the above mentioned states. The relative concentrations of monomers and micelles vary with equilibrium conditions including pressure, temperature, surfactant concentration or electrolyte concentration (in the case of ionic surfactant). At fixed conditions (temperature, pressure and concentration) the amount of adsorbed surfactant monomers at the air/solution interface and the amount of monomers and micelles in the bulk phase are fixed [35-37].

The number of surfactant molecules used and studied is enormous, and while they all have their specificities they are often classified according to the charged groups in their polar headgroups. The first division is into non-ionic surfactants and ionic surfactants. Non-ionic surfactants have no charge in their headgroups and are therefore more resistant to salty environments. Ionic surfactants have charges in their headgroups and can be divided into several types. If the charges are negative, the surfactants are specifically named anionic surfactants. The anionic surfactants are the most widely used type of surfactant in household products such as shampoos and cleaning liquids due to their excellent cleaning properties and low toxicity. The surfactants with positively charged headgroups are called cationic surfactants, which are mostly widely used for their disinfectant and preservative properties. Surfactant molecules containing the headgroups with two opposite charges are called zwitterionic surfactants. Surfactants with two headgroups and two tails are referred to as dimmers or gemini surfactants. A scheme for different types of surfactants is shown in Scheme 2.4.

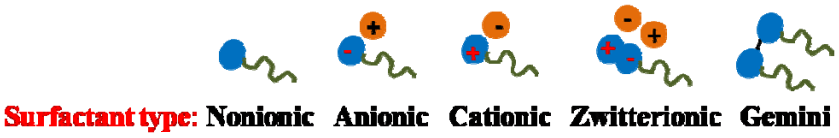

Scheme 2.4 Various types of surfactants, where the blue spot denotes the surfactant headgroup, and the orange spot denotes the counterion

2.2 Micellization of surfactants in the bulk

Micellization is the formation of colloidal-sized clusters of surfactant molecules in solution. In a micellar solution, surfactants are continuously exchanged between micelles and the surrounding solution, which includes entry of surfactants into micelles and their exit. The exchange process is described in Scheme 2.5, where A is

the surfactant monomer, A_S and A_{S-1} are the aggregates formed from S and S-1 monomers (micelles). k_S^+ and k_S^- are the rate constants of association and dissociation of the micelles.

$$A_{s-1} + A \underset{K_s^-}{\overset{K_s^+}{\rightleftharpoons}} A_s$$

Scheme 2.5 Exchange of surfactants between micelles and bulk

It has been recognized that the physical properties of surfactant solutions present an abrupt variation close to a critical concentration corresponding to the onset of surfactant micellization [29]. The physical properties include surface tension, osmotic pressure, electrical conductivity and ability to solubilize non-polar organics in the surfactant solution. The concentration at which micelles begin to appear in the bulk is called the critical micelle concentration (*CMC*) and can be determined from the discontinuity point in the plot of a certain physical property as a function of the surfactant concentration in the system. Surface tension is the free energy per unit area of the liquid surface. The *CMC* is the break point in the plot of the surface tension as a function of surfactant concentration as shown in Scheme 2.6. The *CMC* can be used to determine the monomer concentration in a micellar solution under fixed conditions of temperature, pressure as the concentration of monomers is almost constant above the *CMC*. It has been found that the aggregation number of the micelle increases with the length of hydrophobic chain and decreases with the size of hydrophilic group [38]. The factors which can increase the aggregation number tend to decrease the *CMC*. For example, an increase of the surfactant alkyl chain length decreases the *CMC* [39]. In the case of an ionic surfactant, the presence of electrolyte decreases the *CMC*, due to the screening of the electrostatic repulsions between the charged headgroups, which therefore promotes micelle formation and growth [40].

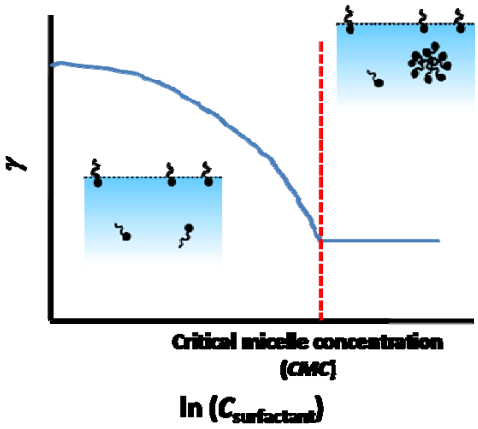

Scheme 2.6 Surface tension as a function of concentration indicating the discontinuity used to determine the *CMC*.

We now turn our attention to the thermodynamics of micelle formation in more detail. We start by looking at the free enthalpy change due to surfactant micellization, ΔG_{mic} given by [29, 41]:

$$\Delta G_{mic} = RT \ln CMC \qquad \text{Equation 2.1}$$

$$\Delta G_{mic} = RT(1+\beta) \ln CMC \qquad \text{Equation 2.2}$$

for non-ionic and ionic uni-valent surfactants respectively, where β is the counterion binding degree of the micelles and T the absolute temperature. For the micellization process, the enthalpy change ΔH_{mic}, the entropy change ΔS_{mic} and ΔG_{mic} are linked by

$$\Delta G_{mic} = \Delta H_{mic} - T\Delta S_{mic} \qquad \text{Equation 2.3}$$

When micellization is thermodynamically favoured, the value of ΔG_{mic} is negative. The negative values of ΔG_{mic} mainly come from the large positive values of ΔS_{mic}, meaning that the micellization process of the surfactant molecules is primarily entropy-driven [29]. When the dissolution of surfactants in the aqueous phase occurs, hydrophobic groups of surfactant molecules change the hydrogen-bonded structure of water and therefore increase the free energy in the system. This energy is recovered after micellization. The interfacial energy may increase when micelles are formed. In addition, in the case of ionic surfactants, electrostatic repulsion between the charged headgroups occurs. These effects may increase the free energy of the system. Hence,

the micellization process depends on the balance between the effects favoring micellization and those opposing it. The hydrophobic effect is considered to be important for the entropy-dominated association of surfactant molecules [29]. Variations of temperature may influence micellization. This is more obvious in the case of non-ionic surfactants. The solubility of non-ionic surfactants can decrease with increasing temperature, due to the loss of hydration water, the head group becoming less hydrophilic, eventually leading to phase separation above a "cloud point" temperature.

In the past decades, self-assembled surfactant aggregates such as cylindrical, lamellar, and reverse micelles have received considerable interest. The assembled structures of surfactant molecules are considered as promising drug delivery carriers [42-44]. Micelles or reversed micelles also play increasingly important roles in catalysis and separation processes [45]. Theories of micellar structure have been developed, and the geometry of the micellar shape is considered to depend on the relative volume occupied by the hydrophilic and hydrophobic groups of surfactant molecules. In aqueous media, surfactant molecules carrying bulky, loosely packed hydrophilic headgroups and long, thin hydrophobic tails tend to form spherical micelles (large spontaneous curvature C_0), while those with small, closely packed hydrophilic headgroups as well as short, bulky hydrophobic tails tend to form lamellar or cylindrical micelles (smaller C_0). Variations in temperature, surfactant concentration or additives in the system may influence the size, shape, aggregation number and stability of the micellar structures [46]. At concentrations slightly above the *CMC*, micelles tend to be of spherical shape. With the increase of surfactant concentration, the structure of a micelle may vary from spherical shape to rod-like or disc-like shape then to lamellar shape.

2.3 Properties of surfactants at the air/water interface

2.3.1 Thermodynamics of surfactant adsorption at the interface

In this section, we will present the Gibbs model which describes surface phenomena in thermodynamic terms, and then the applications of Gibbs model in systems of both ionic surfactants and non-ionic surfactants. As shown in Scheme 2.7, the real system can be divided into three parts: two bulk phases and an interfacial region separating them. In the real system, the interfacial region has a typical thickness of a few molecular diameters, where the physical quantities change sharply but continuously. Gibbs introduced an imaginary reference system, in which the two

bulk phases are separated by an infinitely thin dividing interface, located at $Z=Z_0$, the physical properties remaining constant on each side of the interface [4].

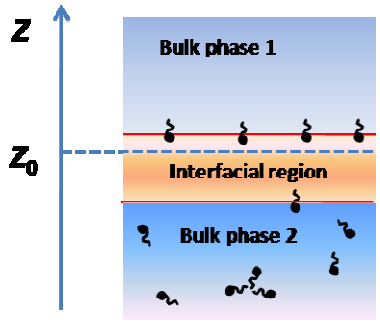

Scheme 2.7 Illustration of a real system (two bulk phases and an interfacial region)

In a multi-component system with volumes in the two phases V^1 and V^2 respectively, the concentrations of the component i in the two phases are C_i^1 and C_i^2. Assuming n_i is the total amount of component i in the system, its quantity at the interface is denoted as

$$n_i^\sigma = n_i - V^1 C_i^1 - V^2 C_i^2 \qquad \text{Equation 2.4}$$

where the subscript σ refers to quantities at the interface.

Let us consider the case of aqueous solutions; for water:

$\Delta C(Z)_{H_2O} = C(Z)_{H_2O} - C_{solution,H_2O}$ for $Z<Z_0$

$$\Delta C(Z)_{H_2O} = C(Z)_{H_2O} - C_{vapor,H_2O} \quad \text{for } Z>Z_0 \qquad \text{Equation 2.12}$$

The surface concentration $\Gamma(H_2O)$is obtained by

$$\Gamma = \int_{-\infty}^{+\infty} \Delta C(Z) dZ \qquad \text{Equation 2.13}$$

The location of the dividing interface is generally chosen such that the surface concentration of the water solvent is zero.

The surface concentration for the component i at the surface area A is defined as

$$\frac{n_i^\sigma}{A} = \Gamma_i \qquad \text{Equation 2.5}$$

In the bulk, we have the differential of the internal energy

$$dU = TdS - PdV + \sum_i \mu_i dn_i \qquad \text{Equation 2.6}$$

Here P is the pressure and μ_i the chemical potential of the species i. Then at the interface an analogous equation is derived with the bulk work term -PdV replaced by the surface work term γdA

$$dU^{\sigma} = TdS^{\sigma} + \gamma d\mathrm{A} + \sum_i \mu_i dn_i^{\sigma} \qquad \text{Equation 2.7}$$

Again, the bulk relation $U = TS - PV + \sum_i \mu_i n_i$ yields the following at the interface

$$U^{\sigma} = TS^{\sigma} + \gamma A + \sum_i \mu_i n_i^{\sigma} \qquad \text{Equation 2.8}$$

Then we differentiate Equation 2.8, compare it with Equation 2.7 and get the Gibbs adsorption equation

$$S^{\sigma} dT + Ad\gamma + \sum_i n_i^{\sigma} d\mu_i = 0 \qquad \text{Equation 2.9}$$

At constant temperature, Equation 2.9 yields

$$-d\gamma = \sum_i \frac{n_i^{\sigma}}{A} d\mu_i = \sum_i \Gamma_i d\mu_i \qquad \text{Equation 2.10}$$

Thus the changes in surface tension dγ and in chemical potential dμ_i have been linked to the surface concentration. In the case of non-ionic surfactant solutions, a gaseous phase is in equilibrium with the solution.Equation 2.10 reduces to

$$-d\gamma = \Gamma_1 d\mu_1 + \Gamma_2 d\mu_2 \qquad \text{Equation 2.11}$$

At a location of the dividing interface such as $\Gamma_1 = \Gamma_{H_2O} = 0$, Equation 2.11 becomes

$$\frac{d\gamma}{d\mu_2} = -\Gamma_2 \qquad \text{Equation 2.14}$$

The surface concentration Γ_i of component *i* is a measurable quantity and the location of the dividing interface has no influence on its value [8]. In order to be able to compare with experimental results, the relationship between the concentration and the chemical potential μ_2 is required, which can be expressed in ideal dilute solutions as:

$$\mu_2 = \mu_2^{\theta} + RT \ln C_2 \qquad \text{Equation 2.15}$$

where R is the gas constant. At constant temperature, Equation 2.15 yields

$$d\mu_2 = RTd \ln C_2 \qquad \text{Equation 2.16}$$

$$\Gamma_2 = -\frac{1}{RT} \frac{d\gamma}{d \ln C_2} \qquad \text{Equation 2.17}$$

Thus a relationship linking Γ_2 to dγ/d(lnC_2) is obtained, which is the result commonly used for the analysis of surface tension data. In many systems, close to the *CMC*, γ varies almost linearly with ln *C*, indicating that the surface coverage is close to a constant maximum value.

The Gibbs adsorption equation can be generalized to ionic surfactants, either with or without added electrolyte [8]. We will consider the case of a cationic surfactant and an electrolyte with the same counter-ion as the surfactant. The surfactant molecule is supposed to becomposed of ν_+ free positive ions and ν_- free negative ions with charge z_+ and z_- respectively.

Assuming that the dissociation of the cationic surfactant in the bulk is complete, one has:

$$RM \rightarrow \nu_+ R^{z_+} + \nu_- M^{z_-} \qquad \text{Equation 2.18}$$

Where RM is the molecular formula for the surfactant, R^{z_+} is the surfactant ion and M^{z_-} is the counter-ion. Similarly, the dissociation reaction for an added inorganic electrolyte is :

$$XM \rightarrow \nu_+^s X^{z_+^s} + \nu_-^s M^{z_-^s} \qquad \text{Equation 2.19}$$

Where *XM* is the electrolyte, $X^{z_+^s}$ is an indifferent co-ion, $M^{z_-^s}$ is the counter-ion. The superscript s denotes the electrolyte which contains ν^s_+ co-ions and ν^s_- counter-ions with charges z_+^s and z_-^s respectively.

Then Equation 2.10 can be expanded over all ionic species in the ideal solution:

$$-d\gamma = \sum_i \Gamma_i d\mu_i = RT\sum_i \Gamma_i d\ln C_i = RT(\Gamma_{M^-} d\ln C_{M^-} + \Gamma_{R^+} d\ln C_{R^+} + \Gamma_{X^+} d\ln C_{X^+})$$

Equation 2.20

The concentrations of surfactant ions and co-ions depend on the bulk concentrations of the surfactant and the salt as:

$$C = \frac{C_{R^+}}{\nu_+}$$
$$C_s = \frac{C_{X^+}}{\nu_+^s}$$
$$\Gamma = \frac{\Gamma_{R^+}}{\nu_+}$$
$$\Gamma_s = \frac{\Gamma_{X^+}}{\nu_+^s} \qquad \text{Equation 2.21}$$

For the cationic gemini surfactant 12-2-12·2Br, ν_+=1, ν_-=2; for the added electrolyte NaBr, ν_+^s=ν_-^s=1. Additionally, the interfacial region is electro-neutral and

the two separate bulk phases are electro-neutral, thus the electro-neutrality requires that

$$C_{M^-} = C_{X^+} + 2C_{R^+}$$
$$\Gamma_{M^-} = \Gamma_{X^+} + 2\Gamma_{R^+} \qquad \text{Equation 2.22}$$

Then with the above equations, Equation 2.20 can be reduced to

$$-d\gamma = RT[(2\Gamma_{R^+} + \Gamma_{X^+})d\ln(C_{X^+} + 2C_{R^+}) + \Gamma_{R^+} d\ln C_{R^+} + \Gamma_{X^+} d\ln C_{X^+}] \qquad \text{Equation 2.23}$$

Assuming the adsorption excess of the salt cation is nearly 0, i.e. $\Gamma_{X^+} \approx 0$, then Equation 2.23 becomes

$$-d\gamma = 2RT\Gamma_{R^+} d\ln(C_{X^+} + 2C_{R^+}) + RT\Gamma_{R^+} d\ln C_{R^+} \qquad \text{Equation 2.24}$$

Therefore the electrolyte concentration affects the adsorption equation. In the case of no added electrolyte (i.e. $C_{X^+} = 0$), Equation 2.24 reduces to

$$-d\gamma = 3RT\Gamma_{R^+} d\ln C_{R^+} \qquad \text{Equation 2.25}$$

At salt concentrations much higher than surfactant concentrations, the first term in Equation 2.24 is close to zero for constant salt concentration, therefore the Gibbs adsorption equation becomes

$$-d\gamma = RT\Gamma_{R^+} d\ln C_{R^+} \qquad \text{Equation 2.26}$$

Our next interest is to understand the equilibrium adsorption of surfactant molecules at the air/water interface, for which many theoretical models have been developed already [9]. According to the Gibbs adsorption equation, the dependence of equilibrium surface tension on surfactant concentration provides information about the amount adsorbed at the interface at equilibrium. For non-ionic and ionic surfactants with sufficient electrolyte, the Gibbs adsorption equation is expressed in Equation 2.27. This equation is commonly used for the analysis of surface tension data in order to obtain the equilibrium surface concentration Γ_{eq}.

$$\Gamma_{eq} = -\frac{1}{RT}\frac{d\gamma}{d\ln C_b} \qquad \text{Equation 2.27}$$

The Gibbs adsorption equation can relate the variation of the surface tension γ_{eq} with bulk surfactant concentration C_b in order to determine the value of the surface concentration Γ_{eq} [4]. Using this method, the equation of state $\gamma_{eq}(\Gamma_{eq})$ (equilibrium surface tension as a function of the surface concentration) can be acquired and eventually compared with theoretical equations of state [9].

The equilibrium surface tension values can be determined from the time-dependent measurements of surface tension at long times [47, 48]. For efficient surfactants with very low critical micelle concentrations (*CMC*), the periods of time required for the equilibration of the surface tension are very long due to the low concentrations studied. For example, hexadecyl trimethyl ammonium bromide (CTAB) in 100 mM sodium bromide (NaBr) has a *CMC* of about 0.03 mM, and it takes more than 3 hours to obtain the equilibrium surface tension for 0.002 mM CTAB. This means that it is indeed time-consuming to determine the complete variation $\Gamma_{eq}(C_b)$ with the Gibbs adsorption equation.

Recently, Moorkanikkara *et al*. [49] developed a novel, combined method of both theoretical as well as experimental analysis to predict the equilibrium surface tension vs surfactant bulk concentration $\gamma(C_b)$ curves for nonionic surfactants using dynamic surface tension data at a single concentration, a single equilibrium surface tension data point and the previously known diffusion constant *D*, and found that they agreed well with those measured by other methods. Pan *et al*. [50] have proposed a method to obtain the equation of state $\gamma(\Gamma)$ using the pendant drop method. The surface area of a bubble is rapidly expanded and subsequently compressed after it has reached the equilibrium state. Assuming the amount of the surfactant molecules on the surface remains constant during this period of time, the equation of state can therefore be calculated rather easily. Lin *et al*. [12] and Taylor *et al*. [51] have proposed similar methods to determine the equations of state using fast bubble expansion. Fainerman *et al*.[52] utilized a comparison between bubble and drop methods, taking the advantage of the surfactant depletion effects commonly occurring in dilute solutions with the drop method.

2.3.2 Dynamics of surfactants at the air/water interface

Besides the surface properties at equilibrium, the time-scales of adsorption also matter in many industrial applications , frequently being even more important than equilibrium properties [3]. Accordingly, intense attention has been paid to the research on the dynamic surface tension of surfactant solutions [3]. The adsorption of the surfactant molecules from the bulk onto the interface includes two steps, as shown in Scheme 1.2:

- diffusion of surfactant molecules from the bulk to the sub-surface.
- transfer of surfactant molecules from the sub-surface to the interface.

For very dilute solutions of non-ionic surfactants, the time-scale for diffusion is

much longer than that of the transfer of surfactant molecules to the surface, meaning that the adsorption processes are solely diffusion-controlled. Diffusion models satisfactorily account for the adsorption kinetics of non-ionic surfactants [53, 54]. In the case of ionic surfactants with high concentrations of added electrolyte, the electrostatic repulsion from the charged surfactant molecules already present at the surface is screened, and therefore the electrostatic adsorption barrier is suppressed. As a result, the adsorption behavior should be similar to that of non-ionic surfactants, i.e., diffusion-controlled [14, 15]. This implies that the local equilibrium is ensured in the interfacial region, and that the concentration in the sub-surface region, C_S, is directly linked to Γ.

A diffusion model for the adsorption of surfactant molecules onto an air/water interface has been developed by Ward and Tordai [55] and afterwards modified by others [56] to account for adsorption onto a spherical surface instead of a planar surface:

$$\Gamma(\mathrm{t}) = 2\sqrt{\frac{D}{\pi}}\left[C_\mathrm{b}\sqrt{t} - \int_0^{\sqrt{t}} C_\mathrm{s}(t-\tau)\mathrm{d}\sqrt{\tau}\right] + \frac{D}{b}\left[C_\mathrm{b}t - \int_0^{t} C_\mathrm{s}(\tau)\mathrm{d}\tau\right] \qquad \text{Equation 2.28}$$

In this equation D is the diffusion constant of surfactant molecules, b the bubble radius, C_b the bulk surfactant concentration, C_S the surfactant concentration close to the interface (sub-surface), t the aging time of the interface and τ the time variable.

At short times, before the surface concentration becomes sufficiently high, desorption is negligible. In addition, for systems with a low ratio of adsorption depth $h=\Gamma_\mathrm{eq}/C_\mathrm{b}$ to the bubble radius b, the effect of curvature is negligible at short time ($t < h^2/D$) [13]. Therefore, at short adsorption times only the first term is required and Equation 2.28 becomes

$$\frac{\Gamma(\mathrm{t})}{\Gamma_\mathrm{eq}} = 2\sqrt{\frac{D}{\pi}}\frac{C_\mathrm{b}}{\Gamma_\mathrm{eq}}\sqrt{t} = 2\sqrt{\frac{D}{\pi}}K \qquad \text{Equation 2.29}$$

In Equation 2.29, Γ_eq is the surface concentration at equilibrium corresponding to the bulk concentration employed. If the adsorption is diffusion-controlled, the normalized surface concentration should increase linearly with the square root of time or with the normalized term $K = \sqrt{t}/h$.

In the case of kinetically controlled adsorption, an adsorption barrier exists in the interfacial region, meaning that the transfer of surfactant molecules from the sub-surface to the air/water interface could be slower than the diffusion of molecules from the bulk to the sub-surface. For example, strong electrostatic interactions in

salt-free ionic surfactant solutions are found to have strong effects on the adsorption process of surfactant molecules, causing the adsorption to be kinetically limited. The adsorption process of ionic surfactants is difficult to model: because of the surface charge, the surface potential increases with time, as indicated in Scheme 2.8.

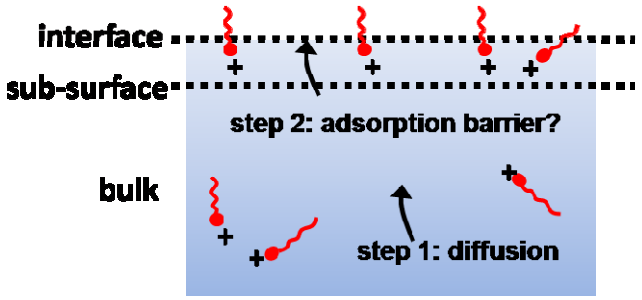

Scheme 2.8 Adsorption of ionic surfactants from the bulk to the air-water interface

The charged surface repels the further arrival of surfactant molecules from the bulk and thus results in the deceleration of the adsorption process. A few models have been developed to understand the adsorption behaviors of the ionic surfactants. Diamant *et al.* [14, 15] proposed a theory for the adsorption kinetics for surfactants (ionic or non-ionic) using a free energy approach and they concluded that at times long enough, the adsorption for ionic surfactants is kinetically controlled rather than diffusion-controlled. In the case of ionic surfactants with high concentrations of added electrolyte, the electrostatic repulsion from the charged surfactant molecules already present at the surface can be screened, and their adsorption becomes diffusion-controlled, which is similar to that of non-ionic surfactant.

There exist various adsorption models to predict the time variation of the surface concentration of molecules. However in general, the interfacial tension changes are measured instead of the surface concentration change. Therefore the models need to be extended to relate the surface tension to the surface concentration. At equilibrium, the relation $\gamma(\Gamma)$ is called the equation of state. The utilization of several assumptions is thus necessary, such as extending equilibrium relations to out of equilibrium situations. Although several different models for the equation of state have been proposed [3], their accuracy is generally not high close to the *CMC* region where the surfactant monolayer at the interface becomes highly compact [57]. In an early experiment by Doss [58] a Langmuir trough was used to determine directly the surface concentration in time, however for an ionic surfactant, where the electrostatic repulsion can easily lead to behaviour that is difficult to model. Therefore, it is necessary to acquire the surface concentration out of experimentally measured surface

tension values, and then to determine the controlling step for the adsorption.

2.3.3 Desorption of surfactants at the air/water interface

In order to better understand the adsorption as well as the desorption processes, many studies have been performed with bubbles and drops which volumes were varied with time [18, 50]. When the diffusion process is relatively slow, it has been assumed that the transport towards and away from the interface is controlled by diffusion. However, when diffusion is sufficiently fast, for instance when dealing with concentrated surfactant solutions, time delays have been observed by Joos *et al*, which were attributed to the presence of adsorption/desorption energy barriers [17, 59, 60].

Denoting the surface concentration by Γ and the bulk concentration near the surface (sub-surface) by C_s with the Langmuir adsorption model, it has been postulated that [16]:

$$\frac{d\Gamma}{dt} = k_a C_s \left(1 - \frac{\Gamma}{\Gamma_\infty}\right) - k_d \frac{\Gamma}{\Gamma_\infty} \qquad \text{Equation 2.31}$$

The parameters k_a and k_d are respectively adsorption and desorption constants, and Γ_∞ is the surface concentration at saturation. k_a and k_d are related to the adsorption and desorption energies E_a and E_d by: $k_{a,d} = k^0_{a,d} \exp(E_{a,d} / k_B T)$, where k_B is the Boltzmann constant and T is the absolute temperature. When diffusion is sufficiently fast, C_s is constant and equal to the bulk concentration C_b so Equation 2.31 can be simplified to:

$$\frac{d\Gamma}{dt} = k \left(\Gamma_{eq} - \Gamma(t)\right) \qquad \text{Equation 2.32}$$

The effective desorption rate k is then:

$$k = \frac{k_a C_b + k_d}{\Gamma_\infty} \qquad \text{Equation 2.33}$$

In the experiments carried out by Joos *et al*. [17, 59, 60], a very fast technique for measuring the dynamic surface tension of aqueous surfactant solutions, the oscillating jet method was used, as the delays were in the order of milliseconds. They have investigated several surface active substances, fatty alcohols and acids, bolaforms (surfactants with two polar heads), an ionic surfactant (SDS, sodium dodecylsulfate) and a series of cationic surfactants with different chain length (C_nTAB, alkyl trimethyl ammonium bromides), with or without small amounts of added salt. It

has been found that for aqueous solutions of these surfactants, k depends linearly on the surfactant bulk concentration; k_d is nearly independent of chain length with k_d/Γ_∞ in the order of 100 s^{-1} for all systems; k_a increases significantly with the chain length roughly as the inverse of the variations of the *CMC* with the chain length. This is opposite to what is nowadays well established for the exchange of surfactant molecules between micelles and bulk: the adsorption rate of surfactant monomers to micelles does not depend on the chain length, whereas the desorption rate decreases considerably with chain length [61]. This is currently explained by saying that when a CH_2 group is translated from a hydrophobic environment to water, the free energy penalty is about $k_BT/2$ [62]. Therefore, there exists an energy barrier for desorption, while not for adsorption. In other words, the adsorption process is simply diffusion controlled [61]. In order to explain their results, Joos *et al*. [17, 59, 60] proposed that an energy barrier for adsorption can also be present, which may be linked to the reorganization of hydration water and be even larger than the desorption energy barrier. Assuming that this interpretation is valid, it would imply that the reorganization of hydration water is more difficult at the air/water interface than at the surface of a surfactant micelle, emphasizing the difference of the adsorption/desorption kinetics between the air/water interface and the micelles.

In addition to the oscillating jet method, other types of methods including the maximum bubble pressure [8], the expanding drop [63], the pendant [50, 64-66] or oscillating drop [67, 68], the surface compression rheology [69] have also been used to address the issue of the transfer of surfactant molecules between bulk solution and interface. Because the times accessible with these methods are longer, more dilute solutions were used in order to measure the surface tension variation due to both the diffusion in the bulk phase and the exchange between subsurface and surface. Below 0.1 s, it was shown that convection is important in the bubble method, and the precise data analysis is difficult [63].

When the concentrations used are relatively small, for instance long chain alcohols with limited water solubility, the transport of surfactant towards the surface was found to be purely diffusion controlled [10], unlike the short chain alcohols studied at larger concentrations [59]. Although there is relative consensus on the adsorption and desorption behavior of dilute solutions, even at low concentrations, fitting adsorption and desorption data with diffusion-controlled transport frequently provides diffusion coefficients smaller than expected. The fitted coefficients can differ by as much as a factor of three between adsorption and desorption experiments, even

when performing experiments with the same solutions [18]. Mixed diffusion-kinetic transport models were therefore proposed [13, 50, 70]. It was found that assuming constant values for k_a and k_d in Equation 2.31 (i.e. constant energy barriers), was not sufficient to fit the data, but that a linear dependence of adsorption and desorption energies on Γ was necessary. This is consistent with the fact that Equation 2.31 leads to the Langmuir equation of state at equilibrium ($\frac{d\Gamma}{dt} = 0$); while with the corrections adopted, a Frumkin equation of state can be obtained, which usually better fits equilibrium surface tension data than the more ideal Langmuir equation of state.

The desorption rates k_d, although scattered, have been found much smaller for alcohols with long chains such as decanol (~10 s^{-1} [64], 2.7 s^{-1} [67], 0.1 s^{-1} [65]) than those ones with shorter chains, from propanol to heptanol (~100 s^{-1}) [59]. However, the concentrations studied were smaller roughly by a factor 1000 (in the range 10 to 100 μM in the references [64, 65, 67] instead of 10 to 100 mM in the reference [59]), and the differences in k_d are possibly due to the influence of the surface concentration on the energy barriers. However, k has not been found concentration dependent for the short chain alcohols and other experiments with decanol did not evidence any energy barrier at all [63, 66]. Besides, it is difficult to determine the desorption rate exactly due to the noise in standard curves of dynamic surface tension, even when diffusion is the major contribution to the transport process.

Experiments with nonionic surfactants, of the alkyl polyoxyethylene glycol ethers series (C_iE_j, a chain with i carbon atoms and j oxyethylene groups) were also performed. For $C_{12}E_6$, Pan *et al*. [13, 50, 70] found $k \sim 1.4\times10^{-4}$ s^{-1}, whereas Lucassen and Giles [69] found that the surfactant transport was diffusion controlled. Pan *et al* claim that the difference is due to the fact that Lucassen and Giles use too many parameters for data fitting. Lee *et al*. [18] studied the series C_iE_8 and, at the difference of alcohols [59], they have found that the desorption rate varies considerably with hydrocarbon chain length (a factor 15 when i changes by a factor 2), whereas the adsorption rate is relatively constant: $k_a \sim 6$ m^3 mol^{-1} s^{-1}. This result is compatible with the findings for surfactant exchanges with micelles, although the rates are lower by many orders of magnitude [61].

In summary, the understanding on desorption of surfactant molecules from the air/water interface is still controversial, therefore further studies of the desorption process are desirable.

2.4 Interactions between surfactants and DNA

The oppositely-charged surfactant and polyelectrolyte system has received intense interest for the past decades [2, 71, 72]. Due to the presence of the electrostatic interactions between the two components and the hydrophobic interactions between the alkyl chains of the surfactants, the surfactant molecules can aggregate around the polyelectrolyte chain at a critical surfactant concentration (shown in Scheme 2.10), which is named *CAC*. The complexation process, phase behavior, the structure of the complexes *etc.* have been widely investigated for this complicated system [73-75].

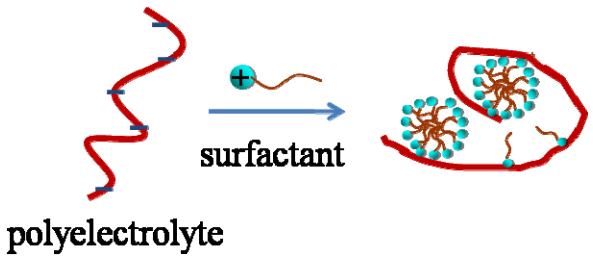

Scheme 2.10 Aggregation process of surfactants around the polyelectrolyte

2.4.1 Interactions between cationic surfactants and DNA

(Deoxyribonucleic acid) DNA is not only an important biological molecule but also a highly charged anionic polyelectrolyte with a unique double helical structure [2, 72, 74]. DNA has the ability to associate with the oppositely charged cosolutes, ranging from simple ions to polymers, proteins, surfactants, lipids and also particles [76-78]. Commonly the association can be strongly enhanced with the increase of the total charges carried by the cosolute or the charge density of the cosolute; on the other hand, the addition of salt can screen the electrostatic interactions and therefore weaken the association.

With the development of biotechnology, cationic surfactants are receiving much interest in biological areas [79, 80]. The oppositely-charged polyelectrolyte/surfactant system has been extensively studied, and the DNA/cationic surfactant system is of interest in many applications, for example, the development of methods for DNA extraction and purification, and lately, the potential use of these systems as efficient non-viral artificial reagents for gene delivery in gene therapy [78, 81]. Complex formation, phase behavior, thermodynamics of interaction processes, morphology of the complexes and surfactant transfection efficiency in the cationic surfactants/DNA

system have been widely investigated by a variety of methods [73, 75, 82-88]. The main driving force for the strong association is due to the electrostatic interactions between the two components (DNA and surfactants) followed by the hydrophobic interactions between the alkyl chains of the surfactant molecules. Typically the electrostatic interactions can lead to an entropy increase due to the release of the counterions, and correspondingly the association of DNA and surfactants can occur at low concentrations [76]. The hydrophobic interactions between the alkyl chains of the surfactant molecules can ensure the cooperative binding of surfactants on the DNA chains. The above studies have shown that the self-assembly of surfactants on DNA chains occurs at a critical concentration, far below the critical micelle concentration (*CMC*). The cooperative binding process of surfactants with DNA, driven by both electrostatic and hydrophobic interactions, plays a significant role in the collapse of DNA molecules [89]. The conformational transition of large DNA molecules from extended coils to collapsed globules, induced by cationic surfactants, has been confirmed by the use of fluorescence microscopy [90]. Recent research on DNA with a relatively low molecular weight revealed that the addition of cationic surfactant could cause changes in the aggregated form of DNA from a loosely packed spherical to a rod-like via a toroidal structure [91]. Recently Profio *et al*. [75] presented a detailed study on the interaction between DNA and cationic amphiphiles with various physicochemical techniques, microscopy observations as well as thermodynamic estimations, and successfully correlated the structural features of the cationic amphiphiles with the induced morphological changes on DNA. It has already been shown that the surfactant structure may be closely related to its interaction with DNA, therefore studies of surfactants with unique structures become interesting and necessary [92-95]. Moreover, the properties of the system may be dependent on its affinity toward the environmental conditions including the additives, temperature and pH. Goracci *et al*. [96] used a pH-dependent probe to detect the interaction between DNA and pH-dependent zwitterionic amine oxide surfactants, which may be of potential use in pH-stimulated gene delivery systems.

2.4.2 Interactions between cationic gemini surfactant and DNA

As a novel class of self-assembling molecules, gemini surfactants have received intense attention in the past decades due to their excellent physicochemical properties [97, 98]. Gemini surfactants are composed of two hydrophobic chains as well as two hydrophilic head groups covalently attached through a spacer, and the typical

structure of gemini surfactants is presented in Scheme 2.11. The gemini surfactants have interesting properties including much lower *CMC*, enhanced efficiency in lowering surface or interfacial tension compared with the traditional surfactants with single head group and single alkyl chain [19]. Goracci *et al*. have reported that the gemini surfactants show high stability at the air/water interface and formation of "dimers" at the interface may account for the compressible nature of the monolayers of traditional surfactants with single chains [99]. Gemini surfactants possess the advantage of rich structural diversity. It is possible to vary the length of alkyl chains, the chemical structure of head groups, the spacer configuration and the counter-ions, therefore intense attention has been paid to the influence of molecular architecture on the properties of gemini surfactants [92, 100]. Rational design of cationic gemini surfactants can ensure high DNA binding ability, low cytotoxicity and enhanced transfection ability [93, 101, 102].

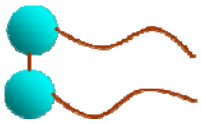

Scheme 2.11 Typical structure of gemini surfactant

2.4.3 Interactions between ionic liquid surfactant and DNA

Typically ionic liquids (ILs) are composed of organic cations and organic/inorganic anions existing as liquids at ambient room temperature. They have attracted considerable attention owing to their unique and excellent physicochemical properties including wide liquid state range, high polarity, negligible vapor pressure, favorable solvation ability, high reactivity and high selectivity [103, 104]. The self-assembly of surfactant molecules or block copolymers in ILs has been widely investigated, and aggregates such as micelles and liquid crystals have been observed [105, 106]. Microemulsions involving ILs have also been prepared, showing advantages including environmental friendliness and high flexibility [33, 34, 107]. The wide applications of ILs in chemical reactions [103, 108], material preparation [109, 110], separation processes [111, 112] and renewable batteries [113, 114] *etc.* have been widely studied in the past decades. The unique physicochemical properties of imidazolium-based ILs have attracted increasing interest due to their potential applications in various areas, especially in the field of life science [115]. For example, 1-butyl-3-methylimidazolium hexafluorophosphate ($[C_4mim]PF_6$) was successfully utilized to extract the double-stranded DNA and showed the potential to become an

appropriate medium for bioprocessing [116]. 1-butyl-3-methylimidazolium tetrafluoroborate ($[C_4mim]BF_4$) and DNA have successfully been assembled into complex films, displaying excellent electrochemical behaviors and potential applications in electrochemical biosensors [117]. IL-robed DNA strands with the characteristics of both ILs and DNA have been formed by fixing 1-alkyl-3-methylimidazolium cations on the phosphate groups of DNA [118]. Some researchers have found that imidazolium-based ILs with certain hydrophobic alkyl groups on the cation possess high surface activity, similar to cationic surfactants therefore they are called IL surfactants which possess the properties of both ionic liquids and surfactants [95]. The surface activity of these types of ILs has recently received extensive attention [25-27, 95, 119].

As a type of novel surfactants, IL surfactants have received much less attention in their interactions with DNA. Recently, Zhang *et al*. [120] studied the application of an imidazolium-based IL in the process of gene transfection and found that the IL displayed high binding ability to DNA with low toxic effects. Xie *et al*. [121] investigated the interactions between 1-butyl-3-methylimidazolium tetrafluoroborate ($[C_4mim]BF_4$) and calf thymus DNA with a surface electrochemical micromethod, and the thermodynamic and kinetic parameters of the binding process were acquired accordingly. Very recently, the molecular mechanism for interactions between 1-butyl-3-methylimidazolium chloride ($[C_4mim]Cl$) and DNA have been shown based on a multi-technique method [94]. Cardoso *et al*. [122] studied the IL/DNA interactions using molecular dynamics (MD) simulation, showing the interactions of IL cations with the DNA main chain and bases, and also interactions between IL anions and DNA bases. It is quite obvious that cationic ionic liquid surfactant/DNA interactions are interesting; however, it is difficult to obtain reliable information for the interaction mechanism based on only instruments or MD simulation. Moreover, the thermodynamics of the interaction process is less studied compared with the complexation process and complex structure, therefore further work is highly necessary.

Chapter 3 Experimental and Numerical Methods

In this chapter, we will describe the materials and methods used in work presented in the thesis.

3.1 Materials

The solvent used in this thesis was Milli-Q water. Different electrolytes have been used: sodium bromide NaBr, sodium chloride NaCl, potassium chloride KCl, magnesium chloride $MgCl_2$, all from Sigma Aldrich.

Several types of surfactant systems were investigated, including non-ionic surfactant hexaethylene glycol monododecyl ether $C_{12}E_6$ (Sigma Aldrich), cationic surfactant hexadecyl trimethyl ammonium bromide CTAB (Sigma Aldrich), cationic surfactant tetradecyl trimethyl ammonium bromide TTAB (Sigma Aldrich), anionic surfactant dioctyl sodium sulfosuccinate AOT (Sigma Aldrich).

Two types of cationic gemini surfactants, 12-2-12·2Br and 12-3-12·2Br, have been used. They have been specifically synthesized for the experiments using the following procedures:

Synthesis of 12-2-12·2Br. Bromododecane (24 mmol) was diluted in the acetonitrile solution (50 mL), while heating and stirring vigorously. The acetonitrile solution (10 mL) containing N,N,N',N'-tetramethylethylenediamine (8 mmol) was added into the system in a dropwise manner for 15 minutes. The reaction was continued for 48 h. Finally the product was filtered out and recrystallised in the acetone/ethanol mixture (17 mL).

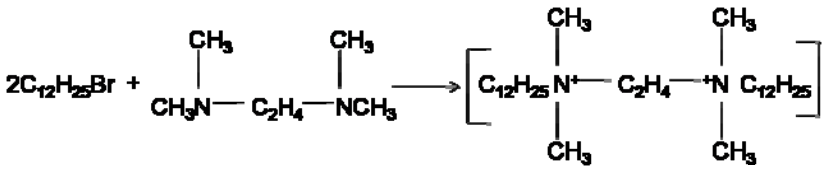

Scheme 3.1 Synthesis of 12-2-12·2Br

Synthesis of 12-3-12·2Br. Gemini surfactant 12-3-12·2Br was prepared by a single-step reaction (Scheme 3.2). First N,N-Dimethyldodecylamine (excess by 5%~10%) was added into alcohol containing 1,3-Dibromopropane. The reaction was performed at a temperature of 373.15 K with reflux for 48 h, and then solvent was removed from the product by the method of reduced pressure. The product was then recrystallized 3~4 times using a mixture of alcohol and ethyl acetate. Finally the

product was dried in the vacuum oven at the temperature range 323.15 K~333.15 K until constant mass of the product is reached.

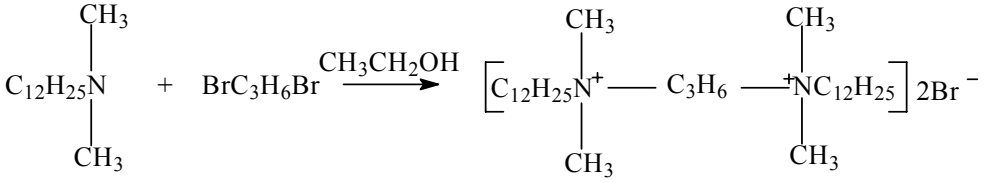

Scheme 3.2 Synthesis of 12-3-12·2Br

Cationic IL surfactant [C_{12}mim]Br was purchased from Chengjie Chemical Inc. (Shanghai, China) with purity 99%, and its chemical structure of is shown in Scheme 3.3.

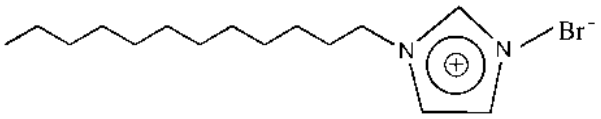

Scheme 3.3 Chemical Structure of cationic IL Surfactant [C_{12}mim]Br

Salmon sperm DNA (Sigma) was used directly without further treatment. The average number of base pairs is around 2000 bp according to the statement of Sigma. DNA stock solution was prepared by dissolving dried DNA in dilute brine. The concentration of DNA phosphate group was determined by UV absorbance measurements assuming a molar extinction coefficient of 6600 $M^{-1}cm^{-1}$ at the wavelength of 260 nm.

3.2 Methods

3.2.1 Surface tension

3.2.1.1 Wilhelmy plate

The Wilhelmy plate technique includes a thin plate made from filter paper, microscope glass slide or platinum plate attached to a balance, which is in contact with the fluid, as shown in Scheme 3.4. The liquid exerts a capillary force on the plate which can be equilibrated by a vertical force *F*. The force *F* is equal to the vertical component of the surface tension (γ*cosθ, where θ is the contact angle) times the length of the plate (2*L*).

$$F = 2\gamma * L * \cos\theta \qquad \text{Equation 3.1}$$

F is measured while the plate is extracted from the solution using a force sensor. F is proportional to γ, provided that the contact angle (θ) between the liquid phase and the plate is zero. This condition of complete wetting (θ=0) is satisfied here because we use a porous paper plate. A vessel containing the sample solution is placed on a platform which can be lowered or lifted manually. The plate is soaked with Milli Q ultra-pure water before measurements. The force sensor is controlled by the software and the processor. The measurements are repeated at least three times to verify reproducibility.

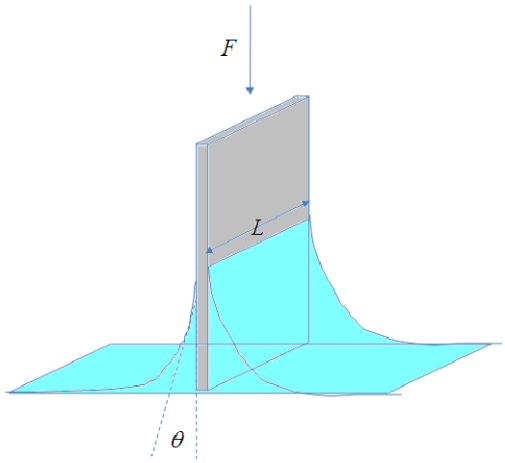

Scheme 3.4 Illustration of the Wilhelmy plate technique

3.2.1.2 Rising bubble

The shape of the bubble is dependent on the balance between the surface tension and gravity forces, therefore measurements of the bubble shape allow to determine the surface tension. Once the bubble images have been recorded, the principle radii of curvature R_1 and R_2 can be obtained. One can determine the surface tension by using the Young-Laplace equation written below, where ΔP is the difference of the internal pressure in the bubble and the external pressure.

$$\Delta P = \gamma(\frac{1}{R_1} + \frac{1}{R_2}) \qquad \text{Equation 3.2}$$

Experiments were performed using a pendant drop tensiometer (Tracker, Teclis, France). The rising bubble configuration (Scheme 3.5) was used in order to avoid bulk depletion effects [52, 123]. The rising bubble is created at the end of a needle with a U form, and the syringe injects air into the surfactant solution under the control of a motor. The air bubble is illuminated with uniform light and the bubble image is projected onto a CCD camera. By analyzing the bubble image with the software, the

surface tension is determined.

Different measurement plans can be chosen depending on the experiments to be performed. In a measurement plan, one executes controlled variations of one of the physical quantities (the drop volume, interface area or tension) and records the response of the other physical quantities versus time.

Scheme 3.5 The rising air bubble configuration

3.2.2 Isothermal titration calorimetry (ITC)

Isothermal titration calorimetry (ITC) is a technique used to calculate the thermodynamic parameters corresponding to the interactions in solution. The unit can directly measure the heat released or absorbed in liquid samples as a result of mixing precise amounts of reactants. As shown in Scheme 3.6, a spinning syringe is utilized to inject and subsequently to mix reactants at a selected spinning rate. Upon the injection and mixing of the reactants, there exists an instant temperature difference between the reference cell and the sample cell, and the release or absorption of heat is detected by maintaining the temperature equilibrium in the two cells.

The calorimetric measurements were performed in a VP-ITC microcalorimetric system (Microcal, USA) with a 1.43 mL sample cell at specified temperatures. The samples were degassed with ThermoVac (Microcal, USA) for 5 min at a constant temperature before measurements. A 250 μL Hamilton injection syringe was used throughout the experiments. The injection speed was 0.5 μL s^{-1} and there was an interval of 240 s between two injections. The stirring speed was kept at 307 rpm throughout the experiments. Raw data curves were integrated with Microcal Origin Software as described in the instrument manual. Measurements were carried out in duplicate and the results were highly reproducible.

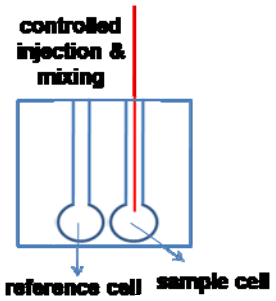

Scheme 3.6 Illustration of the injection system of ITC

3.2.3 Conductivity measurements

The electrical conductivity κ is difined as the ratio of the magnitude of the electric field to the current density with the relation below.

$$\kappa = \frac{E}{J} \qquad \text{Equation 3.3}$$

Electrical conductivity measurements were performed using a conductivity meter (DDS-307, Leici instrument Inc., China). The measurements were performed in a double-walled glass container at 298.15 K controlled by the use of circulating water. A fraction of concentrated surfactant solution was added to the brine in a successive manner. An interval of sufficient time was allowed between two additions to equilibrate the system.

3.2.4 Atomic Force Microscopy (AFM)

AFM is a high-resolution type of scanning probe microscopy, consisting of a cantilever with a sharp tip at its end which is used to scan the sample surface, as shown in Scheme 3.7. The forces between the tip and the sample surface lead to a deflection of the cantilever, which is measured using a laser spot reflected from the top surface of the cantilever into an array of photodiodes. To avoid the collision of the tip with the sample surface, a feedback mechanism is employed to adjust the tip-to-sample distance to maintain a constant force between the tip and the sample.

During the AFM measurements, a 10-20 μL sample solution was deposited onto a piece of freshly cleaved mica and left to adhere for 30 s using spin-coating technique. The sample was then dried overnight before AFM observation. The AFM images were obtained in tapping mode by a scanning probe microscope (AJ-III, Aijian nanotechnology Inc., China) using a triangular micro fabricated cantilever with a length of 100 μm and a spring constant of 48 N m^{-1}.

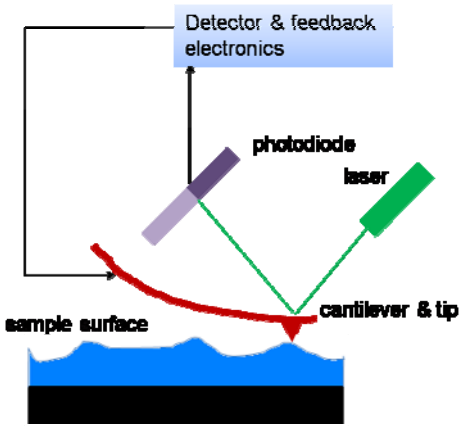

Scheme 3.7 Illustration of AFM

3.2.5 UV-Vis transmittance

The UV-Vis spectrophotometer measures the intensity of light passing through a sample (I) and compares it to the intensity of light before it passes through the sample (I_0). The ratio I/I_0 is the transmittance and is expressed as a percentage (%).

Transmittance of the solutions was measured using a UV spectrophotometer (UV-2450, Shimadzu, Japan) at 298.15 K. All measurements were performed in a 1 cm path length quartz cuvette with the wavelength range of 300~700 nm.

3.2.6 Measurements of particle size and zeta potential

Particle size is measured by dynamic light scattering (DLS), which measures Brownian motion and relates this to the particle size. In the DLS system (Scheme 3.8), the particles are illuminated with a laser, and the intensity fluctuations in the scattered light are detected and analyzed. Measurements were performed using a Zetasizer Instrument (Nano-ZS, Malvern, UK). Size distributions of particles were obtained by measuring the light scattered by particles by using a laser beam at a detecting angle of 173° at 298.15 K.

The zeta potential is measured by determining the electrophoretic mobility and the Henry equation. The electrophoretic mobility is obtained by performing the electrophoresis experiments and measuring the velocity of particles using laser doppler velocimetry. There exists an electrical double layer around the particle, as shown in Scheme 3.9. The double layer consists of two parts: the Stern layer where the ions are strongly bound and a diffuse layer where the ions arefree to move. At the brim of the diffuse layer, there exists a slipping plane, and potential at this boundary is

the zeta potential. Ions within the plane move with the moving particle, but ions beyond the plane move independently. Zeta potentials were measured using a Zetasizer Instrument (Nano-ZS, Malvern, UK). Three measurements were performed for each sample in order to calculate an average value. The data were analyzed with the software supplied by the instrument.

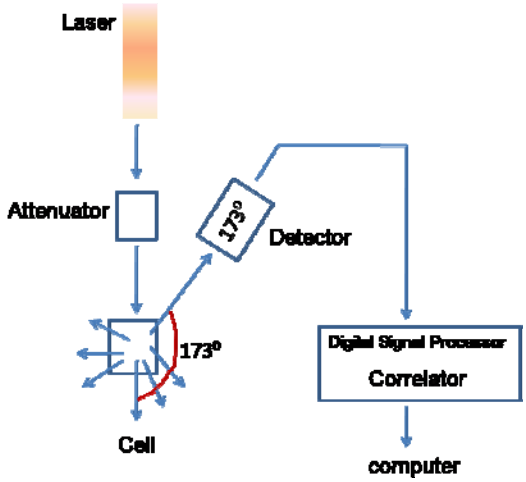

Scheme 3.8 Illustration of the DLS system

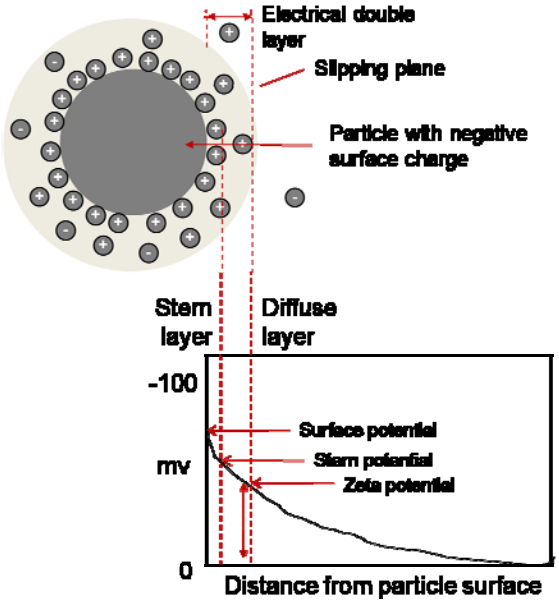

Scheme 3.9 Illustration of the zeta potential and electrical double layer

3.2.7 Micropolarity measurements

Fluorescence spectra were recorded by a fluorescence spectrophotometer (F4500, Hitachi, Japan) at 298.15 K, and pyrene is used as the fluorescent probe to detect the polarity of the microenvironment around the pyrene molecules. Ultrapure water was

saturated by pyrene first and then was used to prepare the samples. The concentration of pyrene in water is kept at 6.53×10^{-7} M. The emission spectrum (λ_{EX}=335 nm) of pyrene presents five peaks at the wavelengths of 373, 379, 384, 390 and 397 nm. The intensity ratio of the first peak (at wavelength 373 nm) to the third peak (at wavelength 397 nm), I_1/I_3, is sensitive to the microenvironment around pyrene molecules and is taken as a measure of polarity, with polarity being high with high I_1/I_3. Measurements were performed in duplicate and the results were highly reproducible.

3.2.8 Gel electrophoresis

The electrophoresis measurements were performed using a gel electrophoresis apparatus (HE-120, Tanon Science and Technology Inc., China) under 160 V for 20 min. Then the agarose gel was stained in ethidium bromide solution for 10 min and photographs of the electrophoresis bands were obtained under ultraviolet light.

3.2.9 Circular dichroism (CD)

CD refers to the differential absorption of left and right circularly polarized light, which can be used for structural studies of certain organic molecules. For the measurements in this thesis, CD spectra were obtained by Jasco spectropolarimeter J-810 (Jasco, Japan). Spectra were measured as the average of three scans from 240 to 340 nm at a scan rate of 50 nm min^{-1} in a 1 cm path length quartz cuvette.

3.2.10 Molecular dynamics (MD) simulation

In the MD simulation, the anionic DNA/cationic ionic liquid system is modeled approximately by an anionic polyelectrolyte/cationic surfactant system, described by a coarse-grained model. The polyelectrolyte is represented by a flexible linear chain of 100 connected negatively-charged spherical segments. A surfactant molecule consists of a head segment with positive unit charge and four neutral tail segments. The solvent is treated as a continuous medium and corresponding counterions of the polyelectrolyte and the surfactant are introduced to reach electroneutrality in the system. In order to simplify the simulation process, all particles including the segments of the polyelectrolyte, surfactant and counterions are assumed to have the same mass m and diameter σ. The Lennard-Jones (LJ) potential is used to model

short-range interactions between the particles. The cut-off length r_c for particles of the polyelectrolyte chains, counterions and surfactant headgroups is assumed to be $2^{1/6}\sigma$ where there exists purely repulsive interaction. For particles of the surfactant chains $r_c=2.5\sigma$ and there exist both repulsive and attractive forces. The Coulombic potential is used to model the long-range interaction between charged particles. A finite extension nonlinear elastic potential (FENE) is used to model the connective interaction of two bonded segments within the polyelectrolyte or surfactant molecules, where the spring constant $k_s=30\varepsilon/\sigma^2$ (ε being the well depth) and maximum extension $R_0=2\sigma$. The motion of the particles is governed by the stochastic Langevin equation, accounting for the viscous force from the solvent and stochastic force form the heat-bath. Ewald summation method is used to calculate the electrostatic interaction, including the contributions from the real space and reciprocal space. The simulation is performed in a cubic box with a length $L=100\sigma$ with periodic boundary conditions in three dimensions. The integral time step is $0.005\tau_s$, where $\tau_s=\sigma(m/\varepsilon)^{0.5}$. The total time steps for simulation are 8×10^6 steps and the last 3×10^6 steps are used to calculate ensemble averages. The temperature T under consideration is such that: $T=\varepsilon/k_B$, where k_B is the Boltzmann constant. The Bjerrum length $\lambda_B=e^2/(4\pi\zeta k_B T)$ is set to be 2σ, where e is the elementary charge, and ζ is the product of the relative dielectric constant of the medium and the vacuum permittivity.

To obtain the amount of surfactants adsorbed on the polyelectrolyte (N_s), an effective cut-off length of 4σ is chosen empirically, within which the surfactant molecules are considered to bind onto the polyelectrolyte chain. The mean-square radius of gyration $<R_g^2>$ is introduced for the polyelectrolyte

$$<R_g^2>=\frac{1}{2N^2}\sum_{i,j}<(r_i-r_j)^2> \qquad \text{Equation 3.4}$$

r_i and r_j are positions of the particle i and j on the polyelectrolyte. Z and Z_c display the (+/-) charge ratio of the positively-charged surfactant to negatively-charged polyelectrolyte in the whole system and in the surfactant/polyelectrolyte complex, respectively.

Chapter 4 Adsorption kinetics of surfactants at the air/water interface

4.1 Introduction

A variety of models have been utilized to understand the adsorption of surfactants onto the air-water interface at equilibrium. Based on the dependence of the equilibrium surface tension γ_{eq} on the bulk surfactant concentration C_b, the equilibrium surface concentration Γ_{eq} can be derived according to the Gibbs adsorption equation. Therefore, the equation of state, the equilibrium surface tension as a function of the surface concentration $\gamma_{eq}(\Gamma_{eq})$, can be obtained. However, it is very time-consuming to determine the equilibrium surface tension for efficient surfactants with very low *CMC*. In this work, we use a bubble compression method with both $C_{12}E_6$ (a nonionic surfactant, hexaethylene glycol dodecyl ether) and CTAB/NaBr solutions. We measured the equation of state using a single experiment by calibration with a known equilibrium surface tension value with its corresponding surface excess concentration, and found it comparable with the one obtained by the traditional method using Gibbs equation.

In addition to the surface properties of the system at equilibrium, the time-dependent adsorption process is also important. The adsorption of the surfactant molecules from the bulk onto the interface includes the diffusion of molecules from the bulk to the sub-surface and then the transfer of molecules from the sub-surface to the interface. The adsorption models commonly predict the time-dependent surface concentration, while experimentally the time-dependent interfacial tension is measured instead. Therefore, the equation of state $\gamma(\Gamma)$ is required to link the surface tension to the surface concentration. In this work, having directly measured the equation of state, we have also been able to perform a series of successive measurements by a proposed bubble compression method to derive the time-dependent surface concentration $\Gamma(t)$.

4.2 Procedures

Two surfactant systems were investigated, a non-ionic surfactant $C_{12}E_6$ and an ionic surfactant CTAB with sufficient NaBr in order to screen the electrostatic interactions. The configuration of rising bubble is used with the Tracker, and two types of measurement plans have been used: measurements with constant interfacial area (area control), and measurements with bubble volume changing linearlyin time (volume linear profile).

The two types of surfactants are selected for their high surface activity (equilibrium surface tension γ_{eq}(CTAB/NaBr) = 31 mN m^{-1}, γ_{eq}($C_{12}E_6$) = 32 mN m^{-1}) and low *CMC* values (for $C_{12}E_6$ 0.07 mM while for CTAB/NaBr 0.03 mM), which can lead to long equilibration times for the dynamic surface tension. Different concentrations for both systems have been studied, all below the *CMC*.

4.3 Results and discussions

4.3.1 Dynamic Surface Tension

The time-dependent surface tension for $C_{12}E_6$ is presented in Fig. 4.1. For the concentration of 0.02 mM, the surface tension drops from 72 mN m^{-1} to 45 mN m^{-1} in the first 100 seconds and continues to decrease slowly until reaching equilibrium (γ_{eq}=42 mN m^{-1}). The shape of the curve is similar for the concentration of 0.004 mM, but the relaxation is slower, the drop from 72 mN m^{-1} down to 54 mN m^{-1} takes 340 s with the equilibrium surface tension γ_{eq}=52 mN m^{-1}. The dynamic surface tensions for CTAB with NaBr are provided in the Fig. 4.2, where full equilibration also takes hundreds of seconds. The equilibrium surface tension values are determined from the limit at long time of the dynamic surface tension data, i.e. after several hours for the lowest concentrations studied.

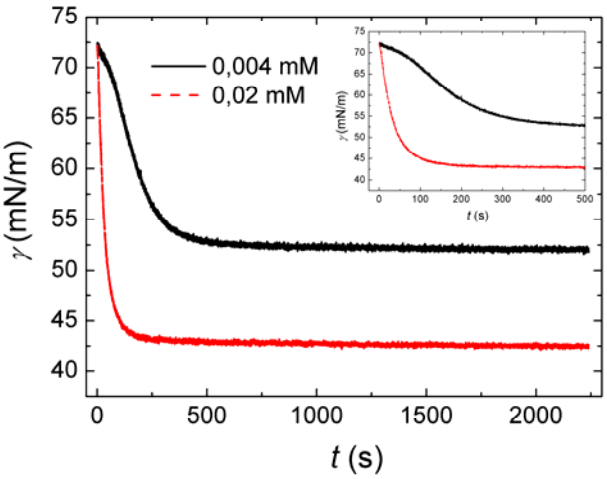

Fig. 4.1 Dynamic surface tension for the $C_{12}E_6$ system with two concentrations (0.004 and 0.02 mM). The inset shows the dynamic surface tensions at short times.

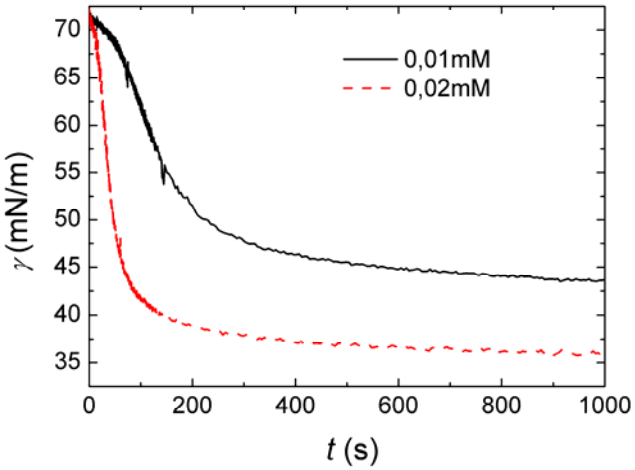

Fig. 4.2 Dynamic surface tension for the CTAB system with two concentrations (0.01 and 0.02 mM) in the presence of 100 mM NaBr.

4.3.2 Measuring surface concentration Γ by the bubble compression method

The Gibbs adsorption equation is utilized to calculate the adsorbed amount of surfactant molecules at equilibrium by linking Γ_{eq} to dγ/dln C_b, however, this method requires a series of measurements to ensure accuracy in the low concentration range. If the area of the bubble interface is abruptly modified as in studies of insoluble monolayers in a Langmuir trough, the equation of state can be directly measured.

The following experiment has been performed. First a bubble with a certain size was formed at t_0. After the evolution at constant area until t_1, we forced a rapid decrease of the surface area of the bubble until t_2 is reached, where the compression is ceased. This process is described in Scheme 4.1.

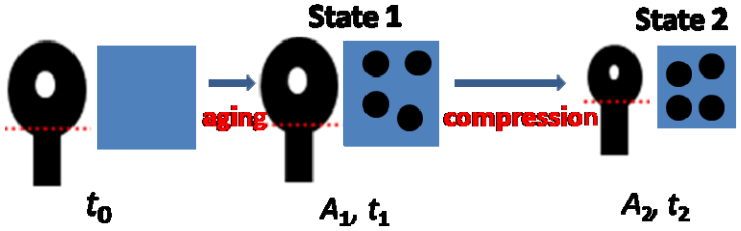

Scheme 4.1 Description of the proposed bubble compression method, with the blue plane denoting the bubble interface and the black spots denoting the surfactant molecules

Fig. 4.3 shows both the surface tension and the surface area of the bubble plotted as functions of time. The initial area of the bubble surface at t_1, before the beginning of the area decrease is denoted as A_1. In the example shown in Fig. 4.3, the area

decrease starts 76.4 s after the bubble formation, t_1. The area decreases from almost 17.7 mm^2 to 9.4 mm^2 in nearly 4.6 seconds. Correspondingly the surface tension is decreased as the surface concentration increases. The minimum surface tension reached is 31 mN m^{-1}, which is below γ_{eq} for this bulk concentration and close to the equilibrium surface tension attained above the *CMC*.

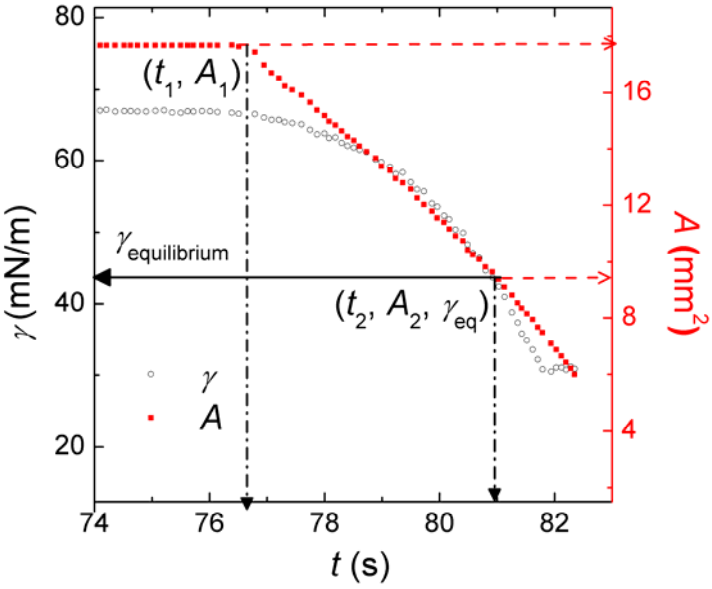

Fig. 4.3 The variations of surface tension (empty circles) and bubble surface area (filled squares) with time. The surface area starts to decrease continuously after t_1 = 76.4 s and at t_2 = 81 s the surface tension measured is equal to γ_{eq} = 42 mN m^{-1} for the system of 0.01 mM CTAB in the presence of 100 mM NaBr.

It is assumed that the decrease in the surface area is much faster than the adsorption or desorption of the molecules, that is to say, we can assume that the number of molecules adsorbed or desorbed during the area change is negligible. This means that $\Gamma_1 A_1 = \Gamma_2 A_2$ holds during the bubble compression process. Choosing A_2 as the point where $\gamma(t_2)=\gamma_{eq}$ means that Γ_2 will be the equilibrium surface concentration Γ_{eq} for the bulk concentration studied (note that Γ_{eq} is dependent on the bulk concentration). During the bubble compression process, assuming that the relation $\Gamma A = \Gamma_{eq} A_{eq}$ always holds, the relation of surface tension γ and surface concentration Γ can be found, that is to say, the equation of state can be measured from the proposed bubble compression method. Such experiments are repeated for a series of t_1, allowing us to measure $\Gamma(t)$ for the studied system. In order to verify our assumption of negligible adsorption or desorption during the bubble compression process, the experiments were carried out at varying compression speeds.

4.3.3 Verification of bubble compression method

4.3.3.1 Effect of the compression speed

Various speeds have been used to compress the bubble in the $C_{12}E_6$ solution with the concentration of 0.02 mM, and the corresponding surface tension vs the calculated surface concentration curves are presented in Fig. 4.4. The curves at higher speeds coincide well with each other, validating the assumption that the adsorption or desorption during the compression is negligible. However, the curves at low compression speeds (lower than 1 μL/s) deviate much from the ones with higher compression speeds. At slower bubble compression speeds, it can be seen that the surface tension decreases more quickly when γ is above γ_{eq} (42 mN/m), and less below. When $\gamma>\gamma_{eq}$, we underestimate the surface coverage as the adsorption occurs during the compression, however as γ reaches γ_{eq} the surface tension decreases more slowly as there is desorption during the compression. Therefore, the surface concentration can only be safely determined at a compression speed sufficiently high (≥1 μL/s), in which case the $\gamma(\Gamma)$ curve is unique. In the following experiments, the bubble compression has been performed at the speed of 1 μL/s.

When decreasing the bubble size at a speed sufficiently high (≥1 μL/s), as shown in Fig. 4.4, γ decreases continuously until around 32 mN m^{-1}, much lower than the equilibrium value γ_{eq}=42 mN/m for 0.02 mM $C_{12}E_6$. Γ/Γ_{eq} increases gradually to 1 (found at $\gamma=\gamma_{eq}$ for 0.02 mM) and then keeps increasing. In other words, the interface is over-occupied, meaning that the surface concentration is beyond Γ_{eq}. The final γ value (around 32 mN m^{-1}) corresponds to the equilibrium surface tension of $C_{12}E_6$ above the *CMC*. This indicates that there exists an "extreme state of packing" at the interface. This process resembles the collapse of insoluble monolayers, where in general the collapse surface pressure (difference between surface tension of water and surface tension in the presence of the monolayer) is higher than the equilibrium surface pressure, but will finally reach equilibrium if sufficient time is given [124]. Note that at high compression speed (≥1 μL/s), a region with constant surface tension can be observed finally, at this stage the interface has already been packed to the maximum state therefore desorption may be involved. Therefore this region should not be considered as part of the equation of state.

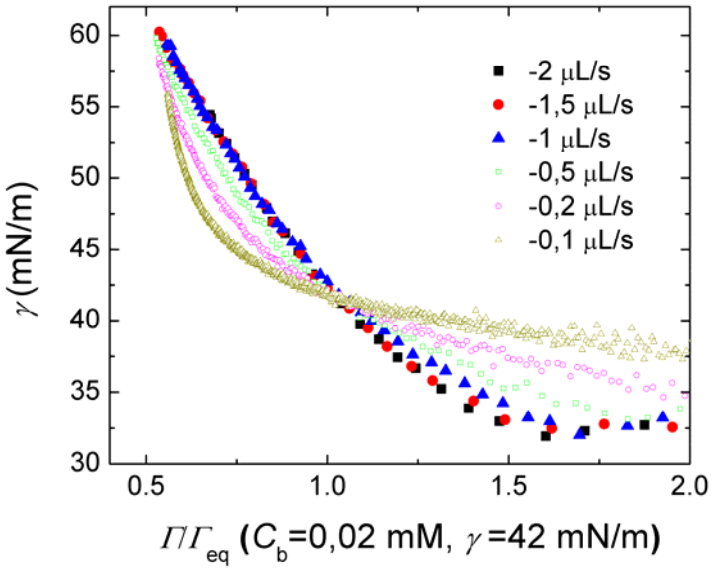

Fig. 4.4 Surface tension γ as a function of the calculated surface concentration Γ, normalized by Γ_{eq} at various compression rates. Γ_{eq} is the equilibrium surface concentration for 0.02 mM $C_{12}E_6$, where the equilibrium surface tension γ_{eq}=42 mN/m. Note that at low compression speeds the calculated value of Γ does not correspond to the actual value of Γ because desorption or adsorption occurs.

4.3.3.2 Reversibility of the compression process

The reversibility of the compression process and the absence of adsorption or desorption was also verified by performing a cycle of compression followed by an equivalent expansion at the same speed. The description for the bubble compression followed by expansion can be seen in Scheme 4.2. Fig. 4.5 present the variations of surface tension and area change with time. The surface tension γ returns to the value before the start of the compression and expansion processes therefore validating the experimental protocol.

Scheme 4.2 Bubble compression followed by bubble expansion

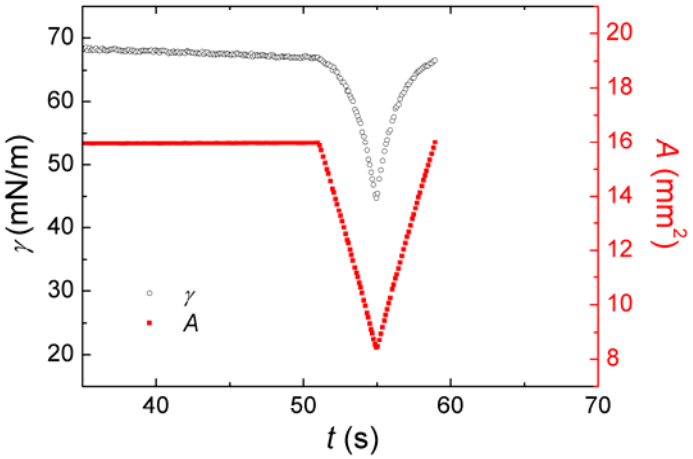

Fig. 4.5 A complete compression and expansion cycle of a bubble in the CTAB/100 mM NaBr system, where the CTAB concentration is 0.01 mM. At 51 s after the creation of the bubble, it was compressed at 1 μL/s and at 55 s, the compression was stopped and an expansion of the bubble was performed at the same speed until 59 s.

4.3.3.3 Comparison with the equation of state

The Gibbs adsorption equation (Equation 4.1) is generally used to analyze the surface tension data in order to obtain the equilibrium surface concentration.

$$\Gamma_{eq} = -\frac{1}{RT}\frac{d\gamma}{d\ln C_b} \qquad \text{Equation 4.1}$$

The surface tension as a function of surfactant concentration was measured for the two systems, non-ionic surfactant $C_{12}E_6$ and ionic surfactant CTAB in the presence of NaBr. The values of $d\gamma/d\ln(C_b)$ were taken at various bulk concentrations and the surface tension vs the surface concentration was obtained. The results are shown in Fig. 4.6 and Fig. 4.7 respectively, together with the values obtained from literature.

Besides, we have recorded the surface tension γ as a function of the surface concentration Γ for both systems using the proposed bubble compression method at a compression speed of 1 μL/s and at various bulk concentrations, as indicated in Fig. 4.6 and Fig. 4.7. Note that the region with constant surface tension should not be considered as trustworthy due to the possible presence of desorption. Here the absolute values of Γ for $C_{12}E_6$ were obtained by calibration using $\Gamma=3\times10^{-6}$ mol/m^2 at γ=42 mN/m, corresponding to a bulk concentration of 0.02 mM. The reference used for calibration was derived from the Gibbs adsorption equation (Fig. 4.6). Neutron reflectivity results have shown that the surface concentrations for 0.01 and 0.04 mM

$C_{12}E_6$ are 2.65 and 3.15×10^{-6} mol/m^2 respectively [125], consistent with the value used. For CTAB, the values of Γ were calculated by calibration using $\Gamma=3.5\times10^{-6}$ mol/m^2 at γ=36 mN/m, again from the Gibbs adsorption equation (Fig. 4.7). As shown, the $\gamma(\Gamma)$ curves derived from bubble compression in solutions with different surfactant concentrations are in good agreement. These data also agree well with those from the Gibbs adsorption equation, although the latter are more scattered, especially for $C_{12}E_6$. This results from the use of the Gibbs adsorption equation, where small uncertainties in the surface tension measurements may result in large differences in the derivatives used to calculate Γ_{eq}. From the compression experiments, we conclude that the relationship found between γ and Γ is unique at least in the experimental range probed, fully validating the procedure used. It implies that one can access the equations of state, based on a single measurement (below the *CMC*) under appropriate conditions (high bubble compression speed, calibration by one equilibrium surface tension value and the corresponding surface concentration).

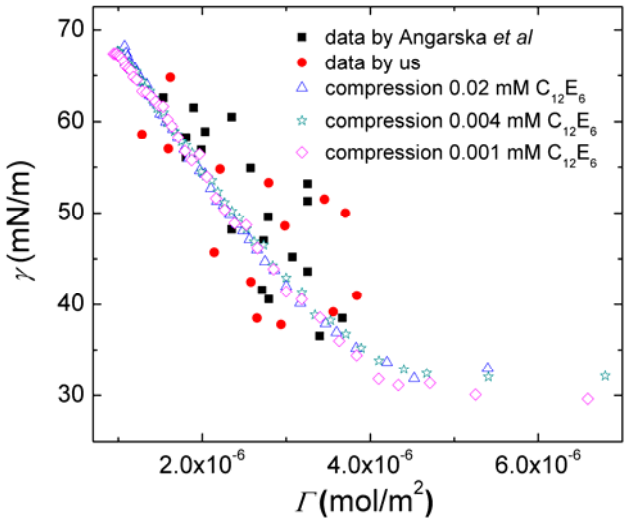

Fig. 4.6 Comparison of data obtained by Gibbs adsorption equation and bubble compression. The filled squares and circles were obtained by derivation of the equilibrium surface tension vs the bulk concentration curve and using the Gibbs adsorption equation: filled circles, from our data; filled squares, from data by Angarska *et al*. [1]. The open symbols were obtained by compressing bubbles at a rate of 1 μL/s in solutions containing different $C_{12}E_6$ concentrations.

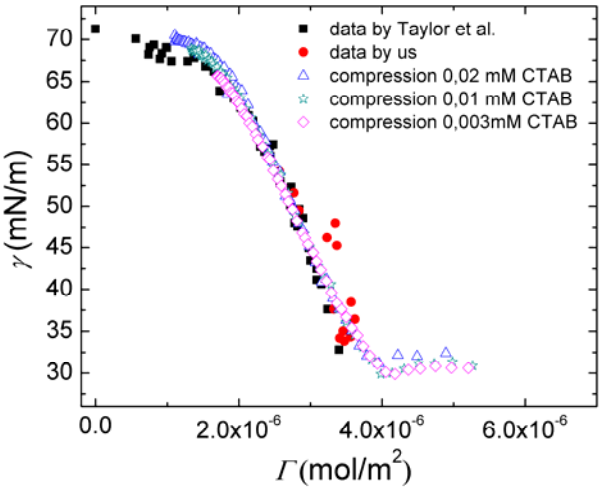

Fig. 4.7 Comparison of data obtained by Gibbs adsorption equation, bubble expansion and bubble compression. The filled circles from our data were obtained by derivation of the equilibrium surface tension vs the bulk concentration curve and using the Gibbs adsorption equation. The filled squares from data by Taylor *et al*. [126] were obtained by a bubble expansion method. The open symbols were obtained by compressing bubble at a rate of 1 μL/s in solutions containing different CTAB concentrations.

4.3.4 Adsorption kinetics

Having shown the validity of our proposed experimental method, the time-dependent surface concentration $\Gamma(t)$ was directly obtained by measuring the surface concentration Γ corresponding to the changing t_1, the time between creation of the bubble and bubble compression. $C_{12}E_6$ and CTAB/NaBr solutions with different concentrations have been studied, and the results are presented in Fig. 4.8 and Fig. 4.9. As shown earlier, there is neither adsorption nor desorption during the compression process at high speed, and the constant number of molecules at the interface during the compression is determined by the amount adsorbed at t_1. In Fig. 4.8 and Fig. 4.9, the insets show Γ/Γ_{eq} as a function of the square root of t_1 at each concentration (Γ_{eq} is the equilibrium surface concentration for the C_b used, so dependent on the bulk concentration). As indicated, Γ/Γ_{eq} is linear with the square root of t_1 at short times, suggesting that the adsorption is diffusion-controlled. The data for the two bulk concentrations for each system were scaled using Γ_{eq} values in Fig. 4.6 and Fig. 4.7 respectively and Equation 4.2

$$\frac{\Gamma(t)}{\Gamma_{eq}} = 2\sqrt{\frac{D}{\pi}}\frac{C_b}{\Gamma_{eq}}\sqrt{t} = 2\sqrt{\frac{D}{\pi}}K \qquad \text{Equation 4.2}$$

The results are shown in the main plot of Fig. 4.8 and Fig. 4.9. The two sets of data superimpose well, supporting the fact that adsorption is diffusion-controlled.

At longer times, i.e. large K values, $\Gamma(t)$ tends to increase more slowly. This can be owing to the fact that the additional terms in Equation 4.3 can no longer be neglected as the desorption and curvature begin to play a role.

$$\Gamma(\mathrm{t}) = 2\sqrt{\frac{D}{\pi}}\left[C_{\mathrm{b}}\sqrt{t} - \int_0^{\sqrt{t}} C_{\mathrm{s}}(t-\tau)\mathrm{d}\sqrt{\tau}\right] + \frac{D}{b}\left[C_{\mathrm{b}}t - \int_0^{t} C_{\mathrm{s}}(\tau)\mathrm{d}\tau\right] \qquad \text{Equation 4.3}$$

The term $D^*C_{\mathrm{b}}^*t/b$ in the Equation 4.3 is of the order of 10^{-7} mol m^{-2} for the longest time studied; therefore the assumption that the curvature effect can be ignored at short time is reasonable.

From the slope of the plot $\Gamma(t)/\Gamma_{\mathrm{eq}}$ vs K at short times and Equation 4.2, we obtain a diffusion coefficient for $C_{12}E_6$: D=(3.8±0.5) $\times 10^{-10}$ m^2 s^{-1}, comparable to the values (in the range of 2.5 to 4.0$\times 10^{-10}$ m^2 s^{-1}) obtained by Lucassen *et al*. [69] with a surface compression rheology technique and the value (6.0×10^{-10} m^2 s^{-1}) obtained by Pan *et al*. [50] using the fit of dynamic surface tensions. Moorkanikkara *et al*. [127] proposed a method to determine the rate-limiting step for the adsorption kinetics of $C_{12}E_6$, using the short time dynamic surface tension data with no assumption for the adsorption isotherm. They found that the adsorption kinetics of $C_{12}E_6$ is diffusion-controlled with a diffusion constant of (3.8± 0.6) $\times 10^{-10}$ m^2 s^{-1}, which agrees well with the diffusion constant derived by us. In the case of CTAB, we find D= (3.0± 0.5) $\times 10^{-10}$ m^2 s^{-1}, comparable to the literature values (1-2$\times 10^{-10}$ m^2 $s^{-1}$from NMR measurements [128]). Therefore, we have successfully confirmed that adsorption is diffusion-controlled at short times for the two types of surfactant solutions studied.

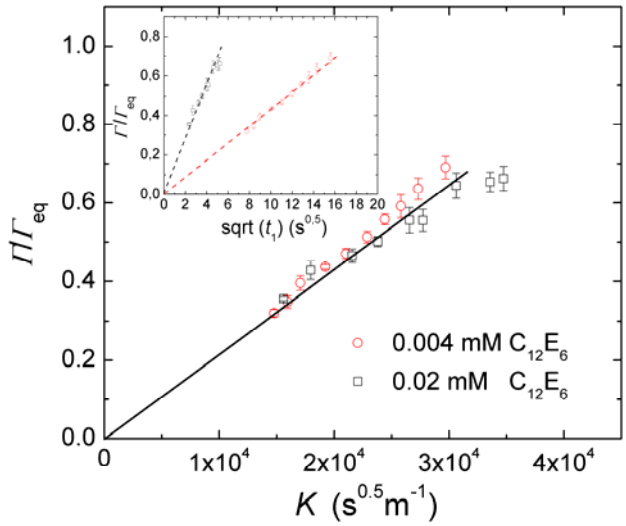

Fig. 4.8 The surface excess ratio Γ/Γ_{eq} as a function of K for two concentrations of $C_{12}E_6$, 0.004 (circles) and 0.02 mM (squares) , where $K = \frac{C_b}{\Gamma_{eq}}\sqrt{t_1}$. The inset shows the Γ/Γ_{eq} as a function of $\sqrt{t_1}$. K was calculated using Γ_{eq}=2.1 ×10^{-6} mol/m^2 for C_b=0.004 mM and 3×10^{-6} mol/m^2 for C_b = 0.02 mM, taken from Fig. 4.6.

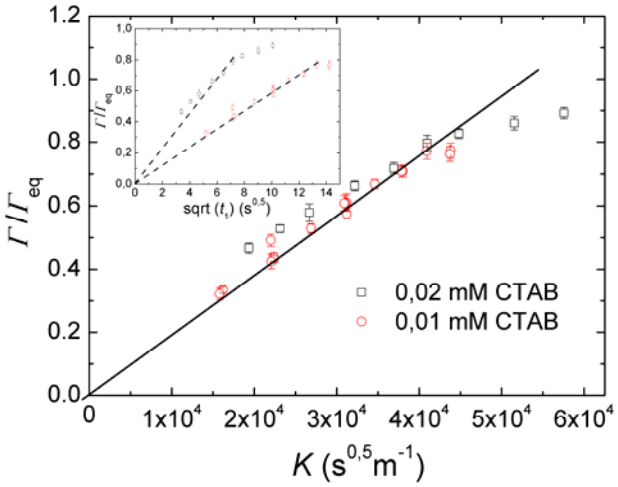

Fig. 4.9 The surface excess ratio Γ/Γ_{eq} as a function of K for two concentrations of CTAB, 0.01 (circles) and 0.02 mM (squares), where $K = \frac{C_b}{\Gamma_{eq}}\sqrt{t_1}$. The inset shows the Γ/Γ_{eq} as a function of $\sqrt{t_1}$. K was calculated using Γ_{eq}=3.25 ×10^{-6} mol/m^2 for C_b=0.01 mM and 3.5×10^{-6} mol/m^2 for C_b = 0.02 mM, taken from Fig. 4.7.

4.4 Conclusions

The equilibrium and dynamic interfacial properties of two types of surfactant systems (non-ionic surfactant $C_{12}E_6$ and ionic surfactant CTAB in the presence of sufficient electrolyte) at the concentration range below *CMC* have been presented. The surfactant systems selected possess very low *CMC* values, therefore have slow adsorption dynamics. We have successfully measured the equation of state (the variation of the surface tension with the surface concentration) from a single bubble compression measurement by calibration with a known value of equilibrium surface tension. It has been found that our results are comparable to those from the traditional methods, which combine the equilibrium surface tension data with the Gibbs adsorption equation.

Moreover, with the proposed bubble compression method, we have directly measured the time-dependent surface concentration for the two types of surfactants, and have shown that the adsorption is diffusion controlled at short times in both cases. The calculated bulk diffusion coefficients for $C_{12}E_6$ and CTAB were found in close agreement with literature values. The proposed method is simple and allows direct access to the adsorption kinetics, opening the way to further test and improve the existing theoretical models.

Chapter 5 Desorption kinetics of surfactants at the air-water interface

5.1 Introduction

Contrary to the adsorption process previously studied in Chapter 4, desorption process is the transfer of molecules from the surface or interface to the bulk phase, and it is considered closely related to the adsorption. This is why, similarly to the adsorption process, the desorption process can be divided into two steps: the transfer of surfactant molecules from the surface/interface to the sub-surface and the diffusion of surfactants in the bulk. To understand the desorption kinetics, many studies have been performed with bubbles or drops with good control of its volumetric variation with time. Diffusion-limited adsorption or desorption may account for the dilute solutions of non-ionic surfactants or ionic surfactants in the presence of sufficient electrolyte. However, in most cases, the energy barrier in the interfacial region may play an important role and become the controlling step. The challenge is to determine the controlling step for the desorption kinetics in the surfactant system.

In Chapter 4, we have investigated the adsorption processes for aqueous solutions of two types of surfactants, $C_{12}E_6$, and CTAB with large amounts of salt. By a bubble compression method, we have successfully determined the equation of state $\gamma(\Gamma)$ and studied the adsorption kinetics of surfactants. In this section, we will introduce the results of our study on the desorption process for the same surfactant systems, based on both the proposed bubble compression method and computer simulations. To better understand the desorption kinetics, the effects of surfactant chain length and counterions have also been studied.

5.2 Procedures

Four surfactant systems were studied, a nonionic surfactant $C_{12}E_6$, two cationic surfactants CTAB and TTAB with NaBr, and an anionic surfactant AOT with NaCl, KCl or $MgCl_2$. The Tracker with a rising bubble configuration was used for all the surface tension measurements. In order to observe the effect of depletion, we compared the maximum amount of adsorbed surfactants at the bubble interface (in the order of 10^{-9} mol) and in the bulk (in the order of 10^{-8}~10^{-7} mol), showing that in all the experiments we have sufficient molecules in the system to cover the air-water interface.

In the experiments, a bubble was first created and then after some time (aging of the interface) it was compressed at a high compression speed (1 μL/s) so as to

increase the surface concentration rapidly above its equilibrium value. As soon as the compression was ceased, the variation of the surface tension γ with time t was recorded. The surface tension increased with time due surfactant desorption leading to the re-equilibration of the surface concentration.

Scheme 5.1 is shown to describe the process more clearly. The bubble compression is performed at t_1 until t_2 is reached. At t_2, the bubble compression is stopped with the over-occupied interface, therefore desorption occurs accompanied by the decrease of surface concentration and increase of surface tension. Finally at t_3, the interface reaches equilibrium.

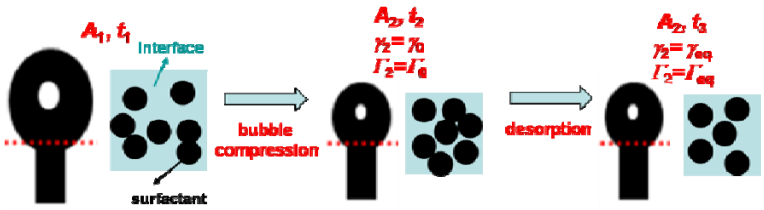

Scheme 5.1 Description of bubble compression and the desorption process, with the blue plane denoting the bubble interface and the black spots denoting the surfactant molecules

In order to compare with the experimental results, Matlab simulations using diffusion models have been performed to study the desorption process of CTAB and $C_{12}E_6$, resulting in the variations of surface concentration with time in the desorption process. By using a diffusion model, the concentration profile from the sub-surface to the bulk infinitive can be obtained. The model is similar to the Ward and Tordai equation adapted for diffusion away from the surface. The input parameters include the initial sub-surface concentration, the diffusion constants and the relation of the surface concentration with the sub-surface concentration derived from the $\gamma_{eq}(C)$ measurements and the equation of state $\gamma_{eq}(\Gamma_{eq})$, which are Equation 5.1 and Equation 5.2 respectively for CTAB and $C_{12}E_6$, where Γ_{CMC} is taken to be 4×10^{-6} mol m^{-2}.

$$C_s = 2.69\text{E-}4 \times e^{4.98\Gamma/\Gamma_{CMC}} - 4.02\text{E-}3 \qquad \text{Equation 5.1}$$

$$C_s = 1.08\text{E-}3 \times e^{4.20\Gamma/\Gamma_{CMC}} - 3.97\text{E-}3 \qquad \text{Equation 5.2}$$

The initial sub-surface concentration can be obtained from the equilibrium relation of the surface concentration with the sub-surface concentration and the known initial surface concentration. The diffusion constant values used were determined from the experimental results in the previous chapter. Therefore, at each step, a concentration profile from the sub-surface to the bulk can be obtained. By

increasing the simulation steps, the concentration profile from the sub-surface to the bulk becomes flatter, meaning that they converge. Accordingly the surface concentration as a function of time can be obtained.

5.3 Results and discussion

5.3.1 Dynamic surface tension

The bubble was compressed until its surface tension γ_0 reached a value below the equilibrium surface tension of γ_{eq} corresponding to the bulk concentration studied. That is to say, when the compression is stopped, the initial surface concentration for the surfactants Γ_0 surpasses the equilibrium value Γ_{eq}. Given enough time, the excess surfactant molecules at the interface will transfer to the bulk, leading to the decrease of the surface concentration Γ as well as the increase of the surface tension γ.

The time-dependent surface tension is recorded during the relaxation processes for the different surfactant systems studied ($C_{12}E_6$, CTAB, TTAB and AOT) and the results are shown in Fig. 5.1. As shown, for each type of surfactant, different bulk concentrations C were studied with different compression degrees to reach various initial surface tension values γ_0. All curves show that γ increases rapidly at the beginning, and then increases more slowly with time followed by a final plateau.

The different surfactant bulk concentrations C and initial surface tensions γ_0 are summarized in Table 5.1, Table 5.2, Table 5.3, Table 5.4 for all the surfactants studied. Several experiments have been performed using the same surfactant solution but with different degrees of compression, however not all of these are included in the tables.

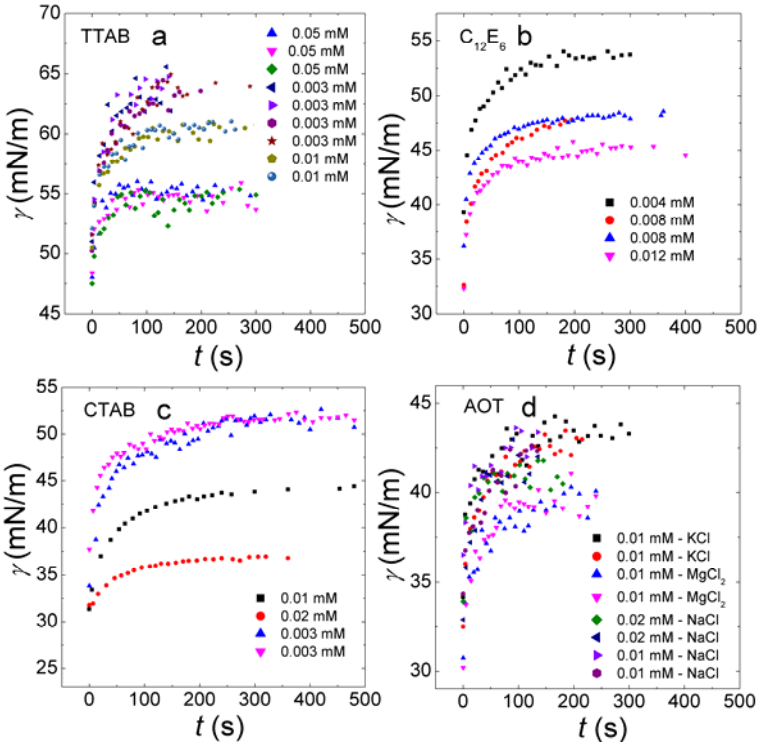

Fig. 5.1 The relaxation of the surface tension $\gamma(t)$ after the compression for different systems studied: a) TTAB/100 mM NaBr; b) $C_{12}E_6$; c) CTAB/100 mM NaBr; d) AOT/100 mM KCl, AOT/100mM NaCl, AOT/50 mM $MgCl_2$.

Table 5.1 Summary of parameters for the $C_{12}E_6$ systems at various surfactant bulk concentrations, where C is the bulk concentration, γ_0 the initial surface tension, γ_{eq} the equilibrium surface tension, Γ_0 the initial surface concentration, Γ_{eq} the equilibrium surface concentration

C (mM)	γ_0 (mN/m)	γ_{eq} (mN/m)	Γ_0 ($\times 10^{-6}$ mol/m^2)	Γ_{eq} ($\times 10^{-6}$ mol/m^2)
0.004	39	54	3.3	2.0
0.008	33	48	4.0	2.5
0.008	36	49	3.6	2.5
0.012	32	45	4.0	2.7

Table 5.2 Summary of parameters for CTAB/100 mM NaBr systems with various surfactant bulk concentrations, where C is the bulk concentration, γ_0 the initial surface tension, γ_{eq} the equilibrium surface tension, Γ_0 the initial surface concentration, Γ_{eq} the equilibrium surface concentration

C (mM)	γ_0 (mN/m)	γ_{eq} (mN/m)	Γ_0 ($\times 10^{-6}$ mol/m^2)	Γ_{eq} ($\times 10^{-6}$ mol/m^2)
0.003	34	51	3.7	2.7
0.003	38	51	3.4	2.7
0.01	31	44	3.9	3.1
0.02	32	37	3.8	3.5

Table 5.3 Summary of parameters for TTAB/100 mM NaBr systems with various surfactant bulk concentrations C and γ_0 is the initial surface tension, and γ_{eq} the equilibrium surface tension

C (mM)	γ_0 (mN/m)	γ_{eq} (mN/m)
0.003	51	62
0.01	50	61
0.031	48	55
0.05	45	50

Table 5.4 Summary of parameters for AOT systems with different types of counterions at various surfactant bulk concentrations, where C is the bulk concentration, γ_0 the initial surface tension, γ_{eq} the equilibrium surface tension

C (mM)	Counterion Type	γ_0 (mN/m)	γ_{eq} (mN/m)
0.01	K^+	34	43
0.01	Mg^{2+}	31	40
0.01	Na^+	37	43
0.01	Na^+	34	42
0.02	Na^+	34	41
0.02	Na^+	33	42

5.3.2 Diffusion-limited desorption model

The systems studied are all at low concentrations, below the *CMC*. The surfactants used include non-ionic surfactants or ionic surfactants in the presence of high concentrations of electrolyte. The adsorption onto a clean interface has been shown previously to be diffusion limited at least at short times, and here we have investigated whether the desorption is also simply diffusion limited, i.e. that the rate limiting step is the diffusion of the molecules from the sub-surface to the bulk phase.

In the case of the diffusion-limited processes, since the interfacial equilibrium always exists, the relationship between the surface tension, surface concentration and the sub-surface concentration is unique and holds even in out of equilibrium situations. Diffusion limited desorption can be described by an approach similar to that of Ward and Tordai, modified to describe diffusion away from an interface, in order to predict the time-dependent surface concentration. In most reported studies, the surface tension is experimentally measured and an equation of state (Langmuir, Frumkin etc.) linking γ and Γ is utilized to derive the surface concentration Γ. Instead of using an existing relationship between γ and Γ, we use a relation $\gamma(\Gamma)$ obtained experimentally, in order to recover $\Gamma(t)$ from the surface tensions measured during the desorption process. The experimental equations of state for $C_{12}E_6$ and CTAB/NaBr are shown in Fig. 5.2. The surface tensions $\gamma(t)$ are then transformed into $\Gamma(t)$ according to the derived equation of state, as shown in Fig. 5.3. Accordingly, the values of Γ_0 and Γ_{eq} can be obtained, as shown in Table 5.1 and Table 5.2.

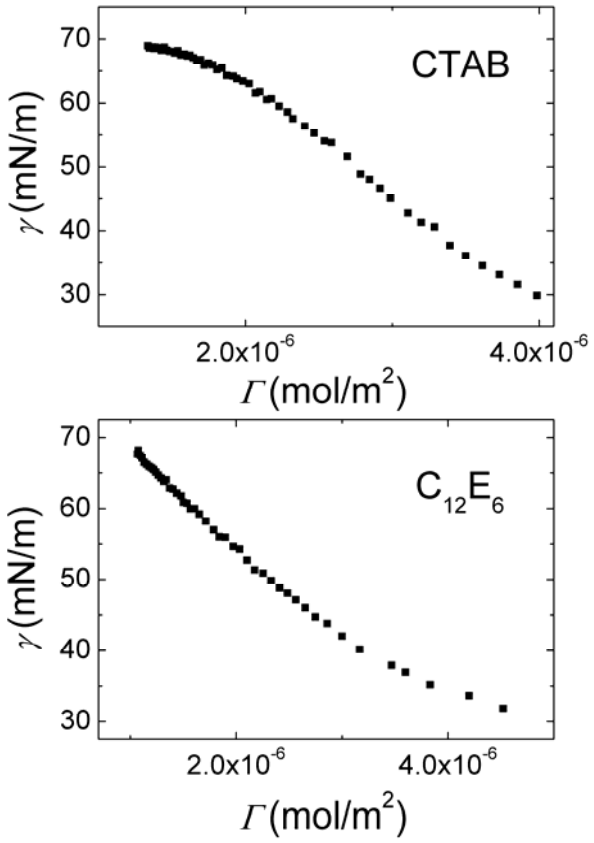

Fig. 5.2 Equilibrium equation of state for $C_{12}E_6$ and CTAB/100 mM NaBr.

Computer simulations were used to model the diffusion limited desorption process and calculations of the theoretical $\Gamma(t)$ have been performed according to the

procedure described in Section 5.2. The relation between the sub-surface concentration and the surface concentration $C_s(\Gamma)$ has been obtained by linking the experimental equilibrium surface tension data $\gamma(C)$ and the equation of state $\gamma(\Gamma)$, the diffusion coefficient is taken as found in adsorption experiments, which means that there are no adjustable parameters in the calculations. The calculated results for $C_{12}E_6$ and CTAB are also shown in Fig. 5.3.

As shown in Fig. 5.3, the calculated values are below the experimentally found surface concentrations in all cases, which means that the desorption is slower than what is expected in a diffusion limited case. For both systems, the difference between calculations and experiments becomes more important at higher surfactant concentrations with higher surface concentrations. This suggests that the relaxation may not be purely diffusion limited, that is to say, there may be a kinetic barrier when the surfactant molecules leave the air-water interface to enter the subsurface. This effect of barrier is more pronounced in the cases with higher surface concentrations.

Let us recall that the adsorption of both surfactants is diffusion controlled, at least at short times. However, during the desorption, $\Gamma(t)$ deviates from the predictions of a diffusion-limited process, suggesting the presence of a desorption barrier.

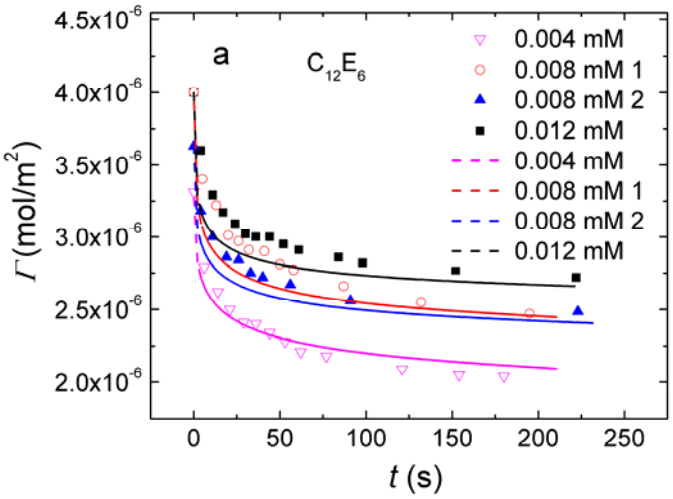

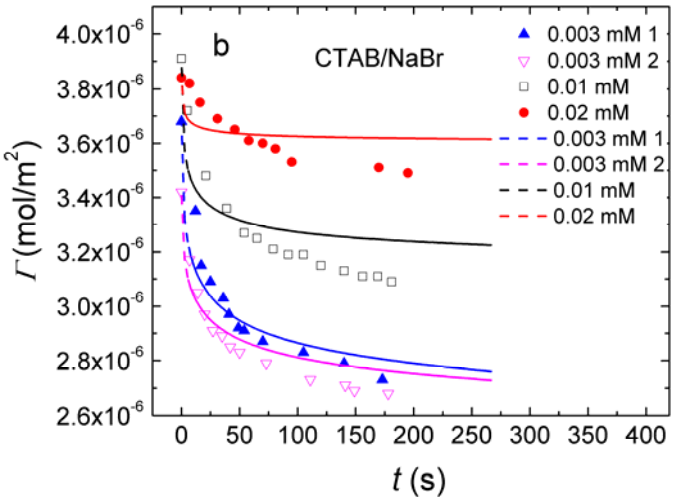

Fig. 5.3 The relaxation of the surface concentration as a function of time for two surfactant systems: $C_{12}E_6$ (a) and CTAB/100 mM NaBr (b). The points with bigger size are the calculated results from surface tension vs time curve while the lines are the simulation results using a diffusion model, assuming that diffusion constant for $C_{12}E_6$ is 3.8×10^{-10} m^2/s and for CTAB 3.0×10^{-10} m^2/s.

5.3.3 Kinetically controlled desorption model

As it has been shown that desorption is not purely diffusion controlled, we will attempt to describe the data by a kinetically-limited desorption model. In the case of kinetically-limited desorption there is no equilibrium between the interface and the subsurface, and it is assumed that the diffusion of the molecules out of the interfacial layer into the bulk is faster than the molecular transfer between interface and sub-surface, meaning that the concentration in the subsurface layer is constant and equal to the bulk concentration at all times.

Recall that in the kinetically controlled desorption model, we have the following relation

$$\Gamma = \Gamma_{eq} + (\Gamma_0 - \Gamma_{eq}) \times e^{-kt} \qquad \text{Equation 5.3}$$

The surface tension is measured experimentally instead of surface concentration. As discussed elsewhere [60], we will assume that the equation of state still applies in the kinetically-limited adsorption kinetics, therefore the $\Gamma(t)$ data are still those of Fig. 5.3. The fit of these data with Equation 5.3 is shown in Fig. 5.4, where Γ_f is the simulated final surface concentration, Γ_0 the initial surface concentrations, and the corresponding k values are included in Table 5.5 and Table 5.6.

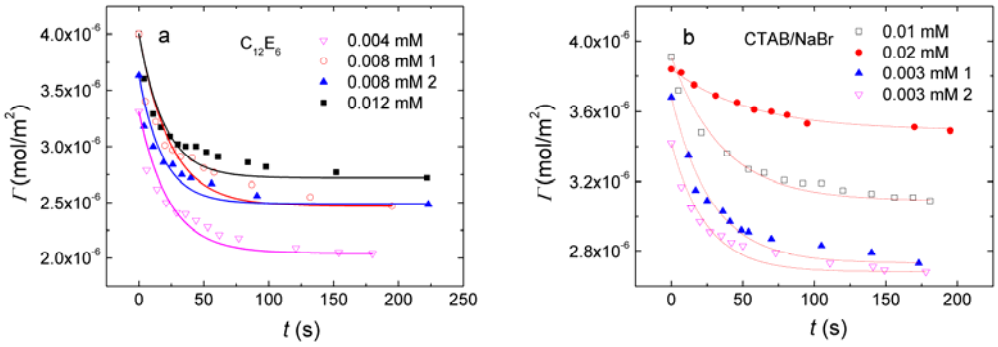

Fig. 5.4 Exponential fits for the calculated surface concentration in time for two systems $C_{12}E_6$ (a) and CTAB/100 mM NaBr (b).

Table 5.5 Fitted k values for the data in Fig. 5.4(a) for the $C_{12}E_6$ system using Equation 5.3

C (mM)	Γ_0 ($\times 10^6$ mol/m^2)	Γ_f ($\times 10^6$ mol/m^2)	k (s^{-1})
0.004	3.3	2.0	0.042
0.008 1	4.0	2.5	0.042
0.008 2	3.6	2.5	0.054
0.012	4.0	2.7	0.050

Table 5.6 Fitted k values for the data in Fig. 5.4(b) for the CTAB/100 mM NaBr system using Equation 5.3

C (mM)	Γ_0 ($\times 10^6$ mol/m^2)	Γ_f ($\times 10^6$ mol/m^2)	k (s^{-1})
0.003 1	3.7	2.7	0.035
0.003 2	3.4	2.7	0.041
0.01	3.9	3.1	0.028
0.02	3.8	3.5	0.018

As seen in Fig. 5.4, the CTAB data can be fitted better with an exponential fit than the diffusion-controlled model (Fig. 5.3). This suggests that the desorption is mainly dominated by the transfer of surfactant molecules from the surface onto the subsurface, especially for the case of CTAB, confirming the presence of a desorption barrier.

In the following we tried to directly interpret the surface tension data using kinetically-limited desorption model. Assuming that the γ vs Γ_{eq} plots for the systems are approximately linear for concentrations not far from the *CMC* (Fig. 5.2), in this case, instead of fitting the $\Gamma(t)$ one can directly use $\gamma(t)$ as:

$$\frac{\gamma_{eq}-\gamma}{\gamma_{eq}-\gamma_0}=e^{-kt}$$ Equation 5.4

Fig. 5.5 shows the variations of $(\gamma_{eq}-\gamma)/(\gamma_{eq}-\gamma_0)$ with time and the fits with Equation 5.4 for $C_{12}E_6$ and CTAB respectively. Separate fits for data points at each surfactant concentration have been performed, and the values of k and the characteristic time τ_1 (inverse of k) are given in Table 5.7 and Table 5.8. Comparing the tables (Table 5.5, Table 5.6, Table 5.7, Table 5.8), the determination of k using the two methods give similar results.

The results suggest that k does not depend appreciably on concentration. Recall Equation 5.5

$$k=\frac{k_a C_b+k_d}{\Gamma_\infty}$$ Equation 5.5

This suggests that k_d is much larger than k_a*C_b, causing k to be independent of C_b. It also further rules out the possibility that desorption could be purely diffusion controlled, in which case the characteristic time should vary as the inverse square of the bulk concentration, i.e. a factor of about 50 for CTAB at the highest and lowest concentrations (0.02 mM and 0.003 mM respectively), clearly incompatible with the results obtained.

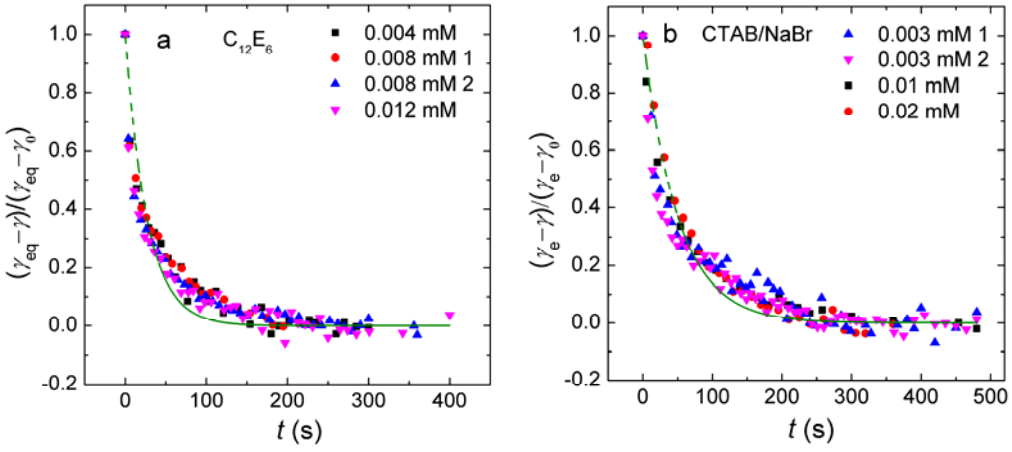

Fig. 5.5 Desorption processes for $C_{12}E_6$ (a) and CTAB/100 mM NaBr (b) with different surfactant concentrations, where the line is the fitting curve for all the data points at different surfactant concentrations using $(\gamma_{eq}-\gamma)/(\gamma_{eq}-\gamma_0)=e^{-kt}$.

Table 5.7 Fitted k and τ_1 values for the data at different surfactant concentrations in Fig. 5.5(a) for the $C_{12}E_6$ system using Equation 5.4

C (mM)	k (s^{-1})	τ_1 (s)
0.004	0.033	30.2
0.008 1	0.035	29.9
0.008 2	0.040	25.0
0.012	0.044	22.9

Table 5.8 Fitted k and τ_1 values for the data at different surfactant concentrations in Fig. 5.5(b) for the CTAB/100 mM NaBr system using Equation 5.4

C (mM)	k (s^{-1})	τ_1 (s)
0.003 1	0.020	49.6
0.003 2	0.024	42.2
0.01	0.018	54.3
0.02	0.017	59.3

5.3.4 Effect of surfactant architecture and counterion type on the desorption kinetics

5.3.4.1 Effect of surfactant chain length

From the above analysis, it can be concluded that there exists an energy barrier for surfactant to desorption from surface to the subsurface. It has been argued that the energy barrier for adsorption was present at high surface concentrations [3]. We propose that the energy barrier for desorption is also linked to high surface coverage with strong mutual interactions between surfactant chains. Therefore, in order to check if hydrophobic interactions affect the desorption kinetics, another ionic surfactant TTAB (in the presence of 100 mM NaBr) was selected for its similar molecular structure to CTAB but a shorter alkyl chain length. Similar to CTAB and $C_{12}E_6$ (Fig. 5.5), the normalized surface tension data $(\gamma_{eq}-\gamma)/(\gamma_{eq}-\gamma_0)$ coincide for various surfactant concentrations C (or initial surface tensions γ_0) for the TTAB system (Fig. 5.6). However, the characteristic time $\tau_1=1/k$ is different: for CTAB τ_1~51 s while TTAB τ_1~23 s. This is because TTAB desorbs faster than CTAB, although the bulk concentrations studied are in the same range. This indicates that the alkyl chain length affects the desorption kinetics, owing to the increasing hydrophobic interactions between the alkyl chains with increasing alkyl chain length.

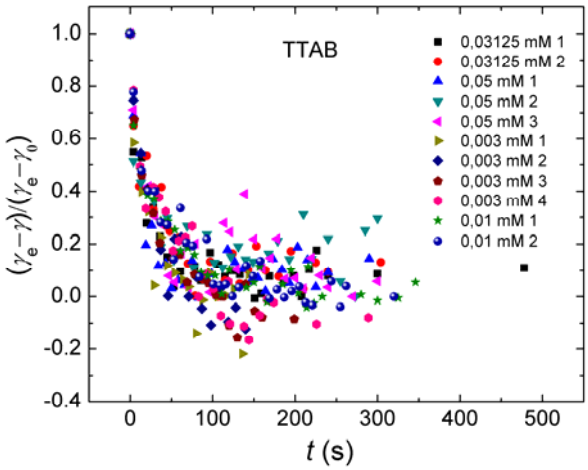

Fig. 5.6 Desorption processes for TTAB with different concentrations in the presence of 100 mM NaBr

5.3.4.2 Effect of counterion type on AOT desorption

It is known that the counterion type has strong effects on the counterion binding degree, therefore affecting the behavior of ionic surfactants in the bulk [129]. Besides, the type of counterion has influence on the interfacial behavior of ionic surfactants due to the effect of counterion type on the surface activity, molecular area, surface viscosity, *etc* [130]. We investigated the influence of the surfactant counterion nature on the desorption process. Anionic surfactant AOT in the presence of various types of counterions (Na^+, K^+, Mg^{2+}) has been studied (Fig. 5.7). Note that due to the short desorption time for AOT, the surface tension data are very scattered, nevertheless it can still be seen that the value of $(\gamma_{eq}-\gamma)/(\gamma_{eq}-\gamma_0)$ does not appear to depend on the nature of counterions or the surfactant concentration. Therefore, we conclude that the counterion type has no obvious effects on the desorption process for the studied system.

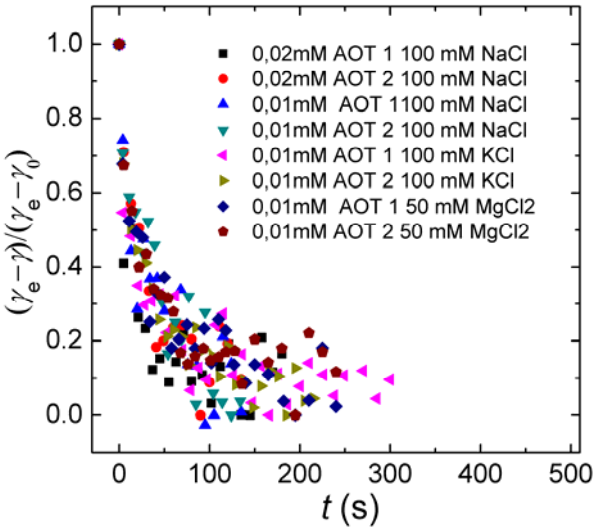

Fig. 5.7 Relaxation processes of AOT with different concentrations in the presence of various types of salts

Note that the characteristic times τ_1 for all the surfactant systems studied in this chapter have been indicated in Fig 5.8. The times are all of the same order of magnitude, between 25 and 55 s. The longest time is for CTAB/100mM NaBr at 55s, longer than all the others. This suggests that it is the length of the alkyl chain that is mainly responsible for the cohesive interaction and for the slowing down of the desorption.

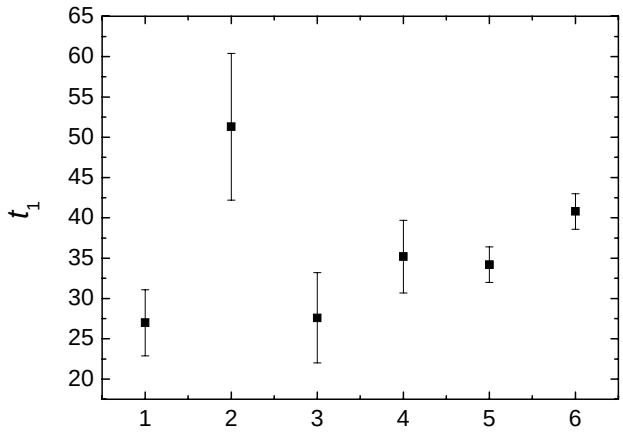

Fig 5.8 Characteristic times for desorption for different surfactant systems, from left to right (1 to 6) are $C_{12}E_6$, CTAB/100 mM NaBr, TTAB/100 mM NaBr, AOT/100 mM NaCl, AOT/100 mM KCl, AOT/50 mM $MgCl_2$ respectively. Each value is based on the measurements for the same surfactant system averaged from measurements at different concentrations.

5.4 Conclusions

In this section, we have studied the desorption process of surfactant molecules from the air-water interface using a bubble compression method. Our studied surfactant systems include non-ionic surfactant $C_{12}E_6$, ionic surfactant CTAB and TTAB in the presence of high concentrations of electrolyte, ionic surfactant AOT in the presence of different types of counterions. By comparing the experimentally derived $\Gamma(t)$ and the calculated $\Gamma(t)$, it has been shown that desorption is not purely diffusion limited. Using a model for the kinetically controlled desorption, we have successfully concluded that desorption is nearly dominated by the transfer of surfactants from the air/water interface onto the subsurface, confirming the presence of a desorption barrier.

Alkyl chain length has been found to affect the desorption kinetics, i.e. TTAB desorbs faster than CTAB at similar concentration range, indicating that the strong mutual interactions between surfactant chains may affect the energy barrier for desorption. We conclude that counterion type has no obvious effects on the desorption process for the studied system.

Having shown that the desorption for the systems studied is not simply diffusion-limited, at present further work is ongoing in order to find out whether the desorption is mixed diffusion-barrier controlled or purely kinetically-limited.

Chapter 6 Adsorption of the gemini surfactant 12-2-12·2Br at the air-water interface

6.1 Introduction

Composed of two hydrophobic chains and two hydrophilic head groups covalently attached through a spacer, gemini surfactants possess superior physicochemical properties including lower *CMC*, greater efficiency in lowering surface or interfacial tension compared with traditional surfactants bearing single head group and single alkyl chain. Therefore, intense attention has been paid to the behaviour of gemini surfactant systems.

As gemini surfactants are ionic surfactants with high charge density [98], the effect of salt influences its bulk and interfacial behavior. Therefore, a number of studies have investigated the effects of salt on the aggregation behavior of gemini surfactants [131-133]. However, there has been much less focus on the effect of electrolyte on the dynamic surface tension of gemini surfactants. Moreover, the adsorption or desorption kinetics of gemini surfactants have been much less studied, compared to the studies on the bulk properties of gemini surfactant systems [98, 131, 134]. Therefore, further study is of particular importance.

In this section, we have investigated the interfacial properties of cationic surfactant dimethylene-1,2-bis (dodecyldimethylammonium bromide) 12-2-12·2Br, similar in structure to two DTAB molecules covalently linked with a spacer, but with superior interfacial properties than DTAB. First, the equilibrium and the kinetic behavior of 12-2-12·2Br in water are studied. Second, the effect of salt concentration on the dynamic surface tensions for the 12-2-12·2Br system has been explored. Third, having studied the adsorption and desorption kinetics for the traditional surfactants in the previous chapters, here we investigate the adsorption and desorption behavior for the 12-2-12·2Br/100 mM NaBr system.

6.2 Procedures

Two types of surfactant systems have been studied, including 12-2-12·2Br in Milli-Q water and 12-2-12·2Br in solutions with different NaBr concentrations. Sodium bromide NaBr was purchased from Sigma Aldrich, France.

Equilibrium surface tensions for 12-2-12·2Br solutions were measured using the method of Wilhelmy plate. Three types of experiments have been performed using the

Tracker with the rising bubble configuration. To measure the dynamic surface tension, we performed experiments with control of constant bubble area. To investigate the adsorption behavior, bubble compression experiments have been performed with control of bubble volume, which decreases at a controlled speed after a period of bubble aging time. To study the desorption behavior, first bubble compression experiments have been performed, and then the time-dependent surface tension are recorded as soon as the bubble compression experiments are stopped.

6.3 Results and discussions

6.3.1 Equilibrium behavior of the 12-2-12·2Br/H_2O system

The equilibrium surface tension vs the surfactant concentration is shown in Figure 6.1. The equilibration is very slow, and the values are taken after several hours of measurements. In order to access the surface concentration from the surface tension measurements, the slope of graph is required. This is why the experimental data were first fitted with the equation

$$\gamma = r_0 + r_1 \times \ln C + r_2 \times (\ln C)^2 + r_3 \times (\ln C)^3 \qquad \text{Equation 6.1}$$

The fitted parameters are shown in Table 6.1. Then Equation 6.2 was used to derive the equilibrium surface concentration Γ_{eq}, and the dependence of equilibrium surface tension γ_{eq} on Γ_{eq} is shown in Fig. 6.2.

$$\Gamma = -\frac{1}{3RT}\frac{d\gamma}{d\ln C} = -\frac{r_1}{3RT} - 2r_2 \times \frac{\ln C}{3RT} - r_3 \times \frac{(\ln C)^2}{RT} \qquad \text{Equation 6.2}$$

The minimum molecule area of 12-2-12·2Br at the air-water interface can be calculated to be 88 Å^2 from the maximum Γ_{eq}, higher than the literature value for the same surfactant (69 Å^2) from surface tension measurements [19], which may be owing to the derived Γ_{eq} value being very sensitive to the $\gamma_{eq}(C)$ curve so that small difference of the curve can cause large difference in the calculated surface concentration. It might also be due to partial condensation of counterions, which would lead to us overestimating the surface area.

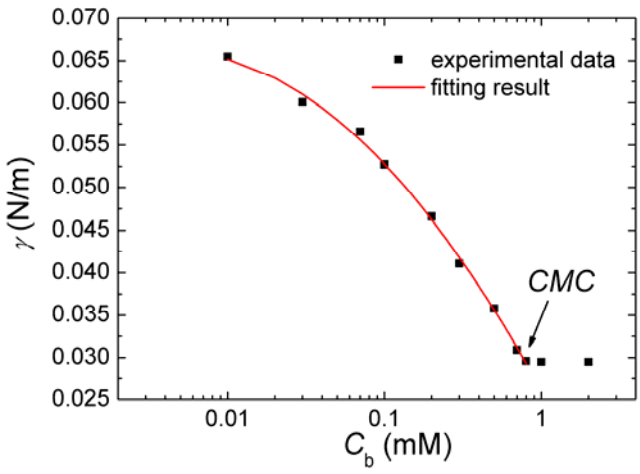

Fig. 6.1 Equilibrium surface tensions as a function of bulk surfactant concentration for 12-2-12·2Br/H_2O solution, compared with the fitting using Equation 6.1.

Table 6.1 Fitting parameters for the data in Fig. 6.1

R=0.99678	Value	Standard Error
r_0	0.02612	5.91042×10^{-4}
r_1	-0.01466	6.41825×10^{-4}
r_2	-0.00134	1.34945×10^{-4}
r_3	4.20222×10^{-18}	-

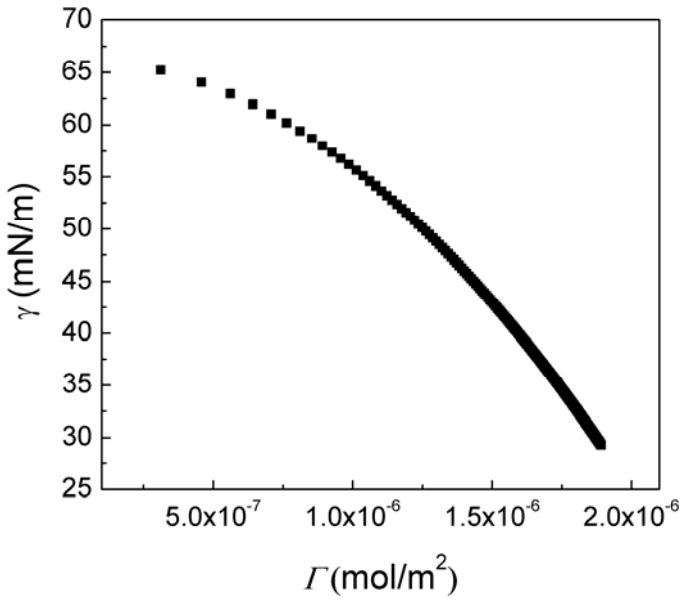

Fig. 6.2 Dependence of equilibrium surface concentration on the bulk surfactant concentration for 12-2-12·2Br/H_2O solutions

The above two figures can provide information about the equilibrium behavior of 12-2-12·2Br, which sets the limit of the adsorption or desorption studied in the following sections.

6.3.2 Adsorption kinetics of the 12-2-12·2Br/H_2O system

The pendant drop method has been used to monitor the dynamic surface tensions for 12-2-12·2Br/H_2O solutions. The time-dependent surface tensions with 12-2-12·2Br concentrations far below *CMC* are presented in Fig. 6.3, while those with 12-2-12·2Br concentrations close to *CMC* are presented in Fig. 6.4.

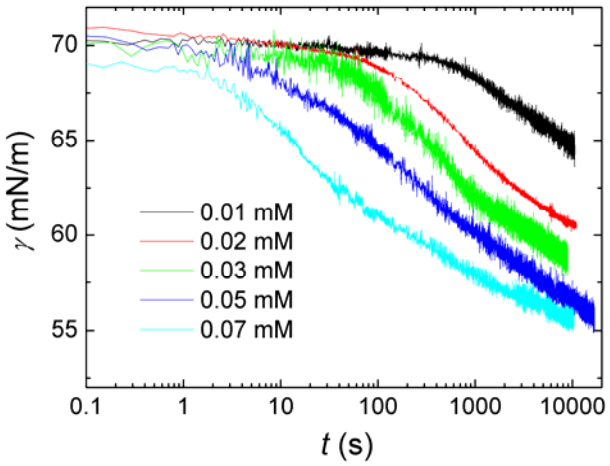

Fig. 6.3 Dynamic surface tensions of 12-2-12·2Br/H_2O solutions, at different concentrations far below *CMC*

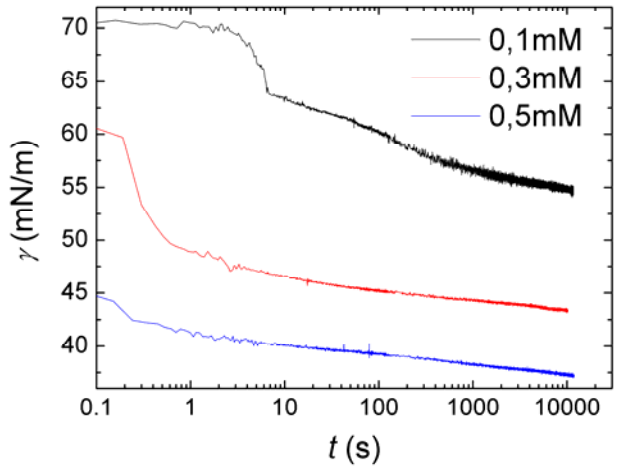

Fig. 6.4 Dynamic surface tensions of 12-2-12·2Br/H_2O solutions, at concentrations close to *CMC*

The surfactant is charged, which is why there exists an energy barrier in the interfacial region, the adsorption is considered to be kinetically limited. Therefore, we have looked at the time-dependent surface tension at longer times using the equation by Andelman *et al*. [15], accounting for the kinetically limited adsorption process.

$$\gamma(t) - \gamma_{eq} \sim e^{-t/\tau_k} \qquad \text{Equation 6.3}$$

Equation 6.3 can be modified as follows:

$$\gamma(t) = \gamma_{eq} + ae^{-t/\tau_k} \qquad \text{Equation 6.4}$$

The fitting results of the time-dependent surface tensions at longer times for 12-2-12·2Br solutions with various concentrations are shown in Fig. 6.5. The fits are good in this case, suggesting that adsorption is kinetically limited at longer times, owing to the presence of the electrostatic adsorption barrier. The derived parameters from the fittings can be seen in Table 6.2. As seen, τ_κ varies from 1700 s to 5400 s for the concentrations studied, although there seems to be no trend for the variation of the characteristic time τ_κ with the surfactant concentration. The τ_κ values are much longer by orders of magnitude than those measured for DTAB adsorption by Ritacco *et al*. [135]. This could be because the dimer has two charged headgroups, and as the interface is charged, the adsorption becomes very slow due to the increased energetic barrier.

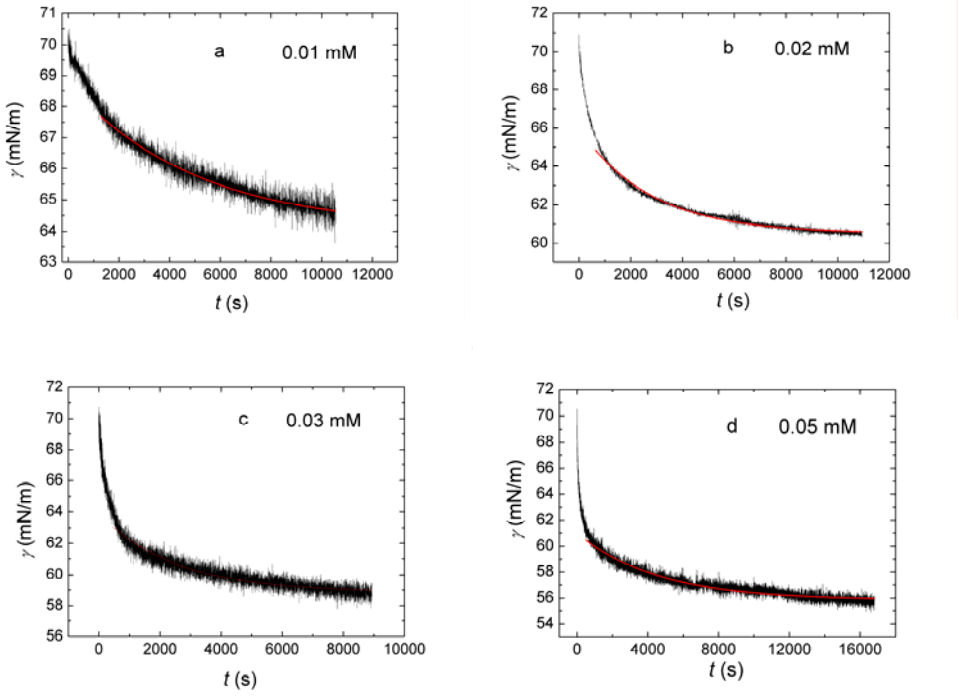

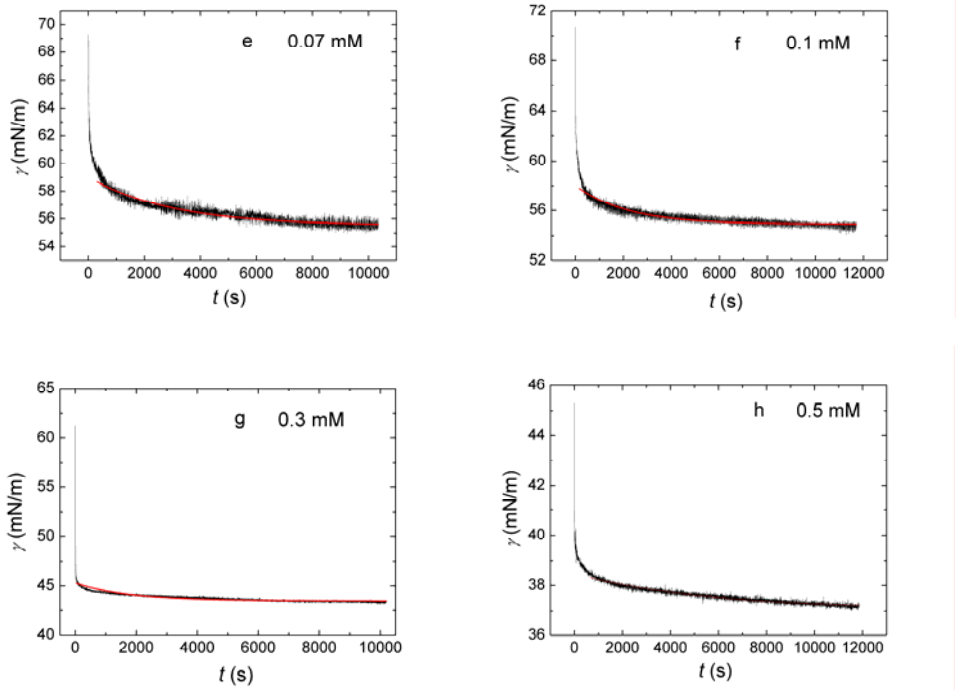

Fig. 6.5 Fitting of the dynamic surface tension data for 12-2-12·2Br solutions with various concentrations using Equation 6.4

Table 6.2 Fitting parameters for the dynamic surface tension data at longer times in Fig. 6.5 using Equation 6.4

C (mM)	γ_{eq} (mN/m)	τ_{κ} (s)	a (mN/m)
0.01	64.1	4890	4.7
0.02	60.5	2720	5.5
0.03	58.8	2540	5.0
0.05	55.9	4500	5.2
0.07	55.5	2940	3.5
0.1	54.9	2140	3.1
0.3	43.5	1760	1.4
0.5	37.1	5380	1.4

6.3.3 Effect of NaBr on dynamic surface tensions for 12-2-12·2Br solutions

As mentioned previously, the adsorption kinetics of 12-2-12·2Br/H_2O system is complicated due to the presence of the electrostatic interactions between the surfactant molecules. Here we introduce salt (NaBr) into the system to see how the addition of electrolyte affects the adsorption kinetics. Fig. 6.6 shows dynamic surface

tension for 0.005 mM 12-2-12·2Br solutions in the absence and presence of 100 mM NaBr. As shown, $\gamma(t)$ decreases continuously even for very long times (10000 s) in the absence of electrolyte. However, for the system with electrolyte, the surface tension reaches equilibrium much more quickly (around 2000 s) after a steep decrease. Note that in both cases in Fig. 6.6, there exists a similar lag time before the surface tension starts to decrease significantly (τ, 520 s-560 s).

Dynamic surface tensions of more concentrated 12-2-12·2Br solutions (0.01 mM) with increasing NaBr concentration were also measured, as shown in Fig. 6.7, again showing a similar lag time τ (110-150 s) for the different NaBr concentrations. This indicates that the presence of electrolyte has no obvious effect on the adsorption kinetics at times shorter than τ. At times longer than τ, the interfacial coverage is sufficiently high, so that the effect of electrostatic barrier becomes obvious.

Dynamic surface tension of still more concentrated 12-2-12·2Br solutions (0.05 mM) with increasing NaBr concentration are shown in Fig. 6.8. As shown, the lag times τ are shorter in this case. When the added NaBr concentration is below 5 mM, similar τ (1.9-2.3 s) was observed for all the systems studied. However, when NaBr concentration is sufficiently high, τ significantly increases (around 10 s and 20 s for 50 mM and 100 mM NaBr respectively). The addition of more salt decreases the adsorption barrier, which should facilitate the adsorption, but the inverse is observed. This is probably because the addition of high concentrations of NaBr decreases the *CMC* strongly. This means that there are fewer monomers and the adsorption is controlled by micellar diffusion, which is slower.

If we assume that at times shorter than the lag time τ the adsorption is diffusion-limited (the surface concentration is still sufficiently low so that the electrostatic barrier is negligible), we expect that at short times:

$$\Gamma_{critical} = 2C\sqrt{\frac{D\tau}{\pi}} \qquad \text{Equation 6.5}$$

In Equation 6.5, Γ_{critical} is the surface concentration at the lag time τ. This means that the strong change in the surface tension begins after Γ_{critical} is attained, implying that at this point the interaction between the surfactants becomes important. Assuming that Γ_{critical} is constant as C changes, from Equation 6.5 it follows that:

$$\log(\tau) \propto \log C^{-2} \qquad \text{Equation 6.6}$$

The experimental lag time τ vs the bulk concentration C is plotted in Fig. 6.9, showing a nice agreement with a power law of -2. This suggests that at times shorter

than the lag time τ, the adsorption is diffusive. In the case of 0.05 mM 12-2-12·2Br solutions with 50 or 100 mM NaBr, τ doesn't meet with the trend line in Fig. 6.9, which may be owing to the micellization of 12-2-12·2Br molecules in the system, which changes the adsorption process.

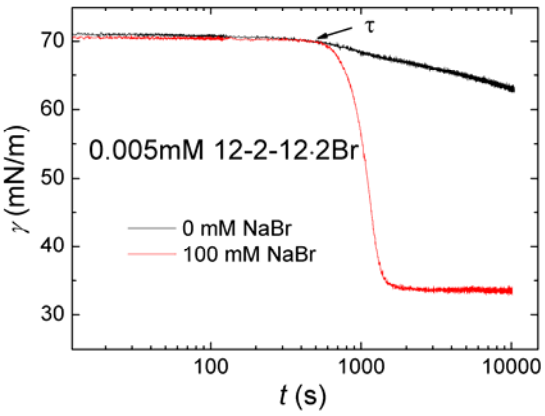

Fig. 6.6 Dynamic surface tensions of 0.005 mM 12-2-12·2Br solution in the absence and presence of 100 mM NaBr

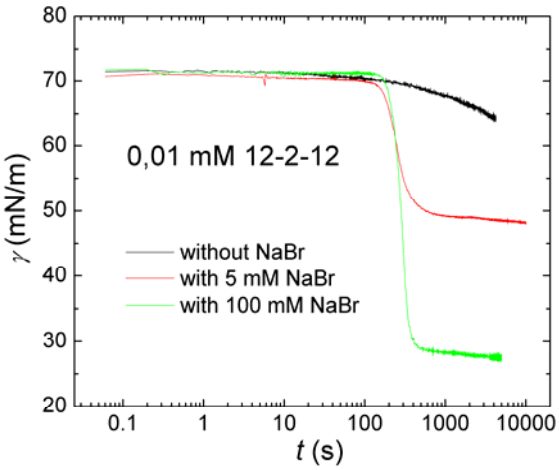

Fig. 6.7 Dynamic surface tensions of 0.01 mM 12-2-12·2Br solution with increasing concentrations of NaBr

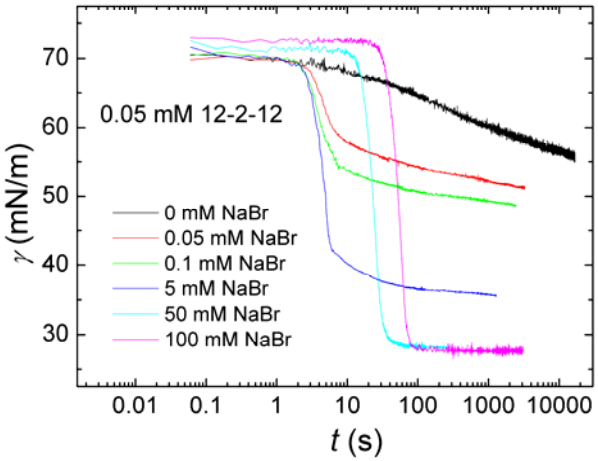

Fig. 6.8 Dynamic surface tension of 0.05 mM 12-2-12·2Br with increasing concentrations of NaBr

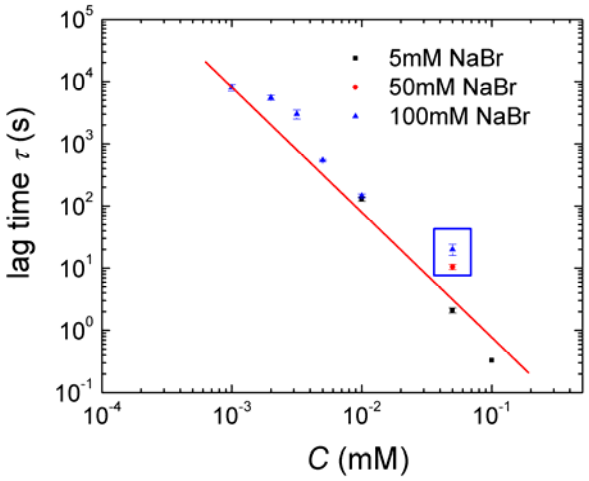

Fig. 6.9 Lag time τ as a function of the bulk surfactant concentration in the presence of different concentrations of NaBr. The red line is a guide line showing a power law behavior.

6.3.4 Interfacial behavior of 12-2-12·2Br solutions in the presence of 100 mM NaBr

In the following, we focus on the system of 12-2-12·2Br solutions in the presence of 100mM NaBr, in which the electrostatic interactions between the surfactant headgroups are largely screened by the added salt. In the 12-2-12·2Br /100 mM NaBr system, the equilibrium behavior of the system, the adsorption kinetics and desorption kinetics of surfactant molecules have been studied.

6.3.4.1 Equilibrium behavior for 12-2-12·2Br/100 mM NaBr system

The equilibrium surface tension values are taken at the longer time limits in the time-dependent measurements of surface tension. According to the Gibbs adsorption equation, the dependence of equilibrium surface tension on the surfactant concentration can provide information about the amount adsorbed at the interface at equilibrium. Note that it is time-consuming to measure the equilibrium surface tension at the low surfactant concentration range for this system; for example, it takes almost one day for the surface tension of 0.001 mM 12-2-12·2Br solution to reach a constant value (Fig. 6.10).

Fig. 6.11(a) shows the equilibrium surface tensions of 12-2-12·2Br in 100 mM NaBr solution as a function of surfactant concentration $\gamma(C)$: the surface tension γ first decreases relatively slowly and then a region of rapid decrease appears before reaching the *CMC* (≈0.0063mM). At such a high concentration of electrolyte, the Gibbs adsorption equation is the same as that for non-ionic surfactant ($-d\gamma = RT\Gamma d\ln C$). The most common (although not the most accurate) way to treat the data is to fit only the rapidly changing part in the $\gamma(C)$ curve. Therefore, we fitted the part with rapidly decreasing surface tension using the following:

$$\gamma = a_0 + a_1 \ln C \qquad \text{Equation 6.7}$$

The fitting result for the rapidly changing part using Equation 6.7 can be seen in Fig. 6.11(a), from which we have calculated the average surface excess Γ_{average} for this region to be 5.93×10^{-6} mol m^{-2} with an error of 3.2×10^{-7} mol m^{-2}.

An alternative and more accurate method was also utilized to analyze the equilibrium surface tension data, where the whole $\gamma(C)$ curve before *CMC* was fitted with Equation 6.8, and the fitting result has been shown in Fig. 6.11(b).

$$\gamma = a_0 + a_1 \ln C + a_2 (\ln C)^2 \qquad \text{Equation 6.8}$$

From the fit in Fig. 6.11(b) we have access to the dependence of Γ with C using the Gibbs adsorption isotherm, and the results are shown in Fig. 6.11(c). Γ increases linearly with the logarithm of the surfactant concentration up to *CMC* with a limiting value of about 7.08×10^{-6} mol m^{-2} with an error of 6.5×10^{-7} mol m^{-2}. Note that the two methods in Fig. 6.11 (a) and (b) are very different, as the first gives constant surface concentration values while the second provides the changing surface concentration depending on the bulk concentration.

It should be noted here that the surface area of the 12-2-12·2Br molecule is calculated to be 0.28 nm^2 ± 0.02 nm^2 from $\Gamma_{\text{average}}=5.93\times10^{-6}$ mol/m^2 ± 3.2×10^{-7} mol/m^2 using Equation 6.7, and is calculated to be 0.24 nm^2 ± 0.03 nm^2 from Γ_{CMC}

=7.08×10^{-6} mol/m^2 ± 6.5×10^{-7} mol/m^2 using Equation 6.8, and these values are much lower than the surface area of the 12-2-12·2Br molecule in the absence of salt (0. 88 nm^2). The surface area per molecule seems surprisingly small and indeed too small to be realistic. This might be because although the NaBr concentration is high (100 mM) we might not have complete counterion condensation. If this is the case we cannot use Equation 2.26, where complete condensation is assumed. This means that there would be a factor between 1 and 3 to take this into account. Therefore, the true surface concentration value could be lower than measured here.

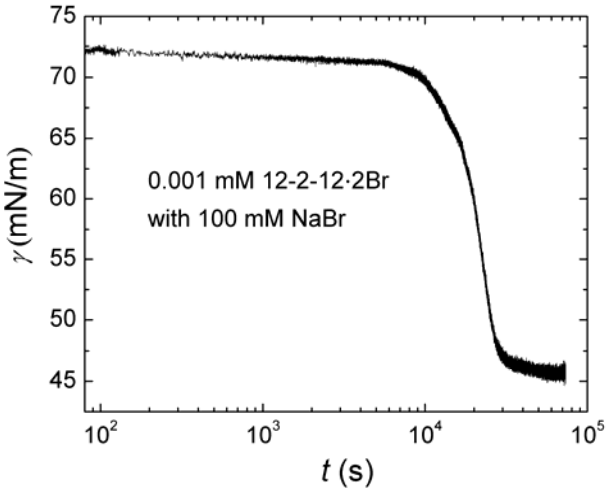

Fig. 6.10 Dynamic surface tension of 0.001 mM 12-2-12·2Br solution in the presence of 100 mM NaBr

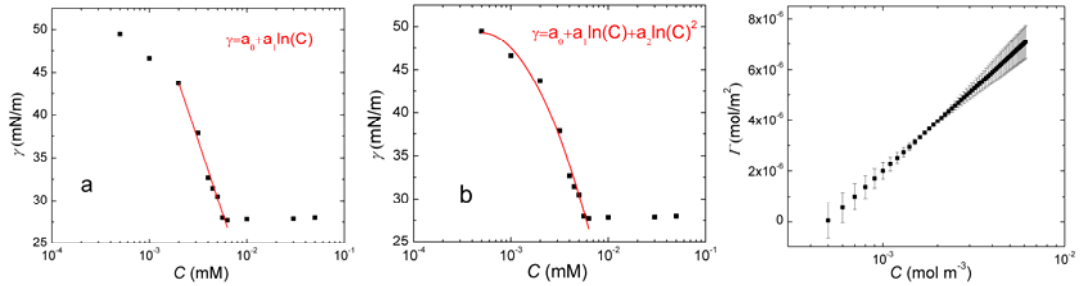

Fig. 6.11 Equilibrium surface tension of 12-2-12·2Br in 100mM NaBr solution as a function of surfactant bulk concentration, fitted with the Equation 6.7 (a) and fitted with Equation 6.8 (b); dependence of surface concentration on the surfactant bulk concentration (c).

Compression and expansion experiments have been performed in order to obtain the equation of state for the 12-2-12·2Br system in the presence of 100 mM NaBr for the whole range of surface concentrations. During the compression experiment, the area of the bubble is forced to decrease after a controlled period of time since the bubble creation, and the relation γ vs Γ/Γ_{eq} can be recorded correspondingly. Details

of the compression method can be found in Chapter 4. Different compression speeds are chosen and a unique dependence of γ on Γ/Γ_{eq} is observed, as shown in Fig. 6.12.

For the expansion experiments, a bubble with a small size is initially formed and sufficient time was utilized to ensure that the interface reached equilibrium. Then the area of the bubble is rapidly increased at a certain speed and the relation γ vs Γ/Γ_{eq} can be recorded during the bubble expansion period. The data for expansion are also shown in Fig. 6.12. A unique dependence of γ on Γ/Γ_{eq} can be found from either the bubble compression or expansion experiments. That is to say, the equation of state can be obtained with these methods. Normalized by the $\Gamma_{average}$ $=5.93\times10^{-6}$ mol m^{-2} obtained from the above analysis, we get the dependence of γ on Γ, as shown in Fig. 6.13.

The equation of state for the 12-2-12·2Br/100mM NaBr system is compared with that for the previously studied CTAB/100mM NaBr system, and the result is shown in Fig. 6.13. Without added salt the two surfactants have similar surface properties and according to the literature, the surface concentration for CTAB/H_2O at the air/water interface is around 3×10^{-6} mol/m^2 and close to that of the 12-2-12·2Br/H_2O system (about 2.4×10^{-6} mol/m^2 in the literature [19] and 2×10^{-6} mol/m^2 in our case), while the *CMC* values of the two systems are also close (0.93 mM for CTAB/H_2O [51] and 0.8 mM for 12-2-12·2Br/H_2O). However, in the presence of 100 mM NaBr, 12-2-12·2Br has a higher surface concentration than CTAB for the same surface tension value as shown in Fig. 6.13. Moreover, the *CMC* of 12-2-12·2Br in the presence of 100 mM NaBr (0.006 mM) is much smaller than that of CTAB (0.03 mM) [51]. The sensitivity of the gemini surfactant 12-2-12·2Br to salt could be due to its peculiar molecular structure. For the conventional surfactant CTAB, the distance between the headgroups is larger than 0.7 nm [136]. For gemini surfactants 12-O-12·2Br with short spacers (less than 6 carbons), as in our case, the length of the spacer d*s* [136]) is: d*s*/(nm)=0.1265(O+1), where O is the number of carbon atoms of the spacer. For O=2, d*s*=0.38 nm and is much smaller than that for CTAB. The charge density of 12-2-12·2Br is higher than CTAB and therefore 12-2-12·2Br is more sensitive to NaBr.

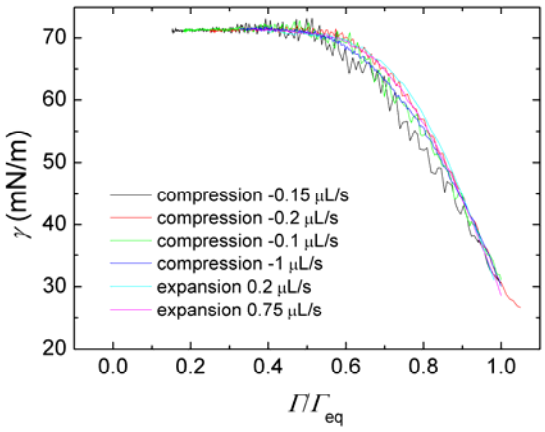

Fig. 6.12 Dependence of surface tension on the surface concentration by the compression or expansion method at different speeds. The surface concentration is calibrated by the $\Gamma_{average}$ value from Fig. 6.11(a)

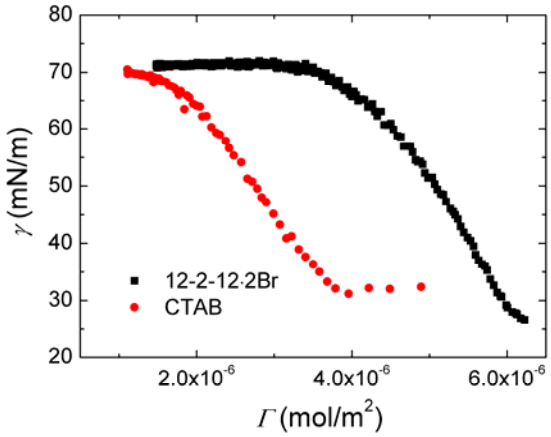

Fig. 6.13 Comparison of equations of state for the 12-2-12·2Br/100 mM NaBr system and CTAB/100 mM NaBr system

6.3.4.2 Adsorption kinetics for 12-2-12·2Br/100mM NaBr system

The adsorption kinetics has been studied using the bubble compression method. Normally the classical Ward-Tordai equation can be used to describe the $\Gamma(t)$ for the diffusion-limited adsorption. At short times, assuming that there is no desorption, we have the Equation 6.9 to describe the adsorption kinetics.

$$\frac{\Gamma(\mathrm{t})}{\Gamma_{\mathrm{eq}}} = 2\sqrt{\frac{D}{\pi}}\frac{C}{\Gamma_{\mathrm{eq}}}\sqrt{t} = 2\sqrt{\frac{D}{\pi}}K \qquad \text{Equation 6.9}$$

The normalized surface concentration Γ derived from the bubble compression experiments is plotted as a function of the square root of the time in Fig. 6.14: Γ is

linear vs $\sqrt{t}$, compatible with the diffusion-limited adsorption kinetics at short times. The simplified Ward-Tordai equation also allows the determination of the value of the diffusion constant, found equal to 4.19×10^{-10} m^2/s and close to the literature value (3.28×10^{-10} m^2 s^{-1}, from NMR measurements) [137]. This confirms that surfactant adsorption is diffusion-limited at short times. We have then estimated the surface concentration corresponding to the lag time τ (Fig. 6.10) using the simplified Ward-Tordai equation and the obtained value of D. For example, for 0.005 mM 12-2-12·2Br, the surface concentration at τ (520-560 s) is estimated to be $2.63\sim2.73\times10^{-6}$ mol/m^2. That is to say, almost 50% of the interface has already been covered by the 12-2-12·2Br molecules before the significant decrease of the surface tension starts.

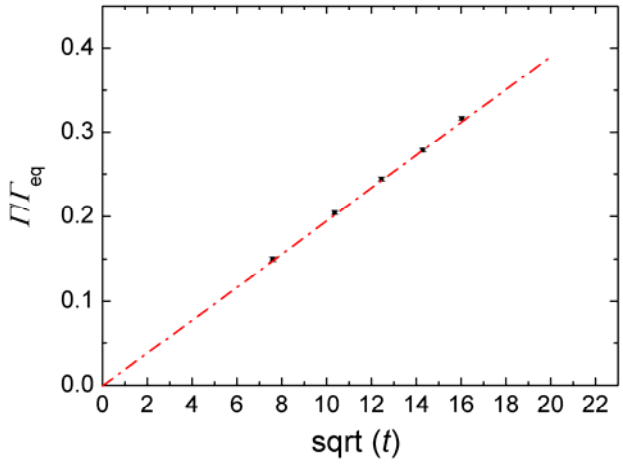

Fig. 6.14 Normalized surface concentration as a function of the square root of the bubble aging time t for 0.005 mM 12-2-12·2Br in the presence of 100 mM NaBr

6.3.4.3 Desorption kinetics for 12-2-12·2Br/100mM NaBr system

To investigate the desorption kinetics for the 12-2-12·2Br/100mM NaBr system, we have measured the time-dependent surface tension with various surfactant bulk concentrations, as indicated in Fig. 6.15. Different measurements with various initial surface tensions for the same surfactant solution have been performed. It can be seen that during the desorption process, the surface tension first increases rapidly and then gradually reaches a stable value, similar to the experimental results for other surfactant systems studied in Chapter 5. The initial surface tensions, equilibrium surface tensions for the surfactant bulk concentrations studied in Fig. 6.15 are shown Table 6.3.

As done for the other surfactants studied we expect that the desorption will be kinetically limited. Following the previous analysis, we normalized the surface tension data using the initial surface tensions as well as the equilibrium surface tensions, and then fitted the normalized surface tensions by the exponential function. The normalized surface tension data are shown in Fig. 6.16. Table 6.4 presents the derived fitting parameters from Equation 6.10. The results show that the characteristic times are between 45 s and 62 s.

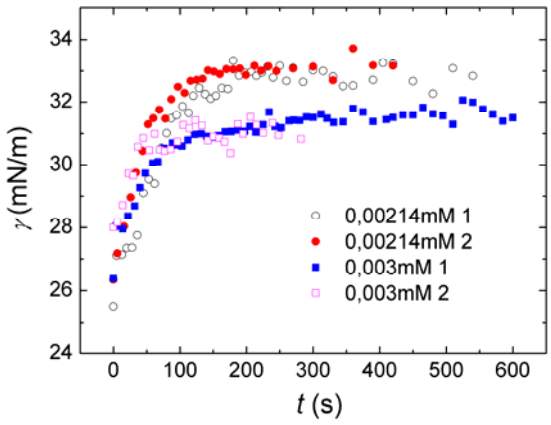

Fig. 6.15 Dependence of surface tension on the time during the desorption process for 12-2-12·2Br systems with different surfactant bulk concentrations

Table 6.3 Initial surface tension, equilibrium surface tension for 12-2-12·2Br/100 mM NaBr systems with various 12-2-12·2Br concentrations

C (mM)	γ_0 (mNm^{-1})	γ_{eq} (mNm^{-1})
0.00214 1	25.5	32.9
0.00214 2	26.4	33.1
0.003 1	26.4	31.6
0.003 2	28.0	31.6

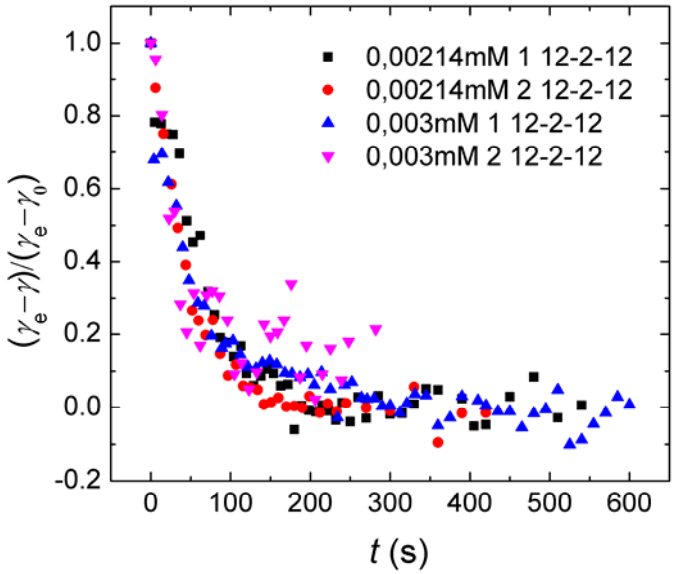

Fig. 6.16 Dependence of normalized surface tension on the time during the desorption process for 12-2-12·2Br systems with different surfactant bulk concentrations, and the line is the fitting of the normalized surface tension data using $\frac{\gamma_{eq}-\gamma}{\gamma_{eq}-\gamma_0}=e^{-kt}$

Table 6.4 Fitting parameters for the 12-2-12·2Br/100 mM NaBr system using Equation 6.10

C(mM)	k (s^{-1})	τ_1 (s)
0.00214 1	0.016	62
0.00214 2	0.022	45.4
0.003 1	0.019	52.5
0.003 2	0.032	53.4

6.4 Conclusions

The equilibrium behavior and kinetic behavior of 12-2-12·2Br/H_2O system have been studied. The relations of equilibrium surface tension as a function of bulk concentration have been recorded by Wilhelmy plate, and the variations of equilibrium surface concentration as a function of surfactant bulk concentration have been calculated using Gibbs adsorption equation. The time-dependent surface tensions have been recorded by the use of pendant drop and fitted using kinetically limited adsorption model. It has been shown that there exists an electrostatic barrier during the adsorption process of 12-2-12·2Br molecules.

Second, we investigated the effect of NaBr concentration on the dynamic surface

tensions for the 12-2-12·2Br system. Addition of NaBr has no obvious influence on the adsorption kinetics at times shorter than the lag time, corresponding to the slow decrease of surface tension. It has been shown that at times shorter than the lag time, the adsorption is diffusive.

Third, for the 12-2-12·2Br/100mM NaBr system, we have calculated the equation of state using both bubble compression and expansion methods. Compared with traditional surfactant CTAB, 12-2-12·2Br has higher charge density and is more sensitive to the presence of NaBr although the result suggests that complete counterion condensation is not achieved. The adsorption of 12-2-12·2Br is proven to be diffusion-limited at short times with the calculated diffusion constant compatible to the literature value. The coverage of surfactant molecules corresponding to the induction time has also been determined, close to 50 %. The desorption process of 12-2-12·2Br is also investigated. The desorption is barrier limited, and the characteristic times are comparable to those found for CTAB with 100 mM NaBr.

Chapter 7 Micellization of cationic gemini surfactant and its interactions with DNA in the bulk

7.1 Introduction

The micellization of gemini surfactants in aqueous solutions and the corresponding thermodynamic parameters have been widely studied for the past decades [138-141]. It has been found that the micellization of gemini surfactants depends on many factors, including temperature [142], the nonpolar chain [143], additives [144] *etc*. In the case of ionic gemini surfactant, the presence of electrolyte can highly influence the electrostatic interactions between the charged headgroups and therefore affect the micellization process of gemini surfactant. The spacer length is also considered to have an influence on the critical micelle concentration *CMC*, micelle ionization degree, thermodynamics of micelle formation and phase behavior [100, 145].

Due to their unique physicochemical properties, cationic gemini surfactants are considered to be potential candidates as gene delivery vectors [88, 102]. Rationally designed cationic gemini surfactants displayed high DNA binding ability, low cytotoxicity and enhanced transfection ability [20, 78, 93, 101]. Several aspects of the interactions between the mixed system of DNA and gemini surfactants have been studied such as the complexation process [72, 86], phase behavior and morphologies of the complexes [146]. The interactions between DNA and cationic gemini surfactants are also dependent on several factors, including the environmental conditions (additives, pH, temperature *etc*.) and the molecular structure of the cationic gemini surfactant (spacer length *etc*.).

In this chapter, the micellization of cationic gemini surfactant 12-3-12·2Br without DNA was first investigated, and the influences of ionic strength and temperature on the micellization of 12-3-12·2Br are studied. Second, the interaction mechanism in the mixed system of 12-3-12·2Br and DNA has been studied using multiple techniques, and the effects of ionic strength, temperature and DNA concentration on the interactions have been examined. Finally, the effect of spacer length on the micellization of cationic gemini surfactant 12-O-12·2Br has been studied with three different spacer lengths O = 3, 4 and 6. The effect of spacer length on the interactions between 12-O-12·2Br and DNA has also been investigated. These experiments have led to a more comprehensive understanding of the studied system,

especially from a quantitative, thermodynamic point of view, thereby providing more fundamental information for the potential biological and biomedical applications.

7.2 Procedures

Cationic gemini surfactant 12-3-12·2Br was synthesized in the lab and salmon sperm DNA was commercially available. 10 mM NaBr aqueous solution was used as solvent in almost all the samples except when studying specifically the effect of electrolyte concentration on 12-3-12·2Br micellization and DNA/12-3-12·2Br interaction. Stock solutions of DNA and 12-3-12·2Br were separately prepared and then mixed at different molar ratios to obtain the required DNA/12-3-12·2Br samples. The samples were kept overnight at 298.15 K to reach equilibrium before measurements.

For the calorimetric measurements, the sample cell was initially loaded with NaBr solution or DNA solution and the concentrated 12-3-12·2Br solution (2.5 mM) was injected into the stirred sample cell in 15-31 portions of 1-10 μL. The enthalpy change caused by DNA dilution was measured under the same circumstances by titrating NaBr solution into DNA solution, which was found to be negilible.

The details for the conductivity, AFM, UV-Vis transmittance, particle size, zeta potential and micropolarity measurements can be seen in Chapter 3.

7.3 Results and Discussion

7.3.1 Micellization of cationic gemini surfactant 12-3-12·2Br

The micellization of surfactants can be influenced by many factors, including the properties of surfactant and the conditions of the bulk solution (ionic strength, temperature, pH, *etc*). In this section, the conductivity and microcalorimetric measurements were performed to study the effects of ionic strength and temperature on the micellization of cationic gemini surfactant 12-3-12·2Br.

7.3.1.1 Effect of ionic strength

Fig. 7.1 shows the dependence of the electrical conductivity (κ) of 12-3-12·2Br in brine on the surfactant concentration (C) at 298.15 K. As shown, κ increases more slowly with the increase of C until a critical surfactant concentration, corresponding to the *CMC*, where the slope changes. The value of *CMC* was determined by the intersection of two linear plots of the $\kappa(C)$ curve, as shown in Fig. 7.1. The degree of

ionization of the micelles α, is the ratio of the values of dκ/dC above and below the *CMC*. The degree of counterion association to micelle β was obtained by the relationship β=1-α. Table 7.1 gives the measured values for both *CMC* and β for 12-3-12·2Br systems with various concentrations of NaBr.

As shown in Table 7.1, the *CMC* decreases with NaBr concentration (C_{NaBr}), however β increases with C_{NaBr}. The addition of NaBr may enhance the binding of the counterion at the micellar surface and also decrease the electrostatic repulsion between the headgroups of the surfactant molecules. Accordingly, the tendency to aggregate has been strengthened with a decreased *CMC*, and β is increased due to the stronger counterion binding [147]. However, even with 50 mM of added NaBr full counterion condensation is not achieved.

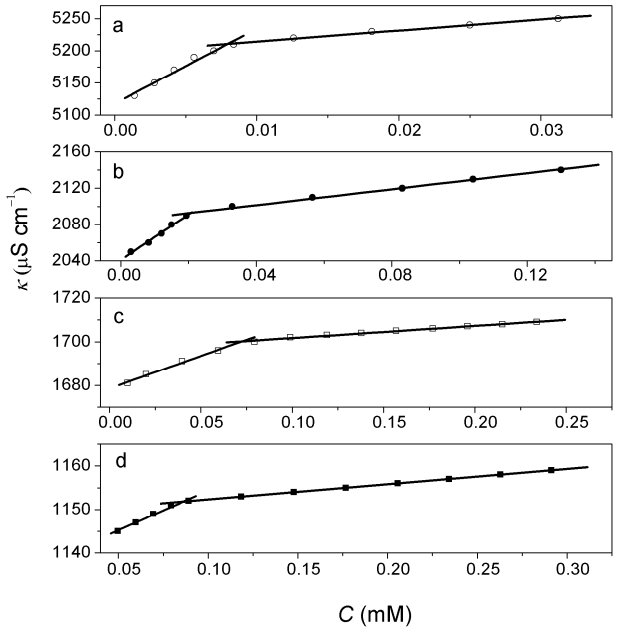

Fig. 7.1 Dependence of conductivity (κ) on the 12-3-12·2Br concentration with various NaBr concentrations: (a) 50 mM; (b) 20mM; (c) 15 mM; (d) 10 mM at 298.15 K

Table 7.1 Critical micelle concentration (*CMC*), the degree of counter-ion association to micelle (β) for the 12-3-12·2Br brine with different NaBr concentrations at 298.15 K using electrical conductivity

C_{NaBr} (mM)	*CMC* (mM)	β
10	0.086	0.810
15	0.070	0.815
20	0.020	0.825
50	0.008	0.853

We have also performed isothermal calorimetric titration measurements at 298.15 K, from which $\Delta H_{obs}(C)$ has been recorded (Fig. 7.2). In Fig. 7.2, ΔH_{obs} denotes the observed enthalpy change corresponding to one mole of 12-3-12·2Br molecules, and C is the surfactant concentration in the sample cell. As shown, the curves for 12-3-12·2Br systems with various NaBr concentrations are all sigmoidal in shape, and each curve can be divided into two concentration regions separated by a transitional concentration associated with micelle formation, namely *CMC*. When C is below the *CMC*, the enthalpy change ΔH_{obs} results from both the breakup of the added micelles and the further dilution of the monomer solution. When C has just passed the *CMC*, some of the added micelles break up into monomers and the rest are only diluted, therefore ΔH_{obs} comes from the breakup of some micelles and the dilution of the remaining micelles and the monomers. When C is much above *CMC*, ΔH_{obs} derives only from the dilution of the added micelles, and is close to zero. The *CMC* values can be obtained from the intersection of the linear extrapolations of the two sections of the curves [148, 149], and agree well with those results obtained from the conductivity measurements. The enthalpy change of micellization (ΔH_{mic}) can be determined by the difference of ΔH_{obs} corresponding to two regionss of the plot [149], as shown in the insert of Fig. 7.2.

In Table 7.2, the measured *CMC* values and thermodynamic parameters (ΔH_{mic}, ΔG_{mic} and $T\Delta S_{mic}$) for 12-3-12·2Br solutions with various concentrations of NaBr are listed. The Gibbs free energy change of micellization (ΔG_{mic}) is calculated based on the values of β and *CMC* according to a standard procedure in the literature [41, 150]. Once ΔG_{mic} is determined, the entropy change of micellization (ΔS_{mic}) can be readily calculated by the classical Gibbs energy relationship, $\Delta G_{mic}=\Delta H_{mic}-T\Delta S_{mic}$. As shown in Table 7.2, the values of ΔH_{mic} are negative for all the experiments, indicating that the formation of 12-3-12·2Br micelles is an exothermic process. $T\Delta S_{mic}$ contributes much more to ΔG_{mic} than ΔH_{mic}, suggesting that the micellization process of 12-3-12·2Br is entropically driven, and this effect can be enhanced with increasing NaBr concentration. The negative values of ΔG_{mic} show that the micellization process is thermodynamically favored, and the C_{NaBr} dependence of ΔG_{mic} suggests that the thermodynamic favorability of micellization is strengthened with increasing addition of NaBr.

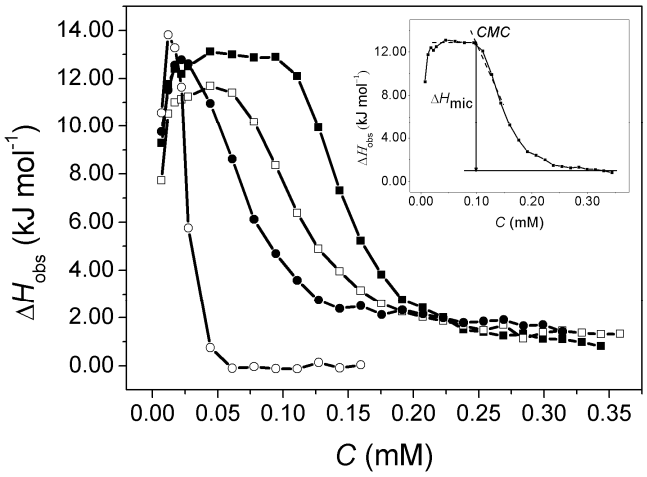

Fig. 7.2 Calorimetric titration curves of 12-3-12·2Br into solutions with various NaBr concentrations: 10 mM (■); 15 mM (□); 20 mM (●); 50 mM (○) at 298.15 K. The insert is the illustration of determination of the *CMC* and ΔH_{mic} from the calorimetric titration curve of 12-3-12·2Br into 10 mM NaBr solution at 298.15 K

Table 7.2 *CMC* and thermodynamic parameters for the 12-3-12·2Br brine with different NaBr concentrations at 298.15 K using calorimetric measurements

C_{NaBr} (mM)	*CMC* (mM)	ΔH_{mic} (kJ/mol)	ΔG_{mic} [a] (kJ/mol)	$T\Delta S_{mic}$ [b] (kJ/mol)
10	0.098	-11.78	-57.17	45.39
15	0.061	-10.32	-60.47	50.15
20	0.027	-10.87	-66.27	55.40
50	0.011	-13.68	-73.66	59.98

[a] Calculated using $\Delta G_{mic}=RT(1+2\beta)\ln(2CMC)$-RTln2 [41, 150]

[b] Calculated from $T\Delta S_{mic}=\Delta H_{mic}-\Delta G_{mic}$

7.3.1.2 Effect of temperature

We have performed the microcalorimetic measurements for 12-3-12·2Br solutions in the presence of 10 mM NaBr at different temperatures to investigate the effect of temperature on the micellization process of 12-3-12·2Br. Fig. 7.3 presents the calorimetric titration curves of 12-3-12·2Br into 10 mM NaBr solutions at temperatures of 298.15 K, 303.15 K and 308.15 K. Table 7.3 presents the *CMC* values and thermodynamic parameters (ΔH_{mic}, ΔG_{mic} and $T\Delta S_{mic}$) for 12-3-12·2Br solutions at fixed NaBr concentration but different temperatures.

As shown in Table 7.3, the *CMC* increases slightly with temperature. It is

considered that increase in the *CMC* is due to the collapse of the structured water surrounding the hydrophobic groups by the temperature increase, which hinders the micellization process [151]. On the other hand, the degree of hydration of the ionic head groups decreases with increasing temperature, which favors the micellization process. The two opposing effects of temperature finally lead to the *CMC* depending only weakly on temperature.

The values of ΔH_{mic}, ΔS_{mic} and ΔG_{mic} at various temperatures were obtained using the same method mentioned above. As shown in Table 7.3, ΔH_{mic} becomes more negative with increasing temperature. Two major competing factors may influence ΔH_{mic} when increasing temperature: a positive contribution is the release of the structured water from the alkyl chains and the hydration layer around the hydrophilic domain, and a negative contribution is the transfer of the chains into the micelle and the restoration of the hydrogen bonding structure of water around the micelles [151, 152]. As the collapse of the structured water occurs with increasing temperature, less energy is needed to destroy the ordered water structures [151, 152], which means that the positive contribution becomes less important. As a result, ΔH_{mic} of 12-3-12·2Br becomes more negative with increasing temperature. ΔS_{mic} is positive over the whole temperature range measured and decreases with temperature. The water structure become less ordered with the temperature increase and thus leads to the decrease of the entropy change. In all cases $T\Delta S_{mic} > -\Delta H_{mic}$, showing that the entropy is the principle driving force towards micellization in all the circumstances investigated here, which results from the collapse of the ordered water structures in the hydrophobic domain [151].

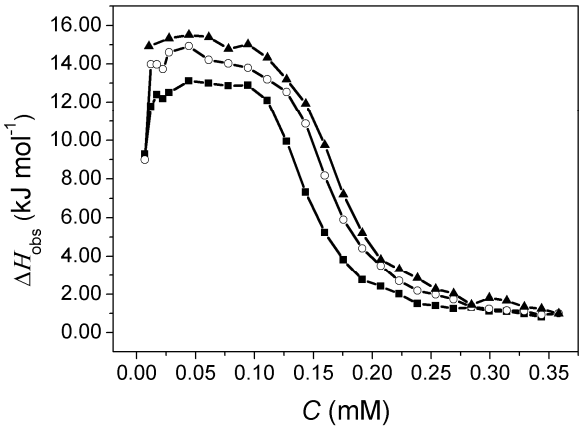

Fig. 7.3 Calorimetric titration curves of 12-3-12·2Br into 10 mM NaBr solution at various temperatures: 298.15 K (■); 303.15 K (○); 308.15 K (▲)

Table 7.3 Critical micelle concentration and thermodynamic parameters for the 12-3-12·2Br brine at various temperatures in 10 mM NaBr solution from calorimetric measurements

T (K)	CMC (mM)	ΔH_{mic} (kJ/mol)	ΔG_{mic} (kJ/mol)	$T\Delta S_{mic}$ (kJ/mol)
298.15	0.098	-11.78	-57.17	45.39
303.15	0.111	-13.04	-57.30	44.26
308.15	0.115	-13.78	-58.01	44.23

7.3.2 Interactions between DNA and 12-3-12·2Br

In this section, our focus is the interactions between DNA and 12-3-12·2Br, which are studied using several techniques. Fig. 7.4(a) presents the surfactant concentration (C) dependence of transmittance of DNA/12-3-12·2Br solutions in the presence of 10 mM NaBr at the wavelength of 450 nm (T^{450}). Fig. 7.4(b) shows two titration curves of the variations of the observed enthalpy change (ΔH_{obs}) with the surfactant concentration (C) at 298.15 K. In Fig. 7.4(b), one curve denotes the dilution of the concentrated 12-3-12·2Br brine into 0.10 mM DNA solution in the presence of 10 mM NaBr, while the other represents the dilution of the concentrated 12-3-12·2Br brine into 10 mM NaBr solution.

As shown in Fig. 7.4(b), in the presence of DNA, the dependence of ΔH_{obs} on 12-3-12·2Br concentration is different from that observed in the absence of DNA. This can be attributed to the strong interactions between DNA and 12-3-12·2Br. When C increases, a sharp endothermic peak is observed in the concentration region of 0~0.027 mM and then the enthalpy change gradually increases to a plateau value, and finally it decreases to a relatively low value. The large endothermic deviation between the two curves in the first few injections indicates the strong interaction between 12-3-12·2Br and DNA at low surfactant concentrations, where 12-3-12·2Br monomers bind to negatively charged sites of DNA through electrostatic attraction. With further addition of 12-3-12·2Br, complex formation occurs, which is also indicated by the decrease of the transmittance at the wavelength of 450 nm, as shown in Fig. 7.4(a). ΔH_{obs} begins to decrease at the surfactant concentration of about 0.012 mM, corresponding to the critical aggregation concentration (CAC). Note that the concentrations in the CAC region are so low that it is difficult to measure the CAC accurately, however, the values are still of use to compare between the different systems. Beyond the CAC, the ΔH_{obs} value mainly result from the disassociation of the added micelles, the dilution of the monomers, the aggregation of the monomers around DNA together with the binding of surfactant aggregates on DNA. As shown,

beyond the *CAC*, ΔH_{obs} first decreases sharply and then increases slowly until the second critical concentration (C_2) is reached. After this point, it can be considered that all DNA chains are bound by 12-3-12·2Br molecules and free 12-3-12·2Br micelles begin to emerge, therefore the titration curve is parallel to the dilution curve without DNA. Eventually the value of ΔH_{obs} approaches zero and hardly changes upon further increase of the surfactant concentration.

As shown in Fig. 7.4(a), there exists no obvious decrease for the transmittance at 450 nm T^{450} at surfactant concentrations below the *CAC*, indicating that aggregation does not occur at low surfactant concentrations. In the surfactant concentration region *CAC*~C_1, T^{450} decreases significantly with the 12-3-12·2Br concentration, indicating that the smaller DNA/12-3-12·2Br complexes may aggregate into larger ones owing to the gradually electrostatic neutralization of DNA and the diminishing repulsion between DNA chains; in the surfactant concentration region C_1-C', the repulsion between DNA chains disappears, which may induce aggregation of the complexes and formation of precipitates; when *C* is above *C'*, the larger aggregates can undergo redissolution due to the electrostatic repulsion between the positively charged complexes, corresponding to the increase of T^{450} with *C*. However, the phase boundaries do not coincide with the turning points of the calorimetric titration curves exactly, emphasizing the complexity of the behavior of the mixed system of DNA and 12-3-12·2Br.

The enthalpy change associated with the aggregation process of 12-3-12·2Br molecules (ΔH_{agg}) is determined by subtracting the observed enthalpy change of the lower valley from that at *CAC*, as shown in Fig. 7.4(b). The values of ΔG_{agg} and $T\Delta S_{agg}$ are obtained by the method previously mentioned, assuming that the degree of counter-ion association to the aggregate (β') remains at the same value as that in the absence of DNA although there exists some uncertainty on how exact it is [148, 150]. The aggregation process of 12-3-12·2Br molecules in the presence of DNA can be considered to be composed of two processes: one is the formation of 12-3-12·2Br micelles, similar to the micellization process without addition of DNA; while the other is the binding of the micelles onto DNA [150]. Therefore, the thermodynamic parameters associated with the binding of 12-3-12·2Br micelles on the DNA chain (ΔH_{bd}, ΔG_{bd}, $T\Delta S_{bd}$) are obtained by subtracting the corresponding parameters (ΔH_{mic}, ΔG_{mic}, $T\Delta S_{mic}$) during the micellization process from the ones (ΔH_{agg}, ΔG_{agg}, $T\Delta S_{agg}$) in the aggregation process. The thermodynamic parameters (ΔH_{bd}, ΔG_{bd}, $T\Delta S_{bd}$) may be associated with the structural reorganization of the surfactant micelle upon its

interaction with DNA. Ghirlando *et al*. [153] have proposed that the CTAB micelles elongated into rod-like aggregates induced by DNA and the two formed hexagonally packed matrix. In addition, the 12-3-12·2Br already forms elongated micelles on its own at higher concentrations, so changing the structure to something different in the presence of DNA is even more probable.

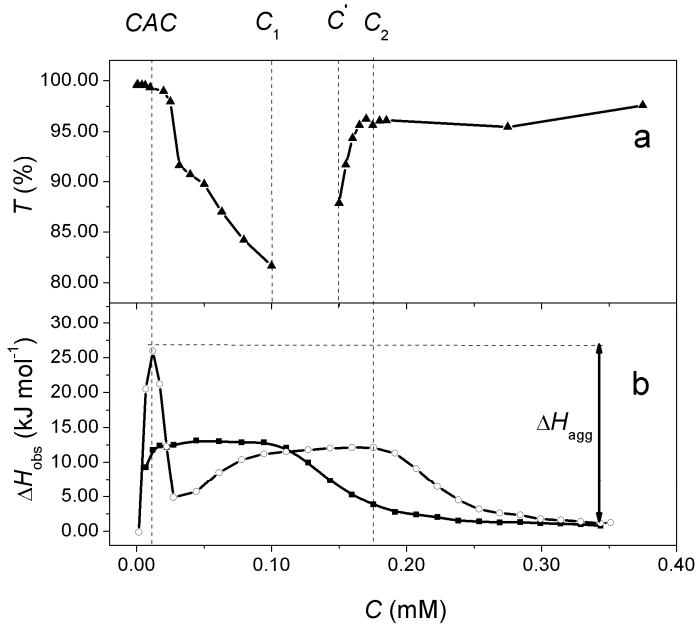

Fig. 7.4(a) Surfactant concentration dependence of T^{450} (%) of DNA/12-3-12 solutions (▲) at 298.15 K with 10 mM NaBr and 0.10 mM DNA; Fig. 7.4(b) calorimetric titration curves of 12-3-12 into brine (■); 0.10 mM DNA (○) at 298.15 K, both in the presence of 10 mM NaBr

DLS experiments have been performed to investigate the variation of the DNA size upon the increasing addition of 12-3-12·2Br in the presence of 10 mM NaBr. Fig. 7.5 gives the typical intensity weighted distribution functions of the DNA solutions with increasing amount of 12-3-12·2Br. It can be seen that the size distribution of the surfactant-free DNA solution presents two peaks with mean hydrodynamic diameters of around 80 nm and 700 nm respectively, as shown in Fig. 7.5(a). The multiple peaks of identical salmon sperm DNA brine was also confirmed by Wang *et al.* [22] using exactly the same DLS technique. Therefore, the two populations of the DNA size may simply arise from the DNA samples already. The hydrodynamic diameters of 12-3-12·2Br/DNA complexes vary with the 12-3-12·2Br concentration. As shown in Fig. 7.5(b), when the concentration of 12-3-12·2Br reaches 0.03 mM, a broad peak with a mean hydrodynamic diameter of approximately 120 nm appears, which indicates the compaction of the DNA molecules in particles with a larger size in Fig.

7.5(a). This peak shows little change when the surfactant concentration is further increased to 0.05 mM, as shown in Fig. 7.5(c). Macroscopic precipitation is observed in the surfactant concentration region of 0.10-0.15 mM, where the charge ratio of surfactant to DNA reaches 2~3. In this region, the zeta potentials of all the DNA/12-3-12·2Br complexes approach zero [23]. As the surfactant concentration reaches 0.16 mM, a second peak with mean hydrodynamic diameter of around 650 nm appears, indicating the existence of large complexes just after the disassociation of the precipitates (Fig. 7.5(d)).

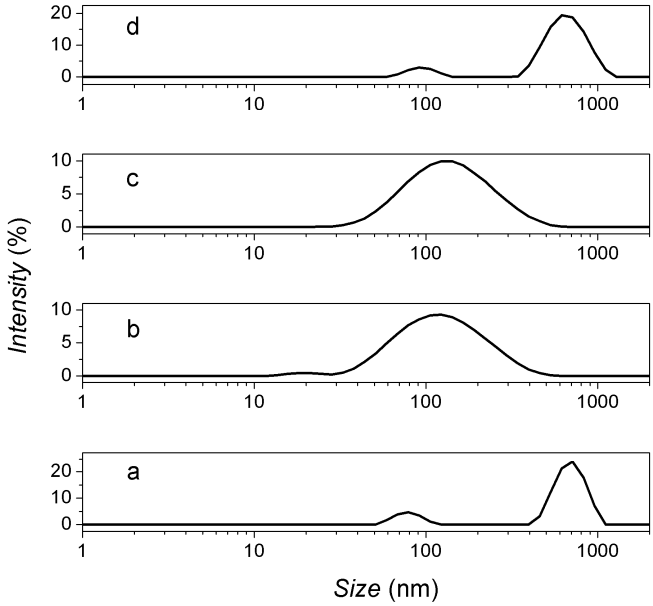

Fig. 7.5 Intensity weighted distribution functions of the DNA solutions with increasing concentration of 12-3-12·2Br: (a) 0 mM; (b) 0.03 mM; (c) 0.05 mM; (d) 0.16 mM, all in the presence of 10 mM NaBr and 0.10 mM DNA

Fig. 7.6 presents the morphological changes of aggregates upon addition of 12-3-12·2Br in the presence of 0.10 mM DNA and 10 mM NaBr observed by AFM and TEM. As shown in Fig 7.6(a), loose coiled structures are observed in the absence of 12-3-12·2Br. Then some beadlike structures appear which are likely to be the condensed DNA due to the presence of surfactant (Fig. 7.6(b)). The existence of this type of aggregate was also proposed by Wang *et al*. [146]. With the further increase of the amount of surfactant, the increasing beadlike structures may have the tendency to approach each other and reassemble to form more condensed aggregates with higher order structures, shown in Fig. 7.6(c), similar to that observed in the CTAB/DNA system according to Nakanishi *et al*. [91]. When the surfactant concentration reaches

0.35 mM, both large aggregates (50-130 nm) and small spherical structures (15-25 nm) appear which may be due to the coexistence of the free 12-3-12·2Br micelles as well as the 12-3-12·2Br/DNA aggregates, corresponding to the results of the microcalorimetric analysis.

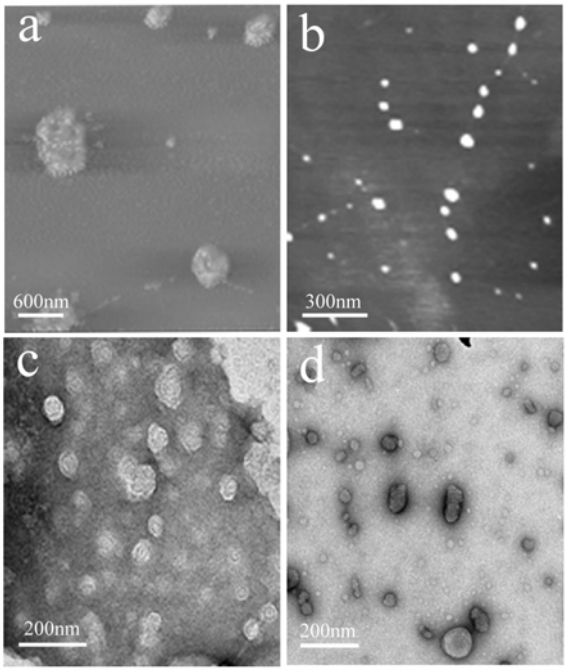

Fig. 7.6 Microstructure of aggregates of DNA/12-3-12·2Br with various 12-3-12·2Br concentration: (a) 0 mM; (b) 0.03 mM; (c) 0.05 mM; (d) 0.35 mM, all in the presence of 10 mM NaBr and 0.10 mM DNA. (a and b) were obtained by AFM observation, while (c and d) were obtained by TEM method

Conformational change of DNA upon its binding with the gemini surfactant has also been confirmed by CD spectrum previously by our group [24]. We have indicated that DNA possess a typical B-form in the absence of 12-3-12·2Br, but it shifts to a longer wavelength upon the addition of 12-3-12·2Br. Meanwhile, in the presence of 12-3-12·2Br, the negative band is enhanced while the positive band becomes flatter with the appearance of a longer tail, which suggests that DNA molecules are packed together to form highly condensed structures in these circumstances.

7.3.3 External Influences on the DNA/12-3-12·2Br interactions

In this section, we have investigated the effects of ionic strength, temperature and DNA concentration on the DNA/12-3-12·2Br interactions with the microcalorimetric method.

7.3.3.1 The effect of ionic strength

The titration curves of the variations of the observed enthalpy change (ΔH_{obs}) with the 12-3-12·2Br concentration (C) in the presence of various concentrations of NaBr are presented in Fig. 7.7. At each NaBr concentration, the dilution of concentrated 12-3-12·2Br brine into a 0.10 mM DNA solution is performed, comparing with the dilution of concentrated 12-3-12·2Br brine into the brine. The measured critical concentrations (CAC, C_2) and the thermodynamic parameters (ΔH_{agg}, ΔH_{bd}, ΔG_{agg}, ΔG_{bd}, $T\Delta S_{agg}$ and $T\Delta S_{bd}$) have been determined (Table 7.4).

For 12-3-12·2Br/DNA systems with different NaBr concentrations, large deviations of the titration curves are observed, showing that ionic strength has great influence on the binding of surfactant with DNA. It can also be seen that the calorimetric titration curves of 12-3-12·2Br diluted into brine and DNA solution become more and more similar with the increase of C_{NaBr}. When C_{NaBr} reaches 50 mM, the two titration curves almost coincide with each other. This can be attributed to the addition of salt weakening the electrostatic attraction between DNA and the surfactant. When C_{NaBr} reaches 50 mM, the interaction is almost fully screened by added salt and the critical concentrations cannot be detectable.

As shown in Table 7.4, the CAC decreases slightly with the increase of salt concentration when C_{NaBr} is below 20 mM, however, the CAC can be considered as infinitely high when C_{NaBr} approaches 50 mM, at which the interaction between DNA and 12-3-12·2Br almost disappears. Wang *et al.* [147] have suggested that the salt has two contrary effects on the systems containing polyelectrolyte and negatively charged surfactant. On the one hand, the addition of salt can weaken the electrostatic attraction between the polyelectrolyte and surfactant. On the other hand, the added salt favors the formation and growth of surfactant micelles. The two competing effects cause the CAC to decrease slightly at lower C_{NaBr} and increase at higher C_{NaBr}. Zhu *et al.* [85] have proposed that there exists a delicate balance between the CAC, the CMC and the ionic strength. The critical ionic strength (I_c) is the concentration of salt at which the values of the CAC and the CMC are equal to each other, and when the ionic strength is below I_c, the CAC is lower than the CMC; when the ionic strength is beyond I_c, DNA does not complex with surfactant. From Table 7.4, we conclude that the value of I_c should be between 20 mM and 50 mM for the studied system. Table 7.4 also shows that the saturation concentration C_2 decreases with C_{NaBr}, indicating that the addition of salt may decrease the number of surfactant molecules needed for saturating the DNA molecules.

The thermodynamic parameters in the aggregation process of 12-3-12·2Br in the presence of DNA (ΔG_{agg}, ΔH_{agg} and $T\Delta S_{agg}$) as well as the thermodynamic parameters relevant to the binding of 12-3-12·2Br micelles onto the DNA chain (ΔG_{bd}, ΔH_{bd} and $T\Delta S_{bd}$) are shown in Table 7.4. Apparently, ΔG_{agg} becomes more negative with increasing ionic strength, indicating that the aggregation of 12-3-12·2Br tends to be more thermodynamically favored at higher ionic strength. However, ΔG_{bd} is much less negative at high ionic strength (20 mM NaBr), suggesting that the thermodynamic favorability of the binding process of DNA with 12-3-12·2Br micelles can be weakened by the screening effect of salt. The increase of ΔH_{bd} and ΔS_{bd} values with C_{NaBr} means that the entropically-driven process is enhanced with increasing NaBr concentration.

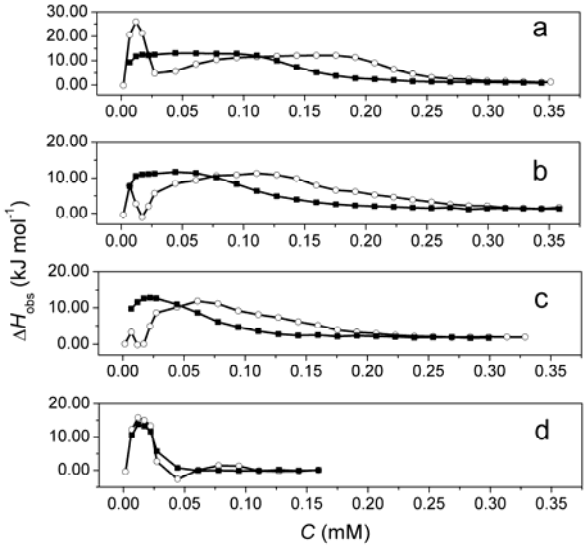

Fig. 7.7 Calorimetric titration curves of 12-3-12·2Br into brine (■) and 0.10 mM DNA solutions (○) with various NaBr concentrations: (a) 10 mM; (b) 15 mM; (c) 20 mM; (d) 50 mM at 298.15 K

Table 7.4 The measured critical aggregation concentration (*CAC*), saturation concentration (C_2) and thermodynamic parameters for the 12-3-12·2Br diluted into DNA with different NaBr concentrations at 298.15 K using calorimetric measurements

C_{NaBr}(mM)	*CAC* (mM)	C_2 (mM)	ΔH_{agg} (kJ/mol)	ΔG_{agg}[a] (kJ/mol)	$T\Delta S_{agg}$[b] (kJ/mol)	ΔH_{bd}[c] (kJ/mol)	ΔG_{bd}[c] (kJ/mol)	$T\Delta S_{bd}$[c] (kJ/mol)
10	0.012	0.176	-25.15	-70.81	45.66	-13.36	-13.64	0.28
15	0.007	0.110	-6.41	-74.59	68.18	3.91	-14.12	18.03
20	0.007	0.061	-1.41	-75.14	73.73	9.46	-8.87	18.33

[a] Calculated using $\Delta G_{agg}=RT(1+2\beta')\ln(2CAC)-RT\ln 2$ assuming that $\beta'=\beta$ [148, 150]

[b] Calculated from $T\Delta S_{agg}=\Delta H_{agg}-\Delta G_{agg}$

[c] Calculated using $\Delta H_{bd}=\Delta H_{agg}-\Delta H_{mic}$, $\Delta G_{bd}=\Delta G_{agg}-\Delta G_{mic}$, $T\Delta S_{bd}=T\Delta S_{agg}-T\Delta S_{mic}$

7.3.3.2 The effect of temperature

We have performed the microcalorimetric experiments at different temperatures to investigate the effect of temperature on the DNA/12-3-12·2Br interactions. Fig. 7.8 shows the calorimetric titration curves of the variations of the observed enthalpy change (ΔH_{obs}) with the surfactant concentration (C) at various temperatures (298.15 K, 303.15 K and 308.15K). In these measurements, 12-3-12·2Br is diluted into 0.10 mM DNA solution in the presence of 10 mM NaBr. As seen, when C is around the CAC region, the ΔH_{obs} value decreases with temperature, while the inverse is observed when C is higher. In the high concentration region, the variation of ΔH_{obs} with temperature is similar to that in the absence of DNA, which may be due to the gradual saturation of DNA with 12-3-12·2Br and the enhanced effect of the 12-3-12·2Br micelle disassociation.

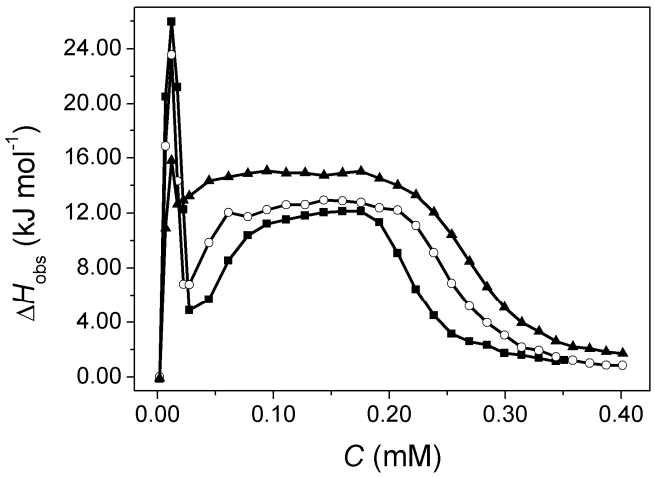

Fig. 7.8 Calorimetric titration curves of 12-3-12·2Br into 0.10 mM DNA solution at various temperatures: 298.15 K (■); 303.15 K (○); 308.15 K (▲), all in the presence of 10 mM NaBr.

7.3.3.3 The effect of DNA concentration

To evaluate the effect of DNA concentration (C_{DNA}) on the interaction between 12-3-12·2Br and DNA, microcalorimetric experiments of concentrated 12-3-12·2Br brine diluted into DNA brine with different DNA concentrations at 298.15 K were performed. Fig. 7.9 shows the corresponding calorimetric titration curves, and the measured critical concentrations (CAC, C_2) and the thermodynamic parameters (ΔH_{agg}, ΔH_{bd}, ΔG_{agg}, ΔG_{bd}, $T\Delta S_{agg}$ and $T\Delta S_{bd}$) for solutions with different DNA concentrations are shown in Table 7.5. It can be seen that at a given temperature, the critical

aggregation concentration *CAC* is independent of DNA concentration, which is consistent with results from the literature [24]. The saturation concentration C_2 increases with DNA concentration, indicating that the appearance of free micelles in the bulk phase is postponed by the increasing DNA concentration. The values of ΔH_{bd}, ΔG_{bd} and ΔS_{bd} change only very slightly or not at all with the variation of DNA concentration.

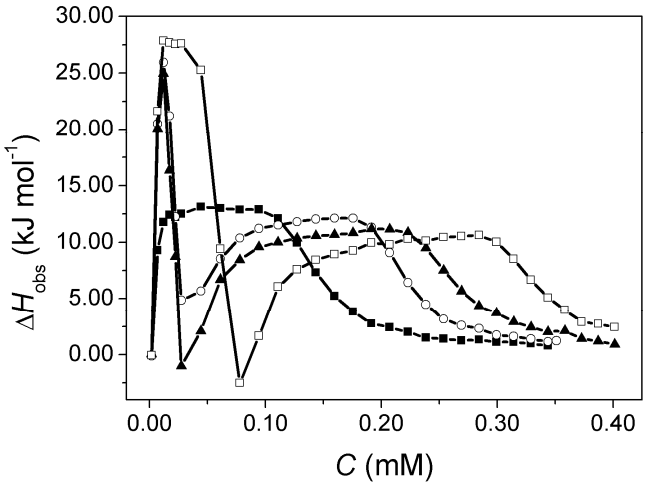

Fig. 7.9 Calorimetric titration curves of 12-3-12·2Br into brine (■), 0.10 mM DNA solution (○), 0.17 mM DNA solution (▲), 0.30 mM DNA solution (□) with 10 mM NaBr at 298.15 K.

Table 7.5 Critical aggregation concentration (*CAC*), saturation concentration (C_2) and thermodynamic parameters for the 12-3-12·2Br diluted into various concentrations of DNA in 10 mM NaBr solution and at 298.15 K from calorimetric measurements

C_{DNA} (mM)	*CAC* (mM)	C_2 (mM)	ΔH_{agg} (kJ/mol)	ΔG_{agg} (kJ/mol)	$T\Delta S_{agg}$ (kJ/mol)	ΔH_{bd} (kJ/mol)	ΔG_{bd} (kJ/mol)	$T\Delta S_{bd}$ (kJ/mol)
0.10	0.012	0.176	-25.15	-70.81	45.66	-13.36	-13.64	0.28
0.17	0.012	0.207	-24.02	-70.81	46.79	-12.23	-13.64	1.41
0.30	0.012	0.284	-26.18	-70.81	44.63	-14.40	-13.64	-0.76

Based on the experimental results obtained, a possible mechanism for interaction between DNA and 12-3-12·2Br with increasing surfactant concentration is proposed. When *C* is below *CAC*, 12-3-12·2Br monomers may bind with the DNA chains through electrostatic attraction. When *C* is in the range *CAC*~C_2, 12-3-12·2Br aggregates begin to form around the DNA chains, and correspondingly, the smaller complexes can aggregate into larger ones due to the partially weakened electrostatic repulsion between DNA chains, followed by a redissolution of the larger aggregates

due to the enhanced electrostatic repulsion between the complexes upon further addition of 12-3-12·2Br. When C reaches the saturation point C_2, all the DNA chains are bound completely by 12-3-12·2Br micelles, and free 12-3-12·2Br micelles begin to emerge in the bulk phase. The interactions between DNA and 12-3-12·2Br are very complicated, with a cooperative mechanism involving both the electrostatic interaction and the hydrophobic interaction which is the main reason for the formation of mixed aggregates of DNA and 12-3-12·2Br.

7.3.4 The effect of spacer length on the micellization of 12-O-12·2Br and its interactions with DNA

In this section, we performed measurements with several techniques (micropolarity, zeta potential, conductivity, isothermal titration calorimetry) to study the effect of spacer length on the micellization of 12-O-12·2Br and its interactions with DNA.

7.3.4.1 Effect of spacer length on 12-O-12·2Br micellization

Fig. 7.10 shows the variations of the electrical conductivity (κ) of 12-O-12·2Br (O=3, 4, 6) with increasing surfactant concentration (C) in the presence of 10 mM NaBr at 298.15 K. As indicated in Fig. 7.10, κ increases linearly with C in the low concentration range. With increasing surfactant concentration, a transition appears at a certain concentration corresponding to the critical micelle concentration (CMC_1 the subscript refers to the CMC being measured using the first method, in this case conductivity), indicating the formation of micellar structures and the binding of counterions. The degree of ionization of the micelles, α, was taken to be the ratio of the values of $d\kappa/dC$ above and below the CMC_1. The degree of counter-ion association to micelle β was obtained by the relationship $\beta=1-\alpha$. The values of CMC_1, α, β for three gemini surfactants 12-O-12·2Br (O=3, 4, 6) measured from the conductivity measurements are indicated in Table 7.6.

As shown in Table 7.6, with increasing spacer length, the CMC_1 first increases then decreases. When the spacer length is increased, the molecular conformation of the surfactant and the relative position of two alkyl chains are changed so that the micellization is hindered leading to the increase of the CMC_1. On the other hand, the spacer is transferred from a polar hydrophobic environment to the micellar surface when forming the micellar structures and this hydrophobic effect is more important

with increasing spacer length, leading to the decrease of CMC_1 [145, 154]. It is shown that the degree of ionization of the micelles α is relatively small when spacer length is short. As the spacer length is short, the distance between the polar groups is relatively short, causing strong binding with counterions [145, 154].

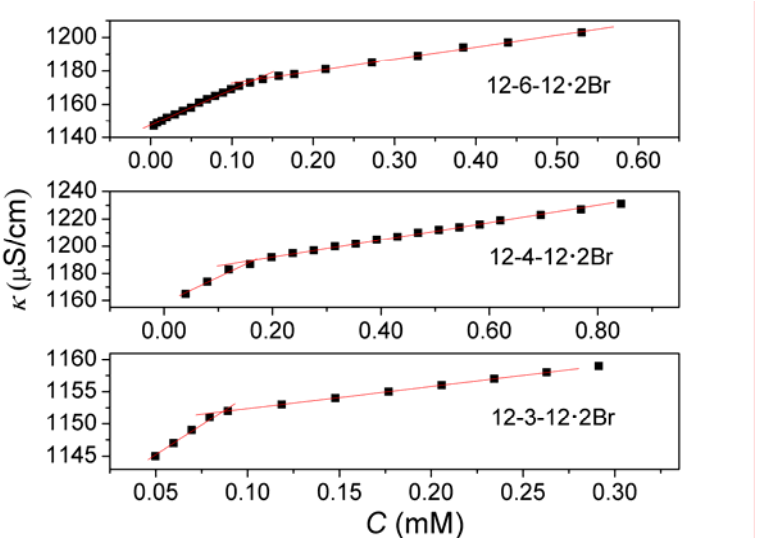

Fig. 7.10 Variation of conductivity with increasing concentration in the 12-O-12·2Br system (O=3, 4, 6) in the presence of 10 mM NaBr

Table 7.6 The counterion disassociation degree α, counterion binding degree β and CMC values (CMC_1 from conductivity, CMC_2 from micropolarity and CMC_3 from isothermal titration calorimetry) in the 12-O-12 system (O=3, 4, 6)

O	α	β	CMC_1(mM)	CMC_2(mM)	CMC_3(mM)
3	0.19	0.81	0.086	0.101	0.100
4	0.34	0.66	0.159	0.155	0.156
6	0.34	0.66	0.132	0.138	0.127

A second method has been used to measure the CMC is the fluorescence technique. To use fluorescence to measure the CMC, a typical S curve of Boltzmann type was utilized to fit the experimental data I_1/I_3~log(C) using the following equation:

$$y = \frac{A_1 - A_2}{1 + e^{(x - x_0)/\Delta x}} + A_2 \qquad \text{Equation 7.1}$$

In Equation 7.1, x_0 representing the abscissa value of the center point on the S curve and Δx is related to the independent variable range in the sharp decrease region of I_1/I_3. Typical S curves with Boltzmann type are presented in Fig. 7.11, and

log(CMC_2/M) is determined by the points of intersection of the tangent at the center point and the line $y_2=A_2$, where log(CMC_2/M)=x_0+2Δx.

Fig. 7.12 shows the dependence of micropolarity in 12-O-12·2Br system on the surfactant concentration in the presence of 10 mM NaBr. As shown, when surfactant concentration C is very low, I_1/I_3 hardly changes with increasing C; when C reaches a certain concentration, I_1/I_3 decreases sharply, indicating the existence of hydrophobic microenvironment; finally I_1/I_3 hardly varies with C, showing that pyrene molecules have all transferred to the hydrophobic microenvironment.

The fitting results for the experimental data using Equation 7.1 are shown in Fig. 7.12, and the parameters derived from the fitting are shown in Table 7.7. Table 7.7 shows that the S curve with Boltzmann type can fit the experimental data I_1/I_3~log(C) quite well, and the CMC_2 values compare well with CMC_1 based on the conductivity measurements, indicating that the proposed methods to determine the critical micelle concentration are rather accurate. It can be observed, in Fig 7.12, that I_1/I_3 decreases at concentrations below the critical micelle concentration, as the pyrene molecules may induce the surfactants to form certain small complex structures before the formation of larger micellar structures [155].

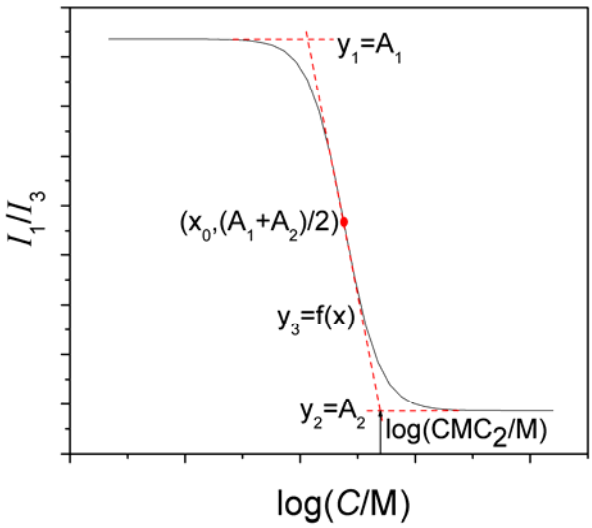

Fig. 7.11 Typical S curve with Boltzmann type, the horizontal axis denotes the logarithmic of surfactant concentration (10 as the base). The lines $y_1=A_1$, $y_2=A_2$ are horizontal, and the line y_3=f(x) is the tangent line to the curve passing the point (x_0,(A_1+A_2)/2). Log(CMC_2/M) is determined by the points of intersection from the lines y_3=f(x) and $y_2=A_2$.

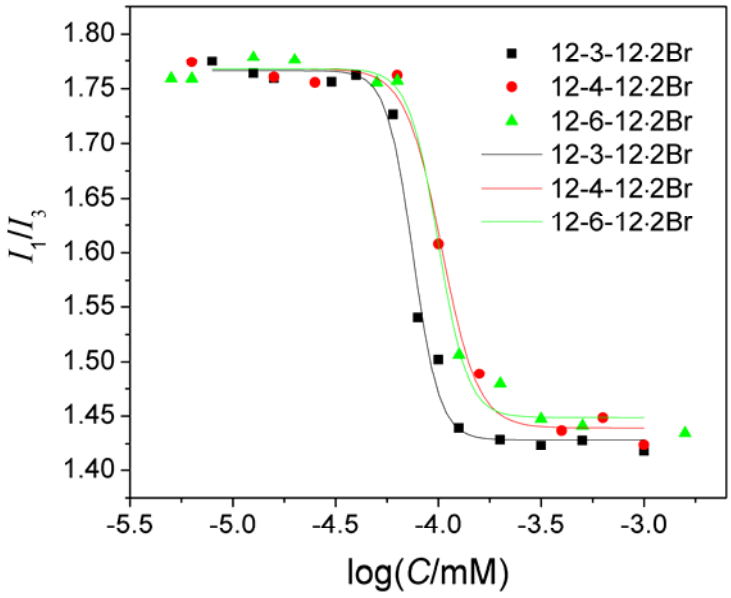

Fig. 7.12 Dependence of micropolarity (I_1/I_3) on 12-O-12·2Br (O=3, 4, 6) concentration in the presence of 10 mM NaBr. The lines are the fitting results using Equation 7.1.

Table 7.7 Fitting results: X_0 denotes the center point of the S curve with Boltzmann type, Δx denotes the steps and r^2 is the square of correlation coefficient

O	X_0	Δx	r^2	χ^2	CMC_2 (mM)
3	-4.12	0.063	0.992	0.00028	0.101
4	-3.98	0.087	0.994	0.00025	0.155
6	-4.00	0.071	0.994	0.00020	0.138

We have also investigated the micellisation process by calorimetry. Fig. 7.13 presents the calorimetric titration curves for three types of gemini surfactants 12-O-12·2Br (O=3, 4, 6). The solution for injection is concentrated 12-O-12·2Br solution while the solution to be titrated is 10 mM NaBr solution. The vertical ordinate of the curve results from the enthalpy change from each injection (ΔH_{obs}), and the horizontal ordinate is the final 12-O-12·2Br concentration (C) in the sample cell. When C reaches a certain concentration, a transition appears on the titration curve with the rapid decrease of ΔH_{obs}, and the critical micelle concentration (CMC_3) is determined correspondingly. When C is lower than CMC_3, the enthalpy change comes from the disassociation of the added surfactant micelles and the dilution of monomers; when C just passes CMC_3, surfactant micelles and monomers coexist in the sample cell, and ΔH_{obs} comes from the disassociation of some of the added micelles, the dilution of the monomers and the remaining micelles; when C is

sufficiently high, ΔH_{obs} comes only from the dilution of micelles, which is relatively small as seen in Fig. 7.13. The CMC_3 is determined from the linear fits of two regions: one is region where ΔH_{obs} decreases slowly and the other is the region where ΔH_{obs} decreases much more rapidly. The enthalpy change for the micellization of 12-O-12·2Br (ΔH_{mic}) is determined by the difference of ΔH_{obs} from the region for the slow variation and the flat region finally, as seen in Fig. 7.13.

Table 7.8 presents the values of the critical micelle concentration CMC_3 and the thermodynamic parameters determined by the microcalorimetric method, which are dependent on the spacer length, as indicated in Table 7.8. With increasing spacer length, CMC_3 first increases and then decreases, comparing well with the previous conductivity and micropolarity results. The $-\Delta H_{mic}$ first decreases significantly and then increases with spacer length, similar to the literature results [154].

The dependence of $-\Delta H_{mic}$ on O can be explained as the result of two effects. For 12-O-12·2Br with spacer length shorter than 4, when the 12-O-12·2Br molecules are transferred from the hydrophilic phase to the micelles, the two hydrophobic chains are closer to each other, therefore the conformation of the micellar surfactant tends to be the cis conformation, while still restricted by the steric effects from the two hydrophobic chains, leading to the decrease of $-\Delta H_{mic}$ with spacer length. While spacer length is further increased, this effect decreases rapidly until it disappears finally, and the other effects on the change of $-\Delta H_{mic}$ become more obvious, mainly from the transfer of the spacer from the hydrophilic phase to the micellar surface and the electrostatic interactions on the micellar surface. In the transfer process of spacer, the microenvironment of the spacer turns from the hydrophilic water environment to the hydrophobic micellar surface, leading to the increase of $-\Delta H_{mic}$ with spacer length.

As indicated in Table 7.8, with the increase of spacer length, the absolute value of Gibbs free energy change corresponding to the micellization process $-\Delta G_{mic}$ is the highest at O=3, and the lowest at O=4. This indicates when O is lower, the thermodynamic favorability for the micellization of the gemini surfactant is higher. However, literature has shown that the spacer length has no obvious effects on the values of $-\Delta G_{mic}$ in the micellization process of 12-O-12·2Br in pure water [156]. The different dependence of $-\Delta G_{mic}$ on the spacer length can be due to the presence of electrolyte in our case, which can screen the electrostatic interactions between the headgroups, thus promoting the micellization of the surfactant. The effect of electrolyte is enhanced for the gemini surfactant with shorter spacer length, for which the distance between the hydrophilic headgroups becomes shorter and

correspondingly the electrostatic interactions become stronger. As indicated in Table 7.8, comparing the contributions of $-\Delta H_{mic}$ and $-\Delta S_{mic}$ on the value of ΔG_{mic}, it can be concluded that the micellization of 12-O-12·2Br is mainly entropically driven.

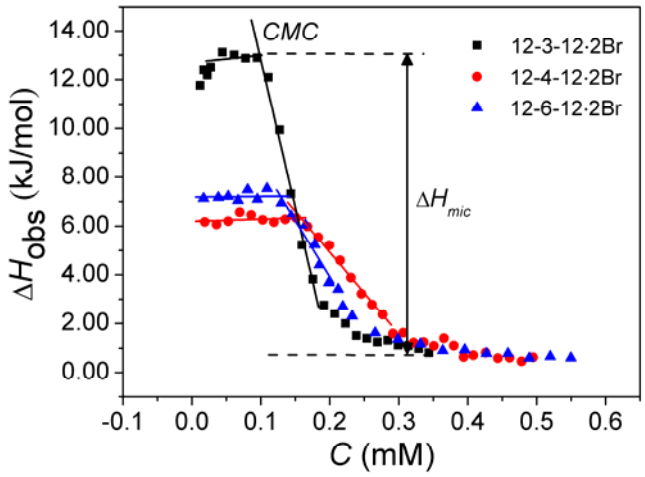

Fig. 7.13 Calorimetric titration curves of 12-O-12·2Br (O=3, 4, 6) into 100 mM NaBr

Table 7.8 CMC_3 values and thermodynamic parameters in the 12-O-12·2Br system (O=3, 4, 6)

O	CMC_3 (mM)	ΔH_{mic} (kJ/mol)	ΔG_{mic} (kJ/mol)	$T\Delta S_{mic}$ (kJ/mol)
3	0.100	-11.79	-57.04	45.25
4	0.156	-5.74	-48.15	42.41
6	0.127	-6.75	-49.33	42.58

$\Delta G_{mic}=RT(1+2\beta)\ln(2CMC)-RT\ln 2$

$T\Delta S_{mic}=\Delta H_{mic}-\Delta G_{mic}$

7.3.4.2 The effect of spacer length on DNA/12-O-12·2Br interactions

The micropolarity in the mixed system of 12-O-12·2Br and DNA is also investigated as shown in Fig. 7.14. In the presence of DNA, I_1/I_3 decreases significantly at very low 12-O-12·2Br concentrations. Note that in the figure the highest concentration is still almost one magnitude lower than CMC_2. Induced by the strong electrostatic interactions between DNA and 12-O-12·2Br, 12-O-12·2Br molecules aggregate around DNA chains with the formation of a hydrophobic microenvironment, therefore the concentration around the DNA chain is higher than that in the bulk phase.

As in Fig. 7.14, when the spacer length is shorter (O=3, 4), the critical concentration corresponding to the sharp decrease of the micropolarity is lower than

that with the longer spacer length (O=6), indicating that the gemini surfactant with shorter spacer length can form the microenvironment at lower concentrations. That is to say, 12-O-12·2Br, with shorter spacer length, has stronger interactions with DNA. This is because that when the spacer length is short, the two hydrophobic alkyl chains are closer. Therefore 12-O-12·2Br can be regarded as a cationic surfactant carrying double charges [20], which is why it has stronger interactions with DNA. When the spacer length becomes longer, the alkyl chains on the spacer can change its conformation flexibility in order to decrease its contact with water, leading to a negative entropic change. This negative entropic change hinders the interactions between the surfactant and DNA, which needs to be compensated by a positive entropic change.

Generally the positive entropic change may come from the hydrophobic interactions between the spacer and other hydrophobic chains, and only the spacer sufficiently long (O is above 10) can take part in the the micellzation of surfactants through hydrophobic interactions. Therefore, the micellization of gemini surfactant with longer spacer length has enhanced thermodynamic favorability.

For the 12-O-12·2Br with medium spacer length (O is around 6), compared with 12-O-12·2Br with short or long spacer length, the negative entropic change caused by the conformation change is more obvious than the positive entropic change arising from the hydrophobic interactions. Thus 12-6-12·2Br has the weakest interactions with DNA with the highest value of critical concentration as shown in Fig. 7.14.

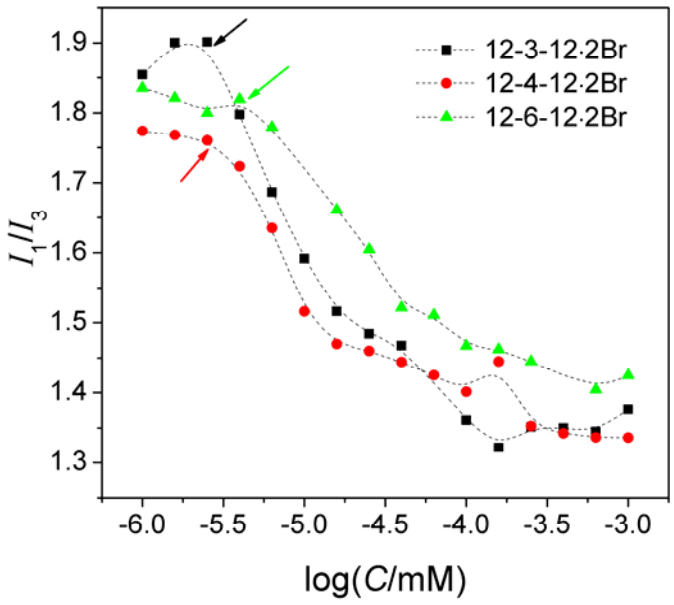

Fig. 7.14 Dependence of micropolarity in 12-O-12·2Br/DNA system on the surfactant concentration, where the DNA concentration is kept at 10^{-4} M.

Now we will focus on the change of charge carried by the 12-O-12·2Br/DNA complex upon the increase of 12-O-12·2Br concentration. Fig. 7.15 presents the variations of zeta potential for the 12-O-12·2Br/DNA system on the surfactant concentration *C*. As shown, for 12-O-12·2Br with different O, the variations of zeta potential with *C* are similar. Note that when *C* is relatively low, the difference in the zeta potential for 12-O-12·2Br for various O is due to the difference of the initial states of DNA, which may come from the preparation of DNA samples. That is to say, when DNA molecules are completely stretched in the solution, the zeta potential may not vary significantly with *C* at first, then transit from negative to positive values with further increase of *C*. For the case when DNA molecules are not completely stretched initially, the negative charges on the DNA chains become more exposed with the increasing addition of surfactants, owing to the strong interactions between the added surfactants and DNA [23]. Therefore, the zeta potential decreases with increasing *C*. When *C* reaches 0.032 mM, most of the negative charges on the DNA become exposed, and then the variations of zeta potential with *C* display a trend from negative to positive values. When *C* reaches around 0.26 mM, zeta potential hardly changes with *C*, indicating the saturation of the complexation between 12-O-12·2Br and DNA. It can be seen that the variations of zeta potential with the surfactant concentration at higher concentrations is hardly affected by the spacer length.

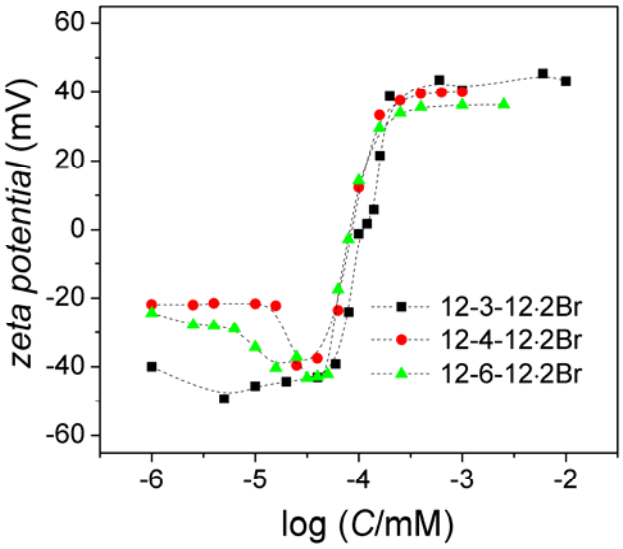

Fig. 7.15 Dependence of zeta potential in 12-O-12·2Br/DNA system on the surfactant concentration, where the DNA concentration is kept at 10^{-4} M

Fig. 7.16 shows the calorimetric titration curves for 12-O-12·2Br with different

O, in which the concentrated 12-O-12·2Br brine is diluted in the DNA solution in the presence of 10 mM NaBr. As shown, when C is relatively low, ΔH_{obs} first increases with C and then decreases with C rapidly; then with further increase of C, ΔH_{obs} first increases and then reaches a platform value, before finally decreasing to around zero.

When C is small, a transition appears on the titration curve with the rapid decrease of ΔH_{obs}, and this transition corresponds to the critical aggregation concentration (*CAC*). When C is smaller than *CAC*, ΔH_{obs} comes from the disassociation of added micelles, the dilution of monomers and the electrostatic interactions between monomers and DNA. When C reaches *CAC*, ΔH_{obs} decreases significantly with C accompanied by the aggregation of 12-O-12·2Br molecules around DNA, and the variation of ΔH_{obs} comes not only from the effects previously mentioned but also from the aggregation of 12-O-12·2Br on DNA through hydrophobic interactions. Further increase of C leads to the gradual saturation of 12-O-12·2Br/DNA interactions, and the micellization of 12-O-12·2Br in the bulk phase gradually becomes dominating, therefore the titration curve becomes similar to that of 12-O-12·2Br injected into NaBr. That is to say, with further increase of C, ΔH_{obs} first remains constant and then decreases to around zero, and the transition point is the critical micelle concentration of 12-O-12·2Br in the mixed system C_{mix}. The enthalpy change corresponding to the binding of 12-O-12·2Br with DNA (ΔH_{bd}) can be determined from the difference of ΔH_{obs} at *CAC* and the platform value in the titration curve for the 12-O-12/NaBr system, as shown in Fig. 7.16. The ΔH_{bd} values for 12-3-12·2Br, 12-4-12·2Br and 12-6-12·2Br are -14.5, -14.4 and -12.5 kJ/mol respectively. The values of *CAC*, C_{mix} and ΔH_{bd} have been presented in Table 7.9.

Based on the effects of spacer length on *CAC*, C_{mix} and ΔH_{bd}, it can be concluded that *CAC* increases slightly with increasing S, showing that the increase of S hinders the interactions between 12-O-12·2Br and DNA for the systems studied, emphasizing the previous micropolarity results. C_{mix} first increases and then decreases with O, and this trend is similar to the dependence of *CMC* on O. It has also been found that spacer length has no obvious influences on ΔH_{bd}.

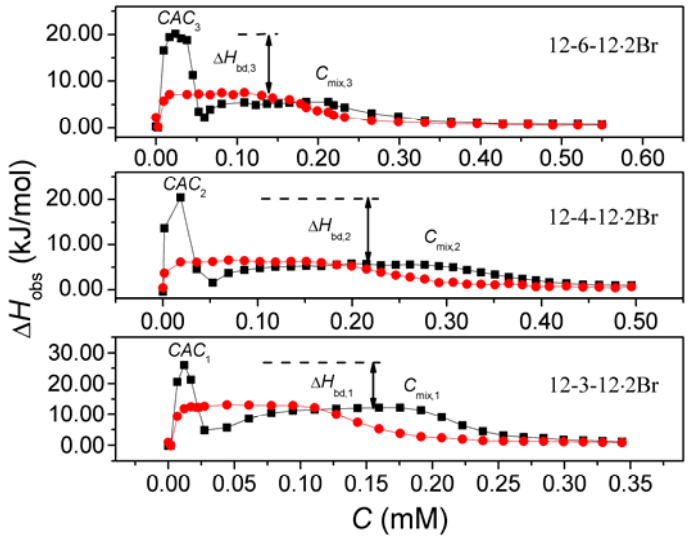

Fig. 7.16 Calorimetric titration curves of 12-O-12·2Br (O=3, 4, 6) into 100 mM NaBr (●) and DNA/NaBr mixtures (■). The DNA concentration is kept at 10^{-4} M.

Table 7.9 Calculated values of *CAC*, ΔH_{bd} and C_{mix} in the mixed system of 12-O-12·2Br (O=3, 4, 6) and DNA

O	*CAC* (mM)	ΔH_{bd} (kJ/mol)	C_2 (mM)
3	0.0120	-14.5	0.191
4	0.0188	-14.4	0.292
6	0.0240	-12.5	0.212

7.4 Conclusions

In this chapter, the micellization process of cationic gemini surfactant 12-3-12·2Br molecules has been investigated, and the influence of ionic strength and temperature on the process have also been studied. The various thermodynamic parameters of these processes are derived based on the measurements of isothermal titration calorimetry and conductivity measurements. It has been found that the micellization of 12-3-12·2Br is entropically driven and thermodynamically favored. The increase of temperature slightly increases the *CMC*, while the increase of the ionic strength lowers the *CMC*. The enthalpy change corresponding to the micellization process of 12-3-12·2Br becomes more negative with the temperature increase, which can be associated with destruction of the structured water around the surfactants with increasing temperature.

The interactions of 12-3-12·2Br with DNA under different environmental conditions were investigated using several techniques. In addition, the effects of ionic strength, temperature and DNA concentration on their interactions have been checked.

It was found that the DNA conformation can be modulated by the addition of 12-3-12·2Br. Loose DNA coils, condensed DNA structures including beadlike structures, highly ordered aggregates, as well as coexistance of large aggregates and small spherical structures in the DNA/12-3-12·2Br system were observed. The addition of electrolyte can screen the DNA/12-3-12·2Br electrostatic attraction, while promoting the formation of free 12-3-12·2Br micelles in the bulk phase or 12-3-12·2Br aggregates on the DNA chain. It has also been proven that the hydrophobic effect is significant in the binding process. The *CAC* value is independent of DNA concentration, due to the DNA chains behaving like a separate phase when in contact with the surfactant molecules. The saturation concentration C_2 increases with the DNA concentration, and this is owing to the postponed appearance of free micelles in the bulk phase. Based on the experimental results, we conclude that 12-3-12·2Br/DNA interactions bear a cooperative mechanism including both the electrostatic and hydrophobic interaction.

The effect of spacer length O on the 12-O-12·2Br micellization is investigated. With increasing spacer length, it can be seen that the *CMC* first increases then decreases. The degree of ionization of the micelles α is relatively small when the spacer length is short. The value of $-\Delta H_{mic}$ first decreases and then increases with spacer length. The *CMC* of the gemini surfactant is lowest at O=3.

The effect of spacer length on the interactions between 12-O-1212-O-12·2Br and DNA has also been investigated. In the presence of DNA, I_1/I_3 decreases significantly at a much lower 12-O-12·2Br concentration than in the absence of DNA. 12-O-12·2Br with a shorter spacer length has stronger interactions with DNA. When increasing the spacer length, the interactions between 12-O-12·2Br and DNA can be hindered, the critical micelle concentration in the mixed system first increases and then decreases. The spacer length has no obvious influences on the enthalpy change corresponding to the binding process of 12-O-12·2Br with DNA (ΔH_{bd}).

Our study on the micellization of the cationic gemini surfactant 12-O-12·2Br, its interaction process with DNA and the influences on these processes are helpful in providing more fundamental information in its interaction with DNA and improving the understanding of oppositely charged polyelectrolyte/surfactant systems.

Chapter 8 Interactions between cationic IL surfactant [C_{12}mim]Br and DNA in the bulk

8.1 Introduction

Typical ionic liquids (ILs) consist of organic cations (imidazolium, pyridinium, pyrrolidinium, ammonium and phosphonium *etc*.) and organic or inorganic anions (acetate, trifluoroacetate, tetrafluoroborate, hexafluorophosphate or bromide anions) [157-159]. ILs possess unique physicochemical properties including high thermal stability, tunable viscosity, negligible vapor pressure, noninflammability as well as excellent solubility for both organic and inorganic compounds [110, 114, 160, 161]. As a result, IL has a wide range of applications in separation and extraction technologies [111, 162-166], electrochemistry and energy use [167-169], solvent and catalysis in synthesis [108, 109, 170] , lubricants [171] *etc*.

Besides, the development of IL in biological and biomedical applications has been increasingly emphasized in the past decades. Studies have shown that functionalized IL has a high binding ability with DNA and could mediate the process of gene expression without the help from any additional agent [120]. The detailed binding characteristics and the molecular mechanism for the interaction system of a typical IL and DNA have also been presented, showing the importance of the electrostatic attraction between the cationic headgroups of IL and the phosphate groups of DNA, as well as the hydrophobic interactions between the alkyl chains of IL and the bases of DNA [94].

As expected, ILs with long hydrophobic alkyl groups can be surface active, similar to cationic surfactants, and the aggregation behavior of these surface active ILs has been investigated [27, 95]. In this chapter, the imidazolium-based cationic surfactant 1-dodecyl-3-methylimidazolium bromide ([C_{12}mim]Br) has been chosen for its superior surface activity and lower *CMC* value compared with DTAB [147] and the potential applications in various areas [27]. In this chapter, the complexation between [C_{12}mim]Br and salmon sperm DNA in the presence of 10 mM NaBr was investigated by the use of combined experimental techniques and computer simulations. The aggregation processes of [C_{12}mim]Br in the absence and presence of DNA have been studied and compared. The size transition and conformational change of the DNA chain, the complex structures formed by [C_{12}mim]Br and DNA and the thermodynamic parameters of the mixed system are presented. For comparison with

the experimental results, Molecular dynamics (MD) simulations were performed to investigate the oppositely charged polyelectrolyte/surfactant system. The equilibrium properties of the system have been recorded by the computer and compared with the results from different types of measurements. Our results may be helpful in the further understanding the interaction mechanism for the oppositely charged surfactant/polyelectrolyte system and in expanding the role of ILs in the biological and biomedical applications.

8.2 Procedures

Cationic surfactant [C_{12}mim]Br was commercially available. 10 mM NaBr solution was utilized as the solvent for all the samples prepared. Stock solutions of DNA and [C_{12}mim]Br were prepared respectively and then mixed up together at a certain ratio to obtain the DNA/[C_{12}mim]Br samples. All DNA/[C_{12}mim]Br samples were prepared using this protocol unless specific methods for sample preparation were otherwise indicated. The samples were kept overnight at 298.15 K before measurements.

For the conductivity and microcalorimetry measurements, the sample cell was initially loaded with the 10 mM NaBr solution or DNA brine. Then the stock brine of [C_{12}mim]Br (150 mM or 10 mM) was injected into the stirred sample cell in portions of 1-15 μL. The description of the measurements of conductivity, micropolarity, particle size, zeta potential, UV-Vis transmittance, gel electrophoresis, AFM and CD as well as the MD simulation can be found in Chapter 3.

8.3 Results and discussion

8.3.1 Conductivity

Fig. 8.1 shows the dependence of the electric conductivity (κ) of [C_{12}mim]Br solution on the [C_{12}mim]Br concentration (C) at 298.15 K. The degree of ionization of the micelles, α, was determined by the intersection of two linear plots of $\kappa(C)$ curve, corresponding to the ratio of $d\kappa/dC$ values above and below the *CMC*. The degree of counterion association to micelle (β) was then calculated using the relationship $\beta=1-\alpha$. It has been found that the values of *CMC* and β determined from the electrical conductivity measurements were 6.80 mM and 0.688, respectively. These values are similar to those obtained for the [C_{12}mim]Br/H_2O system by Wang *et al*. [26, 172], showing that a small amount of salt has no significant effect on the micellization process of [C_{12}mim]Br. This is in agreement with Łuczak *et al*. [172],

who observed that the presence of low concentrations of KCl or KBr (less than 10 mM) in the [C_{10}mim]Cl solution has no obvious effect on the values of *CMC* and *β*.

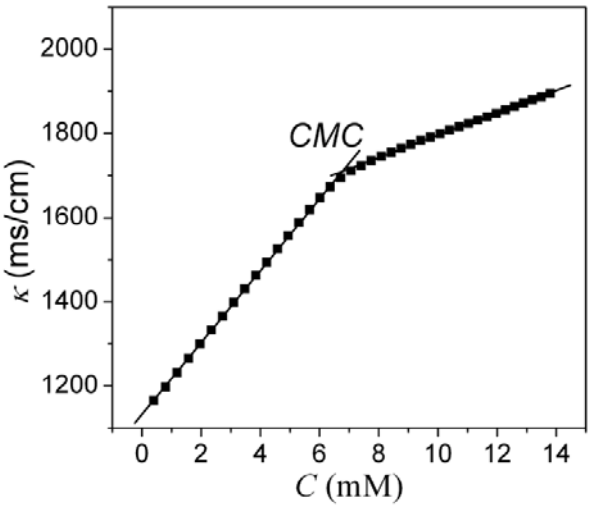

Fig. 8.1 Dependence of electrical conductivity (κ) on [C_{12}mim]Br concentration (C) in 10 mM NaBr solution.

8.3.2 Isothermal titration calorimetry

The microcalorimetric measurements were performed to monitor the interactions of [C_{12}mim]Br with DNA quantitatively. Concentrated [C_{12}mim]Br brine (150 mM) was injected to 10 mM NaBr or 0.1 mM DNA solutions in a stepwise manner. The variations of the observed enthalpy change per mole of the added [C_{12}mim]Br (ΔH_{obs}) with the final [C_{12}mim]Br concentration (C) in the sample cell are presented in Fig. 8.2. It should be noted that the first few titrations may lead to high uncertainty due to instrumental error.

Fig. 8.2 shows the titration curve of the concentrated [C_{12}mim]Br brine diluted into 10 mM NaBr solution. There exists a transition region corresponding to the sudden decrease of ΔH_{obs}, corresponding to the formation of [C_{12}mim]Br micelles. The *CMC* is obtained from the intersection of the two linear extrapolations of two sections of the curve [148, 173], comparing well with the electrical conductivity result. When C is below *CMC*, ΔH_{obs} comes from the breakup of the added [C_{12}mim]Br micelles and further dilution of monomers. When C is close to *CMC*, some of the added micelles break up into monomers and the rest are only diluted in the sample cell, leading to the decrease of ΔH_{obs}. When C is sufficiently high, ΔH_{obs} only results from the dilution of the micelles and is very low. The enthalpy of micellization (ΔH_{mic}) is determined by the difference of ΔH_{obs} corresponding to two sections of the plot in

Fig. 8.2 [149].

Fig. 8.2 shows the titration curve for the dilution of the concentrated [C_{12}mim]Br brine into 0.1 mM DNA solution in the presence of 10 mM NaBr. It can be observed that the titration curve with DNA deviates much from that without DNA even in the low concentration range, indicating that the DNA/[C_{12}mim]Br interaction can occur at low *C*. With the increase of *C*, a sharp endothermic peak appears in the concentration range 0-2.25 mM. With further increase of *C,* ΔH_{obs} remains constant, and finally decreases to a relatively low value.

When *C* is low, the added [C_{12}mim]Br micelles are disassociated into monomers,which may interact with DNA through electrostatic attraction. Upon further addition of [C_{12}mim]Br, the [C_{12}mim]Br molecules begin to aggregate on the DNA chains through the hydrophobic interactions between the alkyl chains, accompanied by the decrease of ΔH_{obs}, also confirmed by the transmittance results discussed below. With further increase of *C*, the binding sites on DNA are further occupied, and finally the titration curve is close to that without DNA.

To obtain information on the interaction in a narrower concentration range, 10 mM [C_{12}mim]Br is injected into 10 mM NaBr and 0.1 mM DNA brine respectively. Fig. 8.3 shows the titration curve of 10 mM [C_{12}mim]Br into DNA brine. The enthalpy changes of 10 mM [C_{12}mim]Br diluted into NaBr are negligible, due to the [C_{12}mim]Br concentration being close to the *CMC* and most [C_{12}mim]Br molecules are in the form of monomers instead of micelles. As shown in Fig. 8.3, ΔH_{obs} first increases and then decreases with *C*, and finally ΔH_{obs} approaches zero. The transition concentration may be associated with the structural rearrangement of the complexes formed by [C_{12}mim]Br and DNA, and accordingly the critical aggregation concentration (*CAC*) is derived [174]. Below *CAC*, the electrostatic interactions between [C_{12}mim]Br and DNA dominate. At *CAC*, the hydrophobic interactions between the alkyl chains of [C_{12}mim]Br may induce the aggregation of [C_{12}mim]Br molecules around DNA. Correspondingly, ΔH_{obs} begins to decrease. The enthalpy change of [C_{12}mim]Br aggregation around the DNA chain (ΔH_{agg}) is obtained from the difference of ΔH_{obs} at *CAC* and the final plateau region [174].

Table 8.1 shows the thermodynamic information for the aggregation of [C_{12}mim]Br in the presence and absence of DNA. The Gibbs free energy change for the micellization of [C_{12}mim]Br (ΔG_{mic}) is determined from β and *CMC* according to a standard procedure [41]. The Gibbs free energy change for the aggregation of [C_{12}mim]Br in the presence of DNA (ΔG_{agg}) is calculated with the same method

assuming that the counterion association degree β' equals to β despite the existence of certain uncertainty [148]. The entropy changes for the micellization and aggregation of [C_{12}mim]Br respectively, ΔS_{mic} and ΔS_{agg}, are obtained by the relationship, $T\Delta S=\Delta H-\Delta G$. As indicated, the aggregation processes of [C_{12}mim]Br in the presence and absence of DNA are both thermodynamically favored, driven by enthalpy and entropy change. Wang *et al*. [175] dertermined the Gibbs free energy change for the binding of [C_{12}mim]Br to calf thymus DNA using a fluorescence spectroscopy technique. By separating the electrostatic and non-electrostatic Gibbs free energy changes, they have shown that electrostatic interactions are predominant for the compexation of IL with DNA. Although an overall ΔG_{agg} is calculated in our study and the contributions of electrostatic or non-electrostatic interactions cannot be separated, the stepwise binding extent of [C_{12}mim]Br molelcules with the DNA chain has been successfully monitored quantitatively, and contributes to the understanding of the interaction mechanism between the cationic surfactant and DNA.

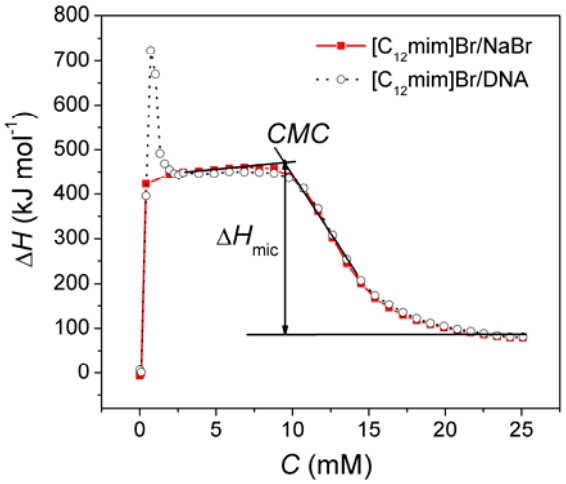

Fig. 8.2 Calorimetric titration curves of 150 mM [C_{12}mim]Br into 10 mM NaBr solution (■); 0.1 mM DNA solution in the presence of 10 mM NaBr (○).

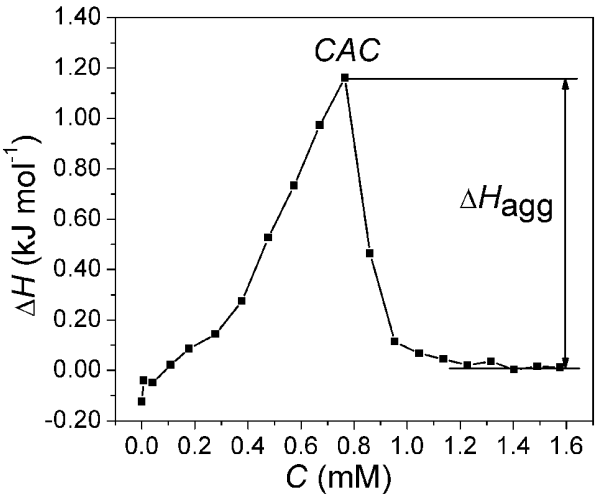

Fig. 8.3 Calorimetric titration curve of 10 mM [C_{12}mim]Br into 0.1 mM DNA solution.

Table 8.1 Thermodynamic properties for the aggregation process of [C_{12}mim]Br with and without DNA, the first two lines correspond to the case without DNA while the lines below denote the case with DNA

β	*CMC* (mM)	ΔH_{mic} (kJ mol^{-1})	ΔG_{mic}[a] (kJ mol^{-1})	$T\Delta S_{mic}$[b] (kJ mol^{-1})
0.688	9.40	-1.61	-19.53	17.92
β'	*CAC* (mM)	ΔH_{agg} (kJ mol^{-1})	ΔG_{agg}[c] (kJ mol^{-1})	$T\Delta S_{agg}$[d] (kJ mol^{-1})
0.688	0.76	-1.15	-30.05	28.90

[a] Caculated using $\Delta G_{mic}=RT(1+\beta)\ln(CMC)$.

[b] $T\Delta S_{mic}=\Delta H_{mic}-\Delta G_{mic}$

[c] Caculated using $\Delta G_{agg}=RT(1+\beta')\ln(CAC)$ assuming that $\beta'=\beta$.

[d] $T\Delta S_{agg}=\Delta H_{agg}-\Delta G_{agg}$

8.3.3 Micropolarity measurements

The variation of the I_1/I_3 value can be used to detect the change of environmental polarity, which can be induced by the aggregation behavior in the bulk phase [155]. We have measured the [C_{12}mim]Br concentration (C) dependence of the intensity ratio (I_1/I_3) for the [C_{12}mim]Br systems in the presence and absence of DNA in 10 mM NaBr, as presented in Fig. 8.4. After a plateau region with a relatively high value, I_1/I_3 decreases rapidly at a certain [C_{12}mim]Br concentration, indicating the formation of the hydrophobic microenvironment and the solubilization of pyrene molecules in the hydrophobic microenvironment. Finally I_1/I_3 changes little with C, showing that all the pyrene molecules may have transferred to the hydrophobic microenvironment.

In the absence of DNA, I_1/I_3 decreases rapidly at the concentration of around 1.6 mM, much lower than the *CMC* (9.4 mM) detected by conductivity and microcalorimetric measurements. This may be due to formation of some premicellar aggregates and transfer of the pyrene molecules from the polar environment to nonpolar premicellar structures [155]. In the presence of DNA, I_1/I_3 decreases around 0.16 mM, lower than the *CAC* determined by the microcalorimetric method (0.76 mM), which can also be explained by the formation of premicellar structures as mentioned previously. This value (around 0.16 mM) is also much lower than the transition concentration in the [C_{12}mim]Br/brine system (around 1.6 mM) detected by similar micropolarity measurements. This can be understood as a consequence of the strong electrostatic attraction between DNA phosphate groups and [C_{12}mim]Br headgroups as well as the hydrophobic interactions between [C_{12}mim]Br alkyl chains, causing the local [C_{12}mim]Br concentration around the DNA to be higher than that in the bulk phase. Similar behaviors have also been observed for other cationic surfactant/DNA systems [23].

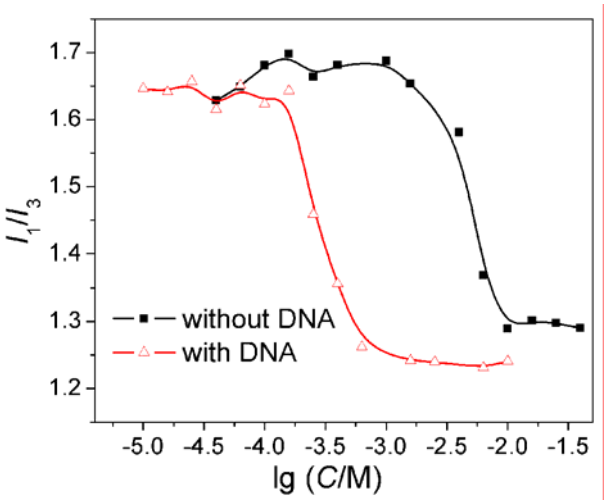

Fig. 8.4 [C_{12}mim]Br concentration dependence of I_1/I_3 with (Δ) and without (■) DNA in 10 mM NaBr solution.

8.3.4 UV-Vis transmittance

The variations of the transmittance (T) with the wavelength (λ) in the DNA brine with different [C_{12}mim]Br concentrations (C) are presented in Fig. 8.5(a). T at the wavelength 450 nm (T^{450}), which is far from the absorption band of DNA, was taken to study the effect of [C_{12}mim]Br concentration on the transmittance of the DNA solution [176]. The dependence of T^{450} on C is shown in Fig. 8.5(b). With the increase of C, T^{450} hardly changes at the beginning followed by a sharp decrease at 0.4 mM,

suggesting the formation of aggregates. This critical concentration on the $T^{450}(C)$ curve seems to compare well with the *CAC* value from the microcalorimetic analysis. As the [C_{12}mim]Br concentration increases, the electrostatic attraction between DNA and [C_{12}mim]Br, as well as the hydrophobic interactions between [C_{12}mim]Br tails, lead to the binding of [C_{12}mim]Br on DNA chains. Accordingly, the DNA charges are neutralized and the electrostatic repulsion between DNA chains is weakened. As a result, larger aggregates are formed followed by precipitates. Excess of [C_{12}mim]Br molecules can redissolve the precipitates due to the electrostatic repulsion between the positively-charged complexes. Correspondingly, T^{450} first decreases and then increases to a higher value after the precipitation region.

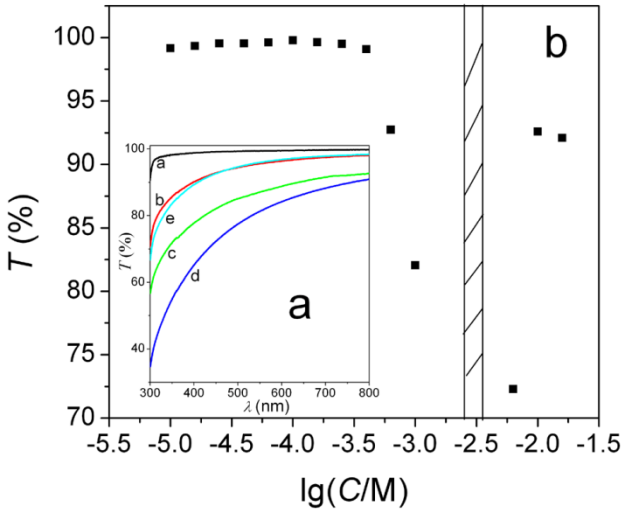

Fig. 8.5(a) Transmittance of [C_{12}mim]Br/DNA solutions (T) as a function of wavelength (λ) at various [C_{12}mim]Br concentrations (C). The [C_{12}mim]Br concentrations (a-e) are 0, 0.63, 1, 6.3, 10 mM; Fig. 8.5(b) [C_{12}mim]Br concentrations (C) dependence of the transmittance at 450 nm T^{450} (%) of [C_{12}mim]Br/DNA solutions. The striped region corresponds to the precipitation region.

8.3.5 Zeta potential and gel electrophoresis analysis

Fig. 8.6 presents the variations of zeta potential of [C_{12}mim]Br/DNA complexes with increasing [C_{12}mim]Br concentration (C). With the increase of C, zeta potential remains constant at the begining, followed by a slight decrease and then a rapid increase to a plateau value. When C is sufficiently low, there exists almost no binding of [C_{12}mim]Br with DNA. With further increasing C, a few [C_{12}mim]Br molecules bind onto the DNA and accordingly the hidden charges of the DNA chains become more exposed due to the complexation between [C_{12}mim]Br and DNA [23]. As a result, the zeta potential has been decreased. With the further increase of C, the DNA

charges become gradually neutralized by the addition of [C_{12}mim]Br, accompanied by the formation of [C_{12}mim]Br/DNA complexes. The zeta potentials of the complexes are negative until *C* approaches the region 2.5-3.5 mM, where the negative charges of DNA are neutralized completely and macroscopic precipitation occurs. As *C* is further increased, the zeta potential is further increased and finally reaches a constant positive value. This can be because the excess [C_{12}mim]Br molecules have the tendency to micellize in the bulk phase instead of binding onto the existing complexes. Therefore, we have successfully shown the neutralization process of DNA charges by the addition of [C_{12}mim]Br molecules with emphasis on the essential role of electrostatic interactions, comparing well with the experimental results from UV-Vis transmittance measurements.

The interactions between [C_{12}mim]Br and DNA have also been confirmed by the use of agarose electrophoresis technique, and the result is shown in Fig. 8.6(b). In the low *C* range, the electrophoresis band is close to that of pure DNA in the absence of [C_{12}mim]Br, suggesting the presence of free DNA molecules. The band becomes vague when *C* approaches 1.58 mM, due to that only a few free DNA molecules exist in the bulk phase and the rest have been bound with [C_{12}mim]Br. Further increase of *C* leads to the disappearance of the white bands, suggesting that all DNA molecules may have combined with [C_{12}mim]Br. Therefore, using the agarose electrophoresis, we have successfully shown the existence of interactions between [C_{12}mim]Br and DNA in a vivid and direct way.

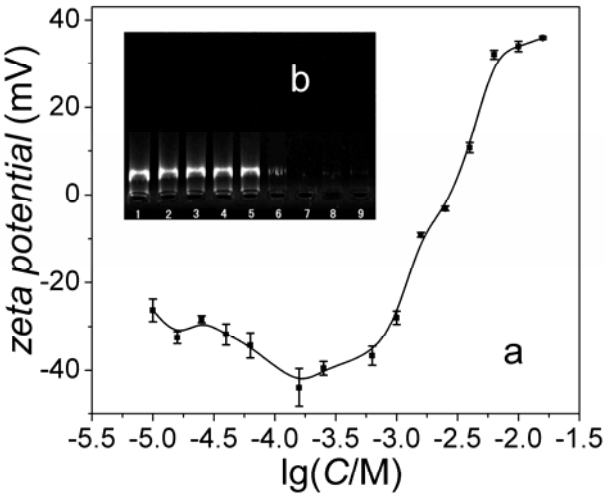

Fig. 8.6(a) [C_{12}mim]Br concentration dependence of the zeta potential in [C_{12}mim]Br/DNA solutions with C_{DNA}=0.1 mM. Each point represents an average value of three experimental data with the error bar denoted. Fig. 6.6(b) Agarose electrophoresis bands of DNA/[C_{12}mim]Br complexes at different [C_{12}mim]Br concentrations with C_{DNA}=0.1 mM, and the [C_{12}mim]Br concentrations from left to right (1-9) are 0, 0.04, 0.10, 0.25, 0.63, 1.58, 3.98, 10.00 and 63.10 mM.

8.3.6 Dynamic light scattering (DLS) measurements

DLS measurements have been performed to investigate the variation of DNA size with increasing [C_{12}mim]Br concentration (C). Fig. 8.7 presents the intensity weighted distribution functions of the DNA brine with increasing C. As shown in Fig. 8.7(a), two peaks with average hydrodynamic diameters of around 80 nm and 700 nm respectively have been observed for the size distribution of the IL-free DNA brine. These peaks hardly change at low C (Fig. 8.7(b)). However, as C reaches 0.63 mM (Fig. 8.7(c)), a broad peak with the average hydrodynamic diameter of approximately 295 nm appears, suggesting that the DNA molecules in the particle family with larger size have been compacted. The dependence of the DNA size on C is similar to that observed by Wang *et al*. [22] for the mixed system of cationic surfactant, lipid and the same type of DNA in 10 mM NaBr solution. When C reaches 100 mM, in addition to the peak corresponding to large complexes, a second peak with an average hydrodynamic diameter of around 1.2 nm is seen (Fig. 8.7(d)). It is comparable with that of the [C_{12}mim]Br brine at the same C in the absence of DNA (Fig. 8.7(e)) and accordingly verifies the existence of free [C_{12}mim]Br micelles in the bulk phase. In

other words, the formation of free [C_{12}mim]Br micelles may occur in the mixed system for the systems with sufficient high *C*.

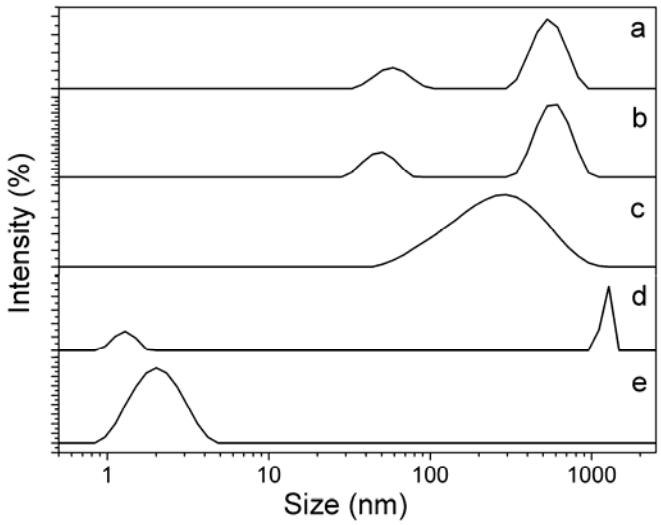

Fig. 8.7 Intensity weighted distribution functions of the solutions at different [C_{12}mim]Br concentration. The surfactant concentrations (a-d) are 0, 0.25, 0.63 and 100 mM with C_{DNA} to be 0.1 mM. The surfactant concentration in e is 100 mM in the absence of DNA.

8.3.7 AFM observation

The morphology of DNA/[C_{12}mim]Br complexes has been observed by the use of AFM, as shown in Fig. 8.8. In the solution which is free of [C_{12}mim]Br, loosely coiled structures are observed, due to electrostatic repulsions between the negatively charged DNA chains. When *C* reaches 0.63 mM, more compact and beadlike structures begin to appear, owing to the strong interactions between DNA and [C_{12}mim]Br. As *C* is further increased (3.98 mM), spherical structures with the size range 100-200 nm are observed. This concentration is just beyond the concentration region for precipitation, thus the aggregates are probably the mutually exclusive complexes bearing positive charges. These AFM results have shown that the complex structure can be appropriately modulated by the concentration ratio of [C_{12}mim]Br to DNA.

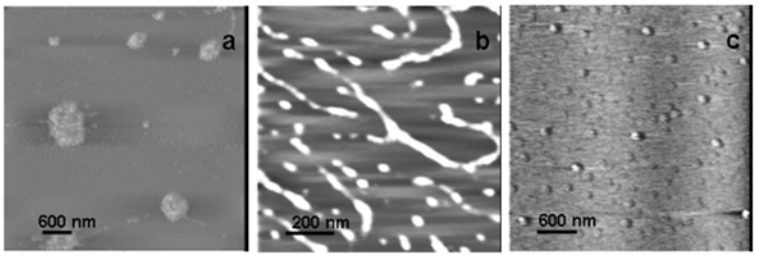

Fig. 8.8 AFM images of DNA/[C12mim]Br complexes at various surfactant concentrations, which are 0, 0.63, 3.98 mM from a to c respectively with C_{DNA} to be 0.1 mM

8.3.8 Circular dichroism analysis

We have investigated the influence of [C_{12}mim]Br concentration on the DNA conformation by the use of CD, as shown in Fig. 8.9. Without [C_{12}mim]Br, CD spectrum presents a positive peak at around 274 nm corresponding to π-π base packing and a negative peak at around 244 nm corresponding to helicity, indicating a typical B form of DNA [94]. The CD spectrum hardly changes at low [C_{12}mim]Br concentration. However, it varies significantly at the [C_{12}mim]Br concentrations which are sufficiently high. It can be observed that the intensity of the negative band is enhanced while no obvious change of intensity is observed for the positive band, and the whole spectrum shifts slightly to the direction of the longer wavelength. This shows that the addition of [C_{12}mim]Br can change the conformation of DNA to a certain extent, especially the helicity of the DNA chains, owing to the electrostatic attraction between DNA phosphate groups and [C_{12}mim]Br headgroups.

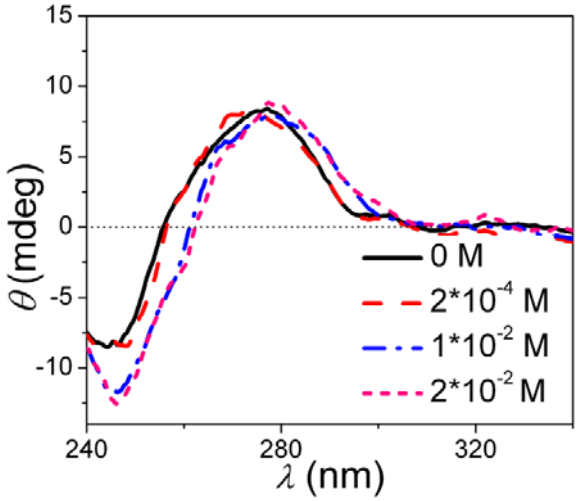

Fig. 8.9 Circular dichroism spectrum of DNA solutions at various [C_{12}mim]Br concentration.

8.3.9 Results by molecular dynamics (MD) simulation

The interactions between the cationic surfactant and anionic polyelectrolyte were also investigated by the coarse-grained MD simulation. Fig. 8.10 shows the dependence of $<R_g^2>$ on Z, where $<R_g^2>$ represents the mean-square radius of gyration of the polyelectrolyte, and Z denotes the charge ratio (+/–) of the cationic surfactant to

the polyelectrolyte in the system. In Fig. 8.10, we have also presented the equilibrium structures of polyelectrolyte/surfactant complexes at different Z to vividly describe the conformational change of the polyelectrolyte upon its interaction with the cationic surfactant.

At Z=0.1, it can be seen that only a few surfactant molecules bind on the polyelectrolyte chain with a high value of $<R_g^2>$. This is because the polyelectrolyte chain displays an extended conformation as a result of the electrostatic repulsion between the monomers with negative charges. At Z=0.2, there exist some spherical surfactant aggregates binding on the polyelectrolyte chain, and therefore the polyelectrolyte becomes more compact. With further increasing Z, $<R_g^2>$ decreases rapidly, indicating the further collapse of the polyelectrolyte. Meanwhile, the size of surfactant aggregates increases. As Z is above 0.75, $<R_g^2>$ hardly varies with Z. It can be seen that the shape of the surfactant aggregates turns from spherical to rod-like at high Z.

The conformational change of the polyelectrolyte with increasing suractant molecules in the simulation system can compare with that observed by AFM for the DNA/[C_{12}mim]Br system with increasing [C_{12}mim]Br concentration, indicating MD simulations have the ability to detect the significant variations of polyelectrolyte/surfactant complexes by fixing the polyelectrolyte concentration and varying the surfactant concentration. Besides, the size transition of the surfactant/polyelectrolyte complex can be compared with the results from the UV-Vis measurements, where the transmittance decreases significantly due to the strong surfactant/DNA complexation. In the DLS experiments, it has also been found that the compaction of DNA occurs at a certain [C_{12}mim]Br concentration, which can be owing to the weakening of electrostatic repulsion between the DNA chains caused by the binding of [C_{12}mim]Br with DNA. Again the strong DNA/[C_{12}mim]Br interactions have been reaffirmed.

Fig. 8.11 presents the dependence of N_s on Z, where N_s denotes the amount of surfactant molecules which bind onto the polyelectrolyte. As shown, with increasing Z, N_s increases rapidly at low Z region. When Z is above 0.75, N_s increases more slowly with Z, showing that gradual saturation of surfactant/polyelectrolyte interactions. This coincides well with Fig. 8.10, in which $<R_g^2>$ remains almost constant as Z is above 0.75.

Fig. 8.12 presents Z_c as a function of Z, where Z_c denotes the electric charge ratio (+/–) of the polyelectrolyte/surfactant complex, and Z is the electric charge ratio (+/–)

in the system. It should be noted that due to the negligible binding of counterions on the polyelectrolyte, Z_c simply represents the charge ratio of the surfactant cations to the negative charges carried by the polyelectrolyte in the complex. As shown, Z_c increases gradually with Z, suggesting that the complex becomes more positively charged due to the binding of cationic surfactants with the polyelectrolyte. In the simulation, Z_c depends on the choice of the effective cut-off length, accounting for the polyelectrolyte/surfactant interaction range, however the simulation results can still predict the trend for the variations of the complex charges as a function of the amount of surfactant in the system. This has reconfirmed the results from the previous zeta potential experiments, in which the zeta potential goes from negative values to zero, and finally a constant positive value with increasing $[C_{12}mim]Br$ concentration.

We have noticed that there were investigations on the oppositely-charged system of polyelectrolyte and macroions using Monte Carlo simulations [177]. The conformational change of the polyelectrolyte (from extended to compact conformation) was shown, induced by polyelectrolyte/macroions electrostatic interactions. For the complexes formed by polyelectrolyte and macroion, charge reversal occurs when the macroion concentration becomes sufficiently high. With the increase of the macroion concentration in the system, a strong and quantitative binding occurs at the beginning followed by slower complexation and finally the saturation of the complexation. These results can compare with our results for the polyelectrolyte/cationic surfactant system using MD simulation. Therefore, the importance of electrostatic interactions for the oppositely-charged systems has been emphasized.

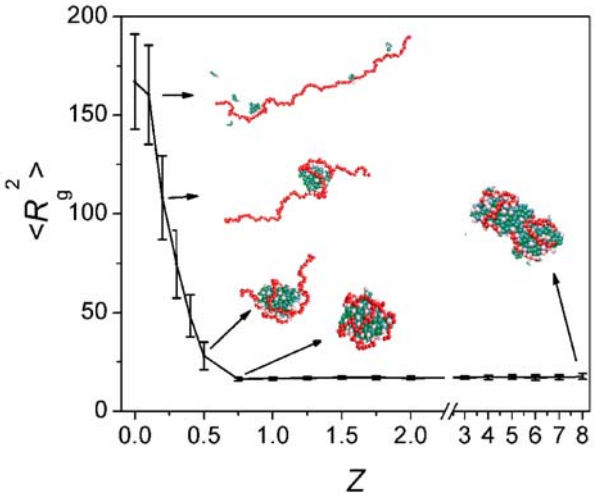

Fig. 8.10 Mean-square radius of gyration $<R_g^2>$ of polyelectrolyte (in the unit of σ^2) as a function of (+/-) charge ratio Z in the system. At each Z, 600 equilibrium simulation steps were

chosen to calculate the average radius of gyration with the error bar denoted. Snapshots of the polyelectrolyte/surfactant complex with increasing Z in the system are also included.

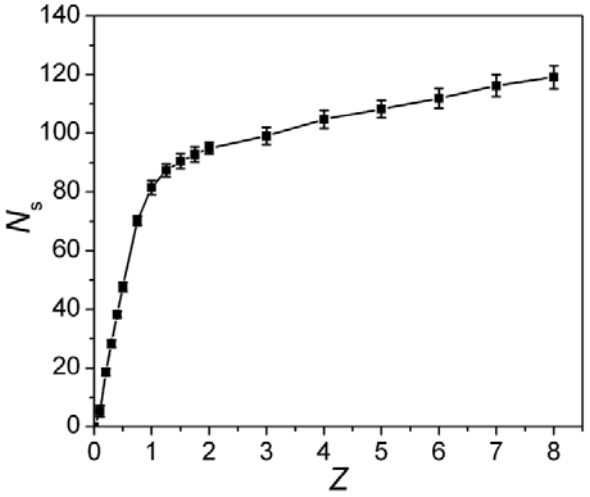

Fig. 8.11 The adsorption amount of surfactant molecules on the polyelectrolyte chain N_s as a function of the (+/-) charge ratio Z. Each point represents an average value of 600 equilibrium steps with the error bar denoted.

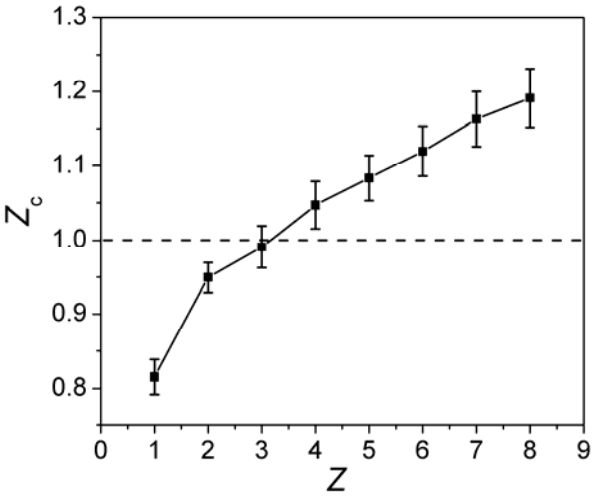

Fig. 8.12 Charge ratio Z_c of the complex as a function of the (+/-) charge ratio Z in the system. Each point represents an average value of 600 equilibrium steps with the error bar denoted.

8.4 Conclusions

In this chapter, the interactions between the cationic surfactant [C_{12}mim]Br and the anionic DNA in the presence of 10 mM NaBr have been systematically studied by the use of combined experimental methods and computer simulations. From the experimental results using multiple techniques including isothermal titration calorimetry, micropolarity, UV-Vis transmittance, we have proposed an interaction mechanism for the studied system. The strong complexation occurs due to the strong

electrostatic attraction between DNA phosphate groups and [C_{12}mim]Br headgroups, as well as the hydrophobic interactions between the alkyl chains of [C_{12}mim]Br.

Based on the microcalorimetic methods, the aggregation processes of [C_{12}mim]Br in the presence and absence of DNA are found to be thermodynamically favored driven by both enthalpy and entropy change. From the DLS, CD and zeta potential measurements, we have found that DNA chain is compacted and the helical structure is altered upon the addition of [C_{12}mim]Br, accompanied by the change of net charges carried by the complexes of DNA and [C_{12}mim]Br. By the use of AFM, the DNA with different conformations have been observed, including the loose coil conformation in nature state, DNA condensed structures, showing the effect of the [C_{12}mim]Br concentration on the structure of the DNA/[C_{12}mim]Br complexes.

In addition, molecular dynamics simulation has shown the collapse process of the polyelectrolyte chain and the neutralization of the negatively charges carried by the polyelectrolyte induced by the addition of surfactant, and reconfirmed the aggregation of surfactant molecules around the polyelectrolyte chain, thereby coinciding well with the experimental results.

Our work helps in understanding the binding characteristics between cationic surfactants and biomacromolecules, showing that ionic liquid surfactants have promising and important roles in biological systems.

Chapter 9 Conclusions

The dissertation is focused on the studies on the interfacial properties of different surfactant solutions and the interactions between oppositely-charged systems of surfactant and DNA.

First, we have looked at the adsorption at equilibrium and adsorption kinetics of surfactant molecules onto the air/water interface, as well as the desorption kinetics of surfactant molecules from the air/water interface mainly by the use of a bubble compression method. The equations of state for different surfactant systems can be obtained and the controlling steps for the adsorption and desorption kinetics of surfactants onto the air/water interface are studied. The detailed conclusions are summarised below:

1. Equilibrium interfacial properties and adsorption kinetics of various surfactant systems (non-ionic surfactant $C_{12}E_6$ and ionic surfactant CTAB with sufficient NaBr) have been investigated. The equation of state (the dependence of the surface tension on the surface concentration) has been determined from a single bubble compression measurement by calibrating with a known value of equilibrium surface tension. Our results are comparable and more complete than the results from the traditional methods, combining the equilibrium surface tension data with the Gibbs adsorption equation.

The time-dependent surface concentrations for $C_{12}E_6$ and CTAB/NaBr systems are determined by the proposed bubble compression method. It is shown that the adsorption is diffusion controlled at short times in both cases. The bulk diffusion coefficients for $C_{12}E_6$ and CTAB have also been calculated and found to agree with literature values.

2. The desorption process of surfactant molecules from the air/water interface has been investigated by using a bubble compression method. Non-ionic surfactant $C_{12}E_6$, ionic surfactant CTAB and TTAB with sufficient NaBr and ionic surfactant AOT in the presence of different types of counterions are studied. We have shown that the desorption process is not purely diffusion-limited by comparing the time-dependent surface concentration derived from experiments and theoretical predictions respectively.

It has been confirmed that the model for the kinetically controlled desorption can better explain the data derived from the measurements, especially for CTAB, showing

that the desorption is nearly controlled by the transfer of surfactant molecules from the air/water interface onto the subsurface. In other words, we have confirmed the presence of a energy barrier in the desorption process.

The influence of the alkyl chain length on the desorption kinetics has been studied by comparing the desorption behaviors of TTAB and CTAB. It has been found that TTAB desorbs faster than CTAB, indicating that the strong mutual interactions between surfactant chains may influence the energy barrier for desorption. It has been also found that the counterion type has no significant effects on the desorption processes for the systems studied.

3. The equilibrium and kinetic behaviors of the cationic gemini surfactant 12-2-12·2Br at the air/water interface were studied. It has been found that for the 12-2-12·2Br system in the absence of electrolyte, there exists an electrostatic barrier for adsorption at longer times. The effect of NaBr concentration on the dynamic surface tensions for the 12-2-12·2Br system has been investigated. Addition of NaBr hardly affects the adsorption kinetics at times shorter than the lag time τ, when the adsorption is diffusive. For the surfactant systems at equilibrium, the cationic gemini surfactant 12-2-12·2Br is more sensitive to the presence of NaBr than CTAB. In the presence of 100 mM NaBr, the adsorption of 12-2-12·2Br is proven to be diffusion-limited at short times. The desorption process of surfactant molecules in the 12-2-12·2Br/100 mM NaBr system has also been investigated and characteristic times for the desorption are obtained, which are comparable for those found with CTAB.

Second, the micellization process of cationic surfactants, the interactions between the cationic surfactants and anionic polyelectrolyte and the influences which affect these processes have been systematically investigated. The interaction mechanisms are proposed correspondingly, the detailed conclusions are shown as:

4. Micellization of cationic gemini surfactant 12-3-12·2Br is investigated, and effects of ionic strength and temperature are studied. Micellization of 12-3-12·2Br is entropically driven and thermodynamically favored. Increasing temperature increases the *CMC* slightly while increasing the ionic strength lowers the *CMC*. The enthalpy change for the micellization of 12-3-12·2Br is more negative with increasing temperature, as the structured water around the surfactants is destroyed.

The 12-3-12·2Br/DNA interactions bear a cooperative mechanism involving the electrostatic and hydrophobic interaction. We have observed coil structures of DNA,

and DNA condensates upon the addition of surfactants, and finally coexistence of large aggregates and spherical structures with increasing 12-3-12·2Br concentration. Salt can screen the DNA/12-3-12·2Br electrostatic attraction and promote the micellization or aggregation of 12-3-12·2Br. *CAC* is independent of DNA concentration, while the saturation concentration C_2 increases with the DNA concentration.

The effects of spacer length O (O=3, 4, 6) on the micellization of 12-O-12·2Br and its interactions with DNA have been investigated. With increasing O, *CMC* first increases then decreases. The degree of ionization of the micelles α is low at low O. The value of $-\Delta H_{mic}$ first decreases and then increases with spacer length. The *CMC* for the 12-O-12·2Br lowest at O=3. With increasing spacer length, the interaction between 12-O-12·2Br and DNA is weakened, and the *CMC* value in the mixed 12-O-12·2Br/DNA system first increases and then decreases. The spacer length hardly affects the enthalpy change for the binding process of 12-O-12·2Br with DNA (ΔH_{bd}).

5. Interactions between the cationic surfactant $[C_{12}mim]Br$ and the anionic DNA in the presence of 10 mM NaBr have been systematically studied. Based on the experimental results using a range of techniques, an interaction mechanism for the studied system was proposed. Strong complexation occurs owing to the electrostatic attraction between DNA and $[C_{12}mim]Br$, and the hydrophobic interactions between the alkyl chains of $[C_{12}mim]Br$.

The aggregation processes of $[C_{12}mim]Br$ with and without DNA are thermodynamically favored driven by enthalpy and entropy change. The DNA chain is compacted and the helical structure is altered by $[C_{12}mim]Br$, accompanied by the change of net charges carried by the DNA/$[C_{12}mim]Br$ complexes. The structure of these complexes suggests the effect of the $[C_{12}mim]Br$ concentration on the conformation of DNA.

Molecular dynamics simulation shows the collapse process of the polyelectrolyte chain and the neutralization of the negatively charges carried by the polyelectrolyte induced by the addition of surfactant, and reconfirms the aggregation of surfactant molecules around the polyelectrolyte chain, thereby coinciding well with the experimental results.

The thesis has shed light on the research on the interfacial properties of surfactants, especially the adsorption/desorption kinetics of surfactant molecules onto the air/water interface, and also on the oppositely-charged DNA/surfactant systems.

Bibliography

[1] Angarska J., Stubenrauch C., Manev E. *Drainage of foam films stabilized with mixtures of non-ionic surfactants.* Colloids and Surfaces a-Physicochemical and Engineering Aspects, 2007. **309**(1-3): p. 189-197.

[2] Dias R.S., Pais A.A.C.C., Miguel M.G. Lindman B. *DNA and surfactants in bulk and at interfaces.* Colloids and Surfaces A: Physicochemical and Engineering Aspects, 2004. **250**(1–3): p. 115-131.

[3] Eastoe J., Dalton J.S. *Dynamic surface tension and adsorption mechanisms of surfactants at the air-water interface.* Advances in Colloid and Interface Science, 2000. **85**(2-3): p. 103-144.

[4] Evans D.F., Wennerstrom H. *The Colloidal Domain: where physics, chemistry, biology and technology meet*. 2nd ed. 1999, New York: Wiley-VCH.

[5] Wilde P.J. *Interfaces: their role in foam and emulsion behaviour.* Current Opinion in Colloid & Interface Science, 2000. **5**(3-4): p. 176-181.

[6] Klitzing R.V., Müller H.J. *Film stability control.* Current Opinion in Colloid & Interface Science, 2002. **7**(1–2): p. 42-49.

[7] Babak V.G., Stébé M.J. *Highly concentrated emulsions: Physicochemical principles of formulation.* Journal of Dispersion Science and Technology, 2002. **23**(1-3): p. 1-22.

[8] Prosser A.J., Franses E.I. *Adsorption and surface tension of ionic surfactants at the air–water interface: review and evaluation of equilibrium models.* Colloids and Surfaces A: Physicochemical and Engineering Aspects, 2001. **178**: p. 1-40.

[9] Chang C.H., Franses E.I. *Adsorption dynamics of surfactants at the air/water interface - a critical-review of mathematical-models, data, and mechanisms.* Colloids and Surfaces a-Physicochemical and Engineering Aspects, 1995. **100**: p. 1-45.

[10] Fainerman V.B., Miller R. *Adsorption kinetics of short-chain alcohols at the water/air interface: Diffusion-controlled adsorption under the conditions of a nonequilibrium surface layer.* Journal of Colloid and Interface Science, 1996. **178**(1): p. 168-175.

[11] Aksenenko E.V., Fainerman V.B., Petkov J.T., Miller R. *Dynamic surface tension of mixed oxyethylated surfactant solutions.* Colloids and Surfaces A: Physicochem. Eng. Aspects, 2010. **365**: p. 210-214.

[12] Lin S.Y., Lee Y.C., Shao M.J., Hsu C.T. *A study on surfactant adsorption kinetics: The role of the data of equation of state γ(Γ) for $C_{14}E_8$.* Journal of Colloid and Interface Science, 2001. **244**(2): p. 372-376.

[13] Lin S.Y., McKeigue K., Maldarelli C. *Diffusion-controlled surfactant adsorption studied by pendant drop digitization.* Aiche Journal, 1990. **36**(12): p. 1785-1795.

[14] Diamant H., Andelman D. *Kinetics of surfactant adsorption at fluid-fluid interfaces.* J. Phys. Chem., 1996. **100**: p. 13732-13742.

[15] Diamant H., Ariel G., Andelman D. *Kinetics of surfactant adsorption: the free energy approach.* Colloids and Surfaces A: Physicochemical and Engineering Aspects, 2001. **183–185**: p. 259–276.

[16] Joos P. *Kinetic-equations for transfer-controlled adsorption-kinetics.* Journal of Colloid and Interface Science, 1995. **171**(2): p. 399-405.

[17] Li B.Q., Geeraerts G., Joos P. *Kinetic-equations for transfer-controlled adsorption-kinetics.* Colloids and Surfaces a-Physicochemical and Engineering Aspects, 1994. **88**(2-3): p. 251-266.

[18] Lee Y.C., Stebe K.J., Liu H.S., Lin S.Y. *Adsorption and desorption kinetics of C_mE_8 on impulsively expanded or compressed air–water interfaces.* Colloids and Surfaces A: Physicochemical and Engineering Aspects, 2003. **220**(1–3): p. 139-150.

[19] Zana R. *Dimeric and oligomeric surfactants. Behavior at interfaces and in aqueous solution: a review.* Advances in Colloid and Interface Science, 2002. **97**(1–3): p. 205-253.

[20] Karlsson L., van Eijk M.C.P., Söderman O. *Compaction of DNA by Gemini surfactants: Effects of surfactant architecture.* Journal of Colloid and Interface Science, 2002. **252**(2): p. 290-296.

[21] Badea I., Verall R., Baca-Estrada M., Tikoo S., Rosenberg A., Kumar P., Foldvari M. *In vivo cutaneous interferon-γ gene delivery using novel dicationic (gemini) surfactant–plasmid complexes.* The Journal of Gene Medicine, 2005. **7**(9): p. 1200-1214.

[22] Wang C., Li X., Wettig S.D., Badea I., Foldvari M., Verrall R.E. *Investigation of complexes formed by interaction of cationic gemini surfactants with deoxyribonucleic acid.* Physical Chemistry Chemical Physics, 2007. **9**(13): p. 1616-1628.

[23] Zhao X., Shang Y., Liu H., Hu Y. *Complexation of DNA with cationic gemini*

surfactant in aqueous solution. Journal of Colloid and Interface Science, 2007. **314**(2): p. 478-483.

[24] Zhao X., Shang Y., Hu J., Liu H., Hu Y. *Biophysical characterization of complexation of DNA with oppositely charged Gemini surfactant 12-3-12.* Biophysical Chemistry, 2008. **138**(3): p. 144-149.

[25] Vanyúr R., Biczók L., Miskolczy Z. *Micelle formation of 1-alkyl-3-methylimidazolium bromide ionic liquids in aqueous solution.* Colloids and Surfaces A: Physicochemical and Engineering Aspects, 2007. **299**(1–3): p. 256-261.

[26] Wang J., Wang H., Zhang S., Zhang H., Zhao Y. *Conductivities, volumes, fluorescence, and aggregation behavior of ionic liquids [C_4mim][BF_4] and [$C_n$mim]Br (n = 4, 6, 8, 10, 12) in Aqueous Solutions.* The Journal of Physical Chemistry B, 2007. **111**(22): p. 6181-6188.

[27] Dong B., Li N., Zheng L. Yu L., Inoue T. *Surface adsorption and micelle formation of surface active ionic liquids in aqueous solution.* Langmuir, 2007. **23**(8): p. 4178-4182.

[28] Israelachvili J. *Physical principles of surfactant self-association into micelles, bilayers, vesicles and microemulsion droplets*, in *Surfactants in Solution*. 1987, Springer US. p. 3-33.

[29] Rosen M.J. *Micelle formation by surfactants*, in *Surfactants and Interfacial Phenomena*. 2004, John Wiley & Sons, Inc. p. 105-177.

[30] Reynolds P.A., Gilbert E.P., Henderson M.J., White J.W. *Structure of high internal phase aqueous-in-oil emulsions and related inverse micelle solutions. 3. Variation of surfactant.* Journal of Physical Chemistry B, 2009. **113**(36): p. 12231-12242.

[31] Reynolds P.A., Gilbert E.P., Henderson M.J., White J.W. *Structure of high internal phase aqueous-in-oil emulsions and related inverse micelle Solutions. 4. Surfactant mixtures.* Journal of Physical Chemistry B, 2009. **113**(36): p. 12243-12256.

[32] Abel S., Abel S., Waks M., Marchi M., Urbach W. *Effect of surfactant conformation on the structures of small size nonionic reverse micelles: A molecular dynamics simulation study.* Langmuir, 2006. **22**(22): p. 9112-9120.

[33] Gao Y., Han S., Han B., Li G., Shen D., Li Z., Du J., Hou W., Zhang G. *TX-100/Water/1-Butyl-3-methylimidazolium hexafluorophosphate microemulsions.* Langmuir, 2005. **21**(13): p. 5681-5684.

[34] Gao H., Li J., Han B., Chen W., Zhang J., Zhang R., Yan D. *Microemulsions with ionic liquid polar domains.* Physical Chemistry Chemical Physics, 2004. **6**(11): p. 2914-2916.

[35] Song Q., Couzis A., Somasundaran P., Maldarelli C. *A transport model for the adsorption of surfactant from micelle solutions onto a clean air/water interface in the limit of rapid aggregate disassembly relative to diffusion and supporting dynamic tension experiments.* Colloids and Surfaces a-Physicochemical and Engineering Aspects, 2006. **282**: p. 162-182.

[36] Danov K.D., Kralchevsky P.A., Denkov N.D., Ananthapadmanabhan K.P., Lips A. *Mass transport in micellar surfactant solutions: 2. Theoretical modeling of adsorption at a quiescent interface.* Advances in Colloid and Interface Science, 2006. **119**(1): p. 17-33.

[37] Danov K.D., Kralchevsky P.A., Denkov N.D., Ananthapadmanabhan K.P., Lips A. *Mass transport in micellar surfactant solutions: 1. Relaxation of micelle concentration, aggregation number and polydispersity.* Advances in Colloid and Interface Science, 2006. **119**(1): p. 1-16.

[38] Shrestha L.K., Dulle M., Glatter O., Aramaki K. *Structure of polyglycerol oleic acid ester nonionic surfactant reverse micelles in decane: Growth control by headgroup size.* Langmuir, 2010. **26**(10): p. 7015-7024.

[39] Abdel-Rahem R.A. *Micellar parameters in solutions with cationic surfactants and N,N-Dimethyldodecan-1-amine oxide: Influence of cationic surfactant chain length.* Journal of Chemical and Engineering Data, 2012. **57**(3): p. 957-966.

[40] Tikariha D., Kumar B., Singh N., Ghosh K.K., Quagliotto P. *Micellization behavior of cationic Gemini surfactants in aqueous-ethylene glycol solution.* Journal of Surfactants and Detergents, 2011. **14**(4): p. 555-562.

[41] Zana R. *Critical micellization concentration of surfactants in aqueous solution and free energy of micellization.* Langmuir, 1996. **12**(5): p. 1208-1211.

[42] Di Marzio L., Marianecci C., Petrone M., Rinaldi F., Carafa M. *Novel pH-sensitive non-ionic surfactant vesicles: comparison between Tween 21 and Tween 20.* Colloids and Surfaces B-Biointerfaces, 2011. **82**(1): p. 18-24.

[43] Tsai C.H., Vivero-Escoto J.L., Slowing I.I., Fang I.J., Trewyn B.G., Lin V.S.Y. *Surfactant-assisted controlled release of hydrophobic drugs using anionic surfactant templated mesoporous silica nanoparticles.* Biomaterials, 2011. **32**(26): p. 6234-6244.

[44] Balachandran V.S., Jadhav S.R., Pradhan P., De Carlo S., George J. *Adhesive vesicles through adaptive response of a biobased surfactant.* Angewandte Chemie-International Edition, 2010. **49**(49): p. 9509-9512.

[45] Bhattacharya S., Kumari N. *Metallomicelles as potent catalysts for the ester hydrolysis reactions in water.* Coordination Chemistry Reviews, 2009. **253**(17-18): p. 2133-2149.

[46] Miraglia D.B., Schulz E.N., Rodriguez J.L.M., Schulz P.C., Salinas D. *Effect of the concentration and composition on the size and shape of micelles of sodium oleate-cetyltrimethylammonium bromide mixtures.* Journal of Colloid and Interface Science, 2010. **351**(1): p. 197-202.

[47] Miller R., Lunkenheimer K. *On the determination of equilibrium surface tension values of surfactant solutions.* Colloid & Polymer Science, 1983. **261**: p. 585-590.

[48] Makievski A.V., Fainerman V.B., Miller R., Bree M., Liggieri L., Ravera F. *Determination of equilibrium surface tension values by extrapolation via long time approximations.* Colloids and Surfaces a-Physicochemical and Engineering Aspects, 1997. **122**(1-3): p. 269-273.

[49] Moorkanikkara S.N., Blankschtein D. *New methodology to determine equilibrium surfactant adsorption properties from experimental dynamic surface tension data.* Langmuir, 2009. **25**(11): p. 6191-6202.

[50] Pan R.N., Green J., Maldarelli C. *Theory and experiment on the measurement of kinetic rate constants for surfactant exchange at an air/water interface.* Journal of Colloid and Interface Science, 1998. **205**(2): p. 213-230.

[51] Taylor C.D., Valkovska D.S., Bain C.D. *A simple and rapid method for the determination of the surface equations of state and adsorption isotherms for efficient surfactants.* Physical Chemistry Chemical Physics, 2003. **5**(21): p. 4885-4891.

[52] Fainerman V.B., Miller R. In Progress in Colloid and Interface Science; Miller, R., Liggieri, L., Eds.; Koninklijke Brill NV: Leiden, 2011; Vol. 2, p 179., 2011.

[53] Lin S.Y., McKeigue K., Maldarelli C. *Diffusion-controlled surfactant adsorption studied by pendant drop digitization.* AIChE Journal, 1990. **36**(12): p. 1785-1795.

[54] Li X., Shaw R., Evans G.M., Stevenson P. *A simple numerical solution to the Ward-Tordai equation for the adsorption of non-ionic surfactants.* Computers

& Chemical Engineering, 2010. **34**(2): p. 146-153.

[55] Ward A.F.H., Tordai L. *Time-dependence of boundary tensions of solutions 1. The role of diffusion in time-effects.* THE JOURNAL OF CHEMICAL PHYSICS, 1946. **14**: p. 453-461.

[56] Mysels K.J. *Diffusion-controlled adsorption kinetics. General solution and some applications.* The Journal of Physical Chemistry, 1982. **86**(23): p. 4648-4651.

[57] Jayalakshmi Y., Ozanne L., Langevin D. *Viscoelasticity of Surfactant Monolayers.* Journal of Colloid and Interface Science, 1995. **170**(2): p. 358-366.

[58] Doss K.S.G. Kolloid Zeits, 1938. **84**: p. 138.

[59] Joos P., Serrien G. *Adsorption-kinetics of lower alkanolsat the air water interface - Effect of structure makers and structure breakers.* Journal of Colloid and Interface Science, 1989. **127**(1): p. 97-103.

[60] Bleys G., Joos P. *Adsorption kinetics of bolaform surfactants at the air/water interface.* The Journal of Physical Chemistry, 1985. **89**(6): p. 1027-1032.

[61] Lang J., Zana R. Chemical Relaxation Methods, in Surfactant Solutions, R. Zana, Editor. Marcel Dekker: New York., 1987: p. 405-452.

[62] Israelachvili J. Intermolecular and Surface Forces. second ed, London: Academic press.

[63] MacLeod C.A., Radke C.J. *Surfactant exchange kinetics at the air/water interface from the dynamic tension of growing liquid drops.* Journal of Colloid and Interface Science, 1994. **166**(1): p. 73-88.

[64] Lin S.Y., Lu T.L., Hwang W.B. *Adsorption kinetics of decanol at the air-water interface.* Langmuir, 1995. **11**(2): p. 555-562.

[65] Lin S.Y., Hwang W.B., Lu T.L. *Adsorption kinetics of soluble surfactants and the phase transition model 2. Experimental demontration of 1-decanol.* Colloids and Surfaces A: Physicochemical and Engineering Aspects, 1996. **114**(0): p. 143-153.

[66] Lin S.Y., McKeigue K., Maldarelli C. *Diffusion-limited interpretation of the induction period in the relaxation in surface-tension due to the adsorption of straight chain, small polar group surfactants - theory and experiment.* Langmuir, 1991. **7**(6): p. 1055-1066.

[67] Johnson D.O., Stebe K.J. *Experimental confirmation of the oscillating bubble technique with comparison to the pendant bubble method: The adsorption*

dynamics of 1-decanol. Journal of Colloid and Interface Science, 1996. **182**(2): p. 526-538.

[68] Chang, C.-H. and E.I. Franses, *Dynamic tension behavior of aqueous octanol solutions under constant-area and pulsating-area conditions.* Chemical Engineering Science, 1994. **49**(3): p. 313-325.

[69] Jacob Lucassen, Giles D. *Dynamic surface properties of nonionic surfactant solutions.* Journal of the Chemical Society, Faraday Transactions 1: Physical Chemistry in Condensed Phases 1975. **71**: p. 217-232.

[70] Chang C.H., Franses E.I. *Modified Langmuir-Hinshelwood kinetics for dynamic adsorption of surfactants at the Air-Water-Interface.* Colloids and Surfaces, 1992. **69**: p. 189-201.

[71] Miguel M.G., Pais A.A.C.C., Dias R.S., Leal L., Rosa M., Lindman B., *DNA–cationic amphiphile interactions.* Colloids and Surfaces A: Physicochemical and Engineering Aspects, 2003. **228**(1–3): p. 43-55.

[72] McLoughlin D., Langevin D. *Surface complexation of DNA with a cationic surfactant.* Colloids and Surfaces A: Physicochemical and Engineering Aspects, 2004. **250**(1–3): p. 79-87.

[73] Dias R., Mel'nikov S., Lindman B., Miguel M.G. *DNA phase behavior in the presence of oppositely charged surfactants.* Langmuir, 2000. **16**(24): p. 9577-9583.

[74] Dias R.S., Magno L.M., Valente A.J.M., Das D., Das P.K., Maiti S., Miguel M.G., Lindman B. *Interaction between DNA and cationic surfactants: Effect of DNA conformation and surfactant headgroup.* The Journal of Physical Chemistry B, 2008. **112**(46): p. 14446-14452.

[75] Di Profio P., Germani R., Goracci L., Grilli R., Savelli G., Tiecco M. *Interaction between DNA and cationic amphiphiles: A Multi-Technique study.* Langmuir, 2010. **26**(11): p. 7885-7892.

[76] Moran M.C., Miguel M.G., Lindman B. *DNA gel particles.* Soft Matter, 2010. **6**(14): p. 3143-3156.

[77] Bilalov A., Olsson U., Lindman B. *Complexation between DNA and surfactants and lipids: phase behavior and molecular organization.* Soft Matter, 2012. **8**(43): p. 11022-11033.

[78] Bhattacharya S., Bajaj A. *Advances in gene delivery through molecular design of cationic lipids.* Chemical Communications, 2009. **0**(31): p. 4632-4656.

[79] Khowdairy M.M., Mohamed M.Z., Mohamed A.S. *Surface and biological*

activity of some prepared quaternary ammonium surfactants. Journal of Dispersion Science and Technology, 2011. **32**(5): p. 760-769.

[80] Infante M.R., Pérez L., Morán M.C., Pons R., Mitjans M., Vinardell M.P., Garcia M.T., Pinazo A. *Biocompatible surfactants from renewable hydrophiles.* European Journal of Lipid Science and Technology, 2010. **112**(1): p. 110-121.

[81] Mintzer M.A., Simanek E.E. *Nonviral vectors for gene delivery.* Chemical Reviews, 2008. **109**(2): p. 259-302.

[82] Santhiya D., Maiti S. *An investigation on interaction between 14mer DNA oligonucleotide and CTAB by fluorescence and fluorescence resonance energy transfer studies.* The Journal of Physical Chemistry B, 2010. **114**(22): p. 7602-7608.

[83] Zhou S., Liang D., Burger C., Yeh F., Chu B. *Nanostructures of complexes formed by calf thymus DNA interacting with cationic surfactants.* Biomacromolecules, 2004. **5**(4): p. 1256-1261.

[84] Kawashima T., Sasaki A., Sasaki S. *Transition of nanostructure in DNA-cationic surfactant complexes with the added salt.* Biomacromolecules, 2006. **7**(6): p. 1942-1950.

[85] Zhu D.M., Evans R.K. *Molecular mechanism and thermodynamics study of plasmid DNA and cationic surfactants interactions.* Langmuir, 2006. **22**(8): p. 3735-3743.

[86] He Y., Shang Y., Shao S., Liu, H., Hu, Y. *Micellization of cationic gemini surfactant and its interaction with DNA in dilute brine.* Journal of Colloid and Interface Science, 2011. **358**(2): p. 513-520.

[87] Dias R., Rosa M., Pais A.C., Miguel M., Lindman B. *DNA-surfactant interactions. Compaction, condensation, decompaction and phase separation.* J. Chin. Chem. Soc., 2004. **51**: p. 447-469.

[88] Kirby A.J., Camilleri P., Engberts J.B.F.N., Feiters M.C., Nolte R.J.M., Söderman O., Bergsma M., Bell P.C., Fielden M.L., Rodríguez C.L.G., Guédat P., Kremer A., McGregor C., Perrin C., Ronsin G., van Eijk M.C.P. *Gemini surfactants: New synthetic vectors for gene transfection.* Angewandte Chemie International Edition, 2003. **42**(13): p. 1448-1457.

[89] Kuhn P.S., Barbosa M.C., Levin Y. *Effects of hydrophobicity in DNA surfactant complexation.* Physica A: Statistical Mechanics and its Applications, 2000. **283**(1–2): p. 113-118.

[90] Mel'nikov S.M., Sergeyev V.G., Yoshikawa K. *Discrete coil-globule transition*

of large DNA induced by cationic surfactant. Journal of the American Chemical Society, 1995. **117**(9): p. 2401-2408.

[91] Nakanishi H., Nakanishi H., Tsuchiya K., Okubo T., Sakai H., Abe M. *Cationic surfactant changes the morphology of DNA molecules.* Langmuir, 2006. **23**(2): p. 345-347.

[92] Bhattacharya S., Haldar J. *Molecular design of surfactants to tailor its aggregation properties.* Colloids and Surfaces A: Physicochemical and Engineering Aspects, 2002. **205**(1–2): p. 119-126.

[93] Bhadani A., Singh S. *Novel Gemini pyridinium surfactants: Synthesis and study of their surface activity, DNA binding, and cytotoxicity.* Langmuir, 2009. **25**(19): p. 11703-11712.

[94] Ding Y., Zhang L., Xie J. Guo R. *Binding characteristics and molecular mechanism of interaction between ionic liquid and DNA.* The Journal of Physical Chemistry B, 2010. **114**(5): p. 2033-2043.

[95] Bowers J., Butts C.P., Martin P.J., Vergara-Gutierrez M.C. *Aggregation behavior of aqueous solutions of ionic liquids.* Langmuir, 2004. **20**(6): p. 2191-2198.

[96] Goracci L., Germani R., Savelli G., Bassani D.M. *Hoechst 33258 as a pH-sensitive probe to study the interaction of amine oxide surfactants with DNA.* ChemBioChem, 2005. **6**(1): p. 197-203.

[97] Hait S.K., Moulik S.P.. Curr. Sci., 2002. **82**: p. 1101.

[98] Zana R. *Gemini (dimeric) surfactants.* Current Opinion in Colloid & Interface Science, 1996. **1**(5): p. 566-571.

[99] Goracci L., Germani R., Rathman J.F., Savelli G. *Anomalous behavior of amine oxide surfactants at the Air/Water interface.* Langmuir, 2007. **23**(21): p. 10525-10532.

[100] Zana R. *Dimeric (Gemini) Surfactants: Effect of the spacer group on the association behavior in aqueous solution.* Journal of Colloid and Interface Science, 2002. **248**(2): p. 203-220.

[101] Wettig S.D., Badea I., Donkuru M., Verrall R.E., Foldvari M. *Structural and transfection properties of amine-substituted gemini surfactant-based nanoparticles.* The Journal of Gene Medicine, 2007. **9**(8): p. 649-658.

[102] Yang P., Singh J., Wettig S., Foldvari M., Verrall R.E., Badea I. *Enhanced gene expression in epithelial cells transfected with amino acid-substituted gemini nanoparticles.* European Journal of Pharmaceutics and

Biopharmaceutics, 2010. **75**(3): p. 311-320.

[103] Kubisa P. *Ionic liquids as solvents for polymerization processes—Progress and challenges.* Progress in Polymer Science, 2009. **34**(12): p. 1333-1347.

[104] Martínez-Palou R. J. Mex. Chem. Soc., 2007. **51**: p. 252-264.

[105] Anderson J.L., Pino V., Hagberg E.C., Sheares V.V., Armstrong D.W. *Surfactant solvation effects and micelle formation in ionic liquids.* Chemical Communications, 2003. **0**(19): p. 2444-2445.

[106] Tran C.D., Yu S. *Near-infrared spectroscopic method for the sensitive and direct determination of aggregations of surfactants in various media.* Journal of Colloid and Interface Science, 2005. **283**(2): p. 613-618.

[107] Liu L., Bauduin P., Zemb T., Eastoe J., Hao J. *Ionic liquid tunes microemulsion curvature.* Langmuir, 2009. **25**(4): p. 2055-2059.

[108] Welton T. *Ionic liquids in catalysis.* Coordination Chemistry Reviews, 2004. **248**(21–24): p. 2459-2477.

[109] Li Z., Jia Z., Luan Y., Mu T. *Ionic liquids for synthesis of inorganic nanomaterials.* Current Opinion in Solid State and Materials Science, 2008. **12**(1): p. 1-8.

[110] Torimoto T., Tsuda T., Okazaki K., Kuwabata S. *New frontiers in materials science opened by ionic liquids.* Advanced Materials, 2010. **22**(11): p. 1196-1221.

[111] Han D., Row K.H. *Recent applications of ionic liquids in separation technology.* Molecules, 2010. **15**(4): p. 2405-2426.

[112] Zhao H., Xia S., Ma P. *Use of ionic liquids as 'green' solvents for extractions.* Journal of Chemical Technology & Biotechnology, 2005. **80**(10): p. 1089-1096.

[113] rmand M., Endres F., MacFarlane D.R., Ohno H., Scrosati B. *Ionic-liquid materials for the electrochemical challenges of the future.* Nat Mater, 2009. **8**(8): p. 621-629.

[114] Galiński M., Lewandowski A., Stępniak I. *Ionic liquids as electrolytes.* Electrochimica Acta, 2006. **51**(26): p. 5567-5580.

[115] Frade R.F.M., Rosatella A.A., Marques C.S., Branco L.C., Kulkarni P.S., Mateus N.M.M., Afonso C.A.M., Duarte C.M.M. *Toxicological evaluation on human colon carcinoma cell line (CaCo-2) of ionic liquids based on imidazolium, guanidinium, ammonium, phosphonium, pyridinium and pyrrolidinium cations.* Green Chemistry, 2009. **11**(10): p. 1660-1665.

[116] Wang J.H., Cheng D.H, Chen X.W., Du Z., Fang Z.L. *Direct extraction of double-stranded DNA into ionic liquid 1-Butyl-3-methylimidazolium hexafluorophosphate and its quantification.* Analytical Chemistry, 2007. **79**(2): p. 620-625.

[117] Gao R., Zheng J., Qiao L. *Direct electrochemistry of hemoglobin in ayer-by-Llayer films assembled with DNA and room temperature ionic liquid.* Electroanalysis, 2010. **22**(10): p. 1084-1089.

[118] Nishimura N., Nomura Y., Nakamura N., Ohno H. *DNA strands robed with ionic liquid moiety.* Biomaterials, 2005. **26**(27): p. 5558-5563.

[119] Malham I.B., Letellier P., Turmine M. *Evidence of a phase transition in water−1-butyl-3-methylimidazolium tetrafluoroborate and water−1-butyl-2,3-dimethylimidazolium tetrafluoroborate mixtures at 298 K: ┌ Determination of the surface thermal coefficient, bT,P.* The Journal of Physical Chemistry B, 2006. **110**(29): p. 14212-14214.

[120] Zhang Y., Chen X., Lan J., You J., Chen L. *Synthesis and biological applications of imidazolium-based polymerized ionic liquid as a gene delivery vector.* Chemical Biology & Drug Design, 2009. **74**(3): p. 282-288.

[121] Xie Y.N., Wang S.F., Zhang Z.L., Pang D.W. *Interaction between room temperature ionic liquid [b_{mim}]BF_4 and DNA investigated by electrochemical micromethod.* The Journal of Physical Chemistry B, 2008. **112**(32): p. 9864-9868.

[122] Cardoso L., Micaelo N.M. *DNA molecular solvation in neat ionic liquids.* ChemPhysChem, 2011. **12**(2): p. 275-277.

[123] Song Q., Couzis A., Somasundaran P., Maldarelli C. *A transport model for the adsorption of surfactant from micelle solutions onto a clean air/water interface in the limit of rapid aggregate disassembly relative to diffusion and supporting dynamic tension experiments.* Colloids and Surfaces A: Physicochemical and Engineering Aspects, 2006. **282-283**: p. 162-182.

[124] Gaines G.L. *Insoluble monolayers at liquid-gas interfaces.* Interscience: New York, 1966.

[125] Lu J.R., Li Z.X., Thomas R.K., Staples E.J., Tucker I., Penfold J. *Neutron reflection from a layer of monododecyl hexaethylene glycol adsorbed at the air-liquid interface: The configuration of the ethylene glycol chain.* J. Phys. Chem., 1993. **97**: p. 8012-8020.

[126] Taylor C.D., Valkovska D.S., Bain C.D. *A simple and rapid method for the*

determination of the surface equations of state and adsorption isotherms for efficient surfactants. Phys. Chem. Chem. Phys., 2003. **5**: p. 4885–4891.

[127] Moorkanikkara S.N., Blankschtein D. *New methodology to determine the rate-limiting adsorption kinetics mechanism from experimental dynamic surface tension data.* Journal of Colloid and Interface Science, 2006. **302**(1): p. 1-19.

[128] Otto W.H., Britten D.J., Larive C.K. *NMR diffusion analysis of surfactant-humic substance interactions.* Journal of Colloid and Interface Science, 2003. **261**(2): p. 508-513.

[129] Marques E.F., Regev O., Khan A., Lindman B. *Self-organization of double-chained and pseudodouble-chained surfactants: counterion and geometry effects.* Advances in Colloid and Interface Science, 2003. **100–102**(0): p. 83-104.

[130] Pandey S., Bagwe R.P., Shah D.O. *Effect of counterions on surface and foaming properties of dodecyl sulfate.* Journal of Colloid and Interface Science, 2003. **267**: p. 160-166.

[131] You Y., Zhao J., Jiang R., Cao J. *Strong effect of NaBr on self-assembly of quaternary ammonium gemini surfactants at air/water interface and in aqueous solution studied by surface tension and fluorescence techniques.* Colloid & Polymer Science, 2009. **287**(7): p. 839-846.

[132] Luo H.S., Wang N., Zhou L.Z., Wang Y.L., Wang J.B., Yan H.K. *Salt effect on the aggregation behaviors of an anionic carboxylate gemini and a cationic surfactant.* Journal of Dispersion Science and Technology, 2008. **29**(5): p. 787-791.

[133] Wattebled L., Laschewsky A. *Effects of organic salt additives on the behavior of dimeric ("Gemini") Surfactants in aqueous solution.* Langmuir, 2007. **23**(20): p. 10044-10052.

[134] Khan I.A., Khanam A.J., Sheikh M.S., ud Din K. *Influence of ionic and nonionic hydrotropes on micellar behavior of a cationic gemini surfactant butanediyl-1,4-bis(dimethylcetylammonium bromide).* Journal of Colloid and Interface Science, 2011. **359**(2): p. 467-473.

[135] Ritacco H., Langevin D.., Diamant H., Andelman D. *Dynamic Surface Tension of Aqueous Solutions of Ionic Surfactants: Role of Electrostatics.* Langmuir, 2011. **27**: p. 1009–1014.

[136] Zana R., *Dimeric and oligomeric surfactants. Behavior at interfaces and in*

aqueous solution: a review. Advances in Colloid and Interface Science, 2002. **97**(1-3): p. 205-253.

[137] Nilsson M., Cabaleiro-Lago C., Valente A.J., Söderman O. *Interactions between gemini surfactants, 12-s-12, and beta-cyclodextrin as investigated by NMR diffusometry and electric conductometry.* Langmuir, 2006. **22**(21): p. 8663-8669.

[138] Batigoc C., Akbas H., Boz M. *Micellization behaviour and thermodynamic parameters of 12-2-12 gemini surfactant in (water plus organic solvent) mixtures.* Journal of Chemical Thermodynamics, 2011. **43**(9): p. 1349-1354.

[139] Zarganian R., Bordbar A.K., Amiri R., Tamannaei M., Khosropour A.R., Mohammadpoor-Baltork I. *Micellization of pentanediyl-1,5-bis(hydroxyethylmethyl hexadecylammonium bromide) as a cationic gemini surfactant in aqueous solutions: Investigation using conductometry and fluorescence techniques.* Journal of Solution Chemistry, 2011. **40**(6): p. 921-928.

[140] ud Din K., Koya P.A., Khan Z.A. *Conductometric studies of micellization of gemini surfactant pentamethylene-1,5-bis(tetradecyldimethylammonium bromide) in water and water-organic solvent mixed media.* Journal of Colloid and Interface Science, 2010. **342**(2): p. 340-347.

[141] Tsubone K., Ghosh S. *Micellization of an anionic gemini surfactant having N,N-dialkylamide, carboxyl, and carboxylate groups in aqueous NaCl solutions.* Journal of Surfactants and Detergents, 2004. **7**(1): p. 47-52.

[142] Koya P.A., ud Din K., Ismail K. *Micellization and thermodynamic parameters of butanediyl-1,4-bis(tetradecyldimethylammonium bromide) gemini surfactant at different temperatures: Effect of the addition of 2-Methoxyethanol.* Journal of Solution Chemistry, 2012. **41**(8): p. 1271-1281.

[143] Chavda S., Bahadur P. *Micellization of a cationic gemini surfactant in aqueous solutions with different alkanols and alkanediols as additives: Effect of nonpolar chain and position of hydroxyl groups.* Journal of Molecular Liquids, 2011. **161**(2): p. 72-77.

[144] Sohrabi B., Bazyari A., Hashemianzadeh M. *Effect of ethylene glycol on micellization and surface properties of Gemini surfactant solutions.* Colloids and Surfaces a-Physicochemical and Engineering Aspects, 2010. **364**(1-3): p. 87-93.

[145] Zana R., Benrraou M., Rueff R.

Alkanediyl-.alpha.,.omega.-bis(dimethylalkylammonium bromide) surfactants. 1. Effect of the spacer chain length on the critical micelle concentration and micelle ionization degree. Langmuir, 1991. **7**(6): p. 1072-1075.

[146] Wang X.L., Zhang X.H., Cao M., Zheng H.Z., Xiao B., Wang Y., Li M. *Gemini surfactant-induced DNA condensation into a beadlike structure.* The Journal of Physical Chemistry B, 2009. **113**(8): p. 2328-2332.

[147] Wang X., Li Y., Li J., Wang J., Wang Y., Guo Z., Yan H. *Salt effect on the complex formation between polyelectrolyte and oppositely charged surfactant in aqueous solution.* The Journal of Physical Chemistry B, 2005. **109**(21): p. 10807-10812.

[148] Bai G., Wang Y., Yan H. *Thermodynamics of interaction between cationic gemini surfactants and hydrophobically modified polymers in aqueous solutions.* The Journal of Physical Chemistry B, 2002. **106**(9): p. 2153-2159.

[149] Meagher R.J., Hatton T.A., Bose A. *Enthalpy measurements in aqueous SDS/DTAB solutions using isothermal titration microcalorimetry.* Langmuir, 1998. **14**(15): p. 4081-4087.

[150] Jiang N., Li P., Wang Y., Wang J., Yan H., Thomas R.K. *Micellization of cationic gemini surfactants with various counterions and their interaction with DNA in aqueous solution.* The Journal of Physical Chemistry B, 2004. **108**(39): p. 15385-15391.

[151] Łuczak J., Jungnickel C., Joskowska M., Thöming J., Hupka J. *Thermodynamics of micellization of imidazolium ionic liquids in aqueous solutions.* Journal of Colloid and Interface Science, 2009. **336**(1): p. 111-116.

[152] Šarac B., Bešter-Rogač M. *Temperature and salt-induced micellization of dodecyltrimethylammonium chloride in aqueous solution: A thermodynamic study.* Journal of Colloid and Interface Science, 2009. **338**(1): p. 216-221.

[153] Ghirlando R., Wachtel E.J., Arad T., Minsky A. *DNA packaging induced by micellar aggregates: a novel in vitro DNA condensation system.* Biochemistry, 1992. **31**(31): p. 7110-7119.

[154] Grosmaire L., Chorro M., Chorro C., Partyka S., Zana R. *Alkanediyl-alpha,omega-bis(dimethylalkylammonium bromide) surfactants - 9. Effect of the spacer carbon number and temperature on the enthalpy of micellization.* Journal of Colloid and Interface Science, 2002. **246**(1): p. 175-181.

[155] Aguiar J., Carpena P., Molina-Bolívar J.A., Ruiz C.C. *On the determination of*

the critical micelle concentration by the pyrene 1:3 ratio method. Journal of Colloid and Interface Science, 2003. **258**(1): p. 116-122.

[156] Bai G., Wang J., Yan H., Li Z., Thomas R.K. *Thermodynamics of Molecular Self-Assembly of Cationic Gemini and Related Double Chain Surfactants in Aqueous Solution.* The Journal of Physical Chemistry B, 2001. **105**(15): p. 3105-3108.

[157] El Seoud O.A., Koschella A., Fidale L.C., Dorn S., Heinze T. *Applications of ionic liquids in carbohydrate chemistry: A window of opportunities.* Biomacromolecules, 2007. **8**(9): p. 2629-2647.

[158] Patel D.D., Lee J.M. *Applications of ionic liquids.* Chemical Record, 2012. **12**(3): p. 329-355.

[159] Fei Z., Geldbach T.J., Zhao D., Dyson P.J. *From dysfunction to bis-function: On the design and applications of functionalised ionic liquids.* Chemistry-a European Journal, 2006. **12**(8): p. 2123-2130.

[160] Olivier-Bourbigou H., Magna L., Morvan D. *Ionic liquids and catalysis: Recent progress from knowledge to applications.* Applied Catalysis a-General, 2010. **373**(1-2): p. 1-56.

[161] Zhao H. *Innovative applications of ionic liquids as "greem" engineering liquids.* Chemical Engineering Communications, 2006. **193**(12): p. 1660-1677.

[162] Han D., Tang B., Lee Y.R., Row K.H. *Application of ionic liquid in liquid phase microextraction technology.* Journal of Separation Science, 2012. **35**(21): p. 2949-2961.

[163] Kubota F., Goto M. *Application of ionic liquids to solvent extraction.* Solvent Extraction Research and Development-Japan, 2006. **13**: p. 23-36.

[164] Ma J., Hong X. *Application of ionic liquids in organic pollutants control.* Journal of Environmental Management, 2012. **99**: p. 104-109.

[165] Wang Y., Tian M., Bi W., Row K.H. *Application of ionic liquids in high performance reversed-phase chromatography.* International Journal of Molecular Sciences, 2009. **10**(6): p. 2591-2610.

[166] Meindersma G.W., Sánchez L.M.G., Hansmeier A.R., de Haan A.B. *Application of task-specific ionic liquids for intensified separations.* Monatshefte Fur Chemie, 2007. **138**(11): p. 1125-1136.

[167] Abbott A.P., McKenzie K.J. *Application of ionic liquids to the electrodeposition of metals.* Physical Chemistry Chemical Physics, 2006. **8**(37): p. 4265-4279.

[168] Wei D., Ivaska A. *Applications of ionic liquids in electrochemical sensors.* Analytica Chimica Acta, 2008. **607**(2): p. 126-135.

[169] Wishart J.F. *Energy applications of ionic liquids.* Energy & Environmental Science, 2009. **2**(9): p. 956-961.

[170] Li L., Wang J., Wu T., Wang R. *Click ionic liquids: A family of promising tunable solvents and application in Suzuki-Miyaura cross-coupling.* Chemistry-a European Journal, 2012. **18**(25): p. 7842-7851.

[171] Zhou F., Liang Y., Liu W. *Ionic liquid lubricants: designed chemistry for engineering applications.* Chemical Society Reviews, 2009. **38**(9): p. 2590-2599.

[172] Łuczak J., Markiewicz M., Thöming J., Hupka J., Jungnickel C. *Influence of the Hofmeister anions on self-organization of 1-decyl-3-methylimidazolium chloride in aqueous solutions.* Journal of Colloid and Interface Science, 2011. **362**(2): p. 415-422.

[173] Zheng P., An X., Peng X., Shen W. *Interactions and aggregations in aqueous and brine solutions of poly(diallydimethylammonium chloride)/sodium bis(2-ethylhexyl) sulfosuccinate.* The Journal of Physical Chemistry B, 2009. **113**(41): p. 13566-13575.

[174] Jiang N., Wang J., Wang Y., Yan H., Thomas R.K. *Microcalorimetric study on the interaction of dissymmetric gemini surfactants with DNA.* Journal of Colloid and Interface Science, 2005. **284**(2): p. 759-764.

[175] Wang H., Wang J., Zhang S. *Binding Gibbs energy of ionic liquids to calf thymus DNA: a fluorescence spectroscopy study.* Physical Chemistry Chemical Physics, 2011. **13**(9): p. 3906-3910.

[176] Uhríková D., Zajaca I., Dubničková M., Pisárčik M. , Funari S.S., Rapp G., Balgavý P. *Interaction of gemini surfactants butane-1,4-diyl-bis(alkyldimethylammonium bromide) with DNA.* Colloids and Surfaces B: Biointerfaces, 2005. **42**(1): p. 59-68.

[177] Jonsson M., Linse P. *Polyelectrolyte--macroion complexation. I. Effect of linear charge density, chain length, and macroion charge.* The Journal of Chemical Physics, 2001. **115**(7): p. 3406-3418.

List of symbols

A Surfactant monomer

$A_{s\text{-}1}$, $A_{s\text{-}1}$ Surfactant micelles

β Counterion binding degree of micelles

β' Counterion binding degree of aggregates

α Degree of ionization of the micelles

ΔG_{mic} Gibbs free energy change of micellization

ΔG_{agg} Gibbs free energy change of aggregation

ΔG_{bd} Gibbs free energy change of binding

ΔH_{mic} Enthalpy change of micellization

ΔH_{agg} Enthalpy change of aggregation

ΔH_{bd} Enthalpy change of binding

ΔH_{obs} Observed enthalpy change per mole of solution

ΔS_{mic} Entropy change of micellization

ΔS_{agg} Entropy change of aggregation

ΔS_{bd} Entropy change of binding

V Volume

dV Differential of the volume change in the bulk

V^1 Volume of phase 1

V^2 Volume of phase 2

C Surfactant concentration

C_i Concentration of component i

C_i^1 Concentration of component i in phase 1

C_i^2 Concentration of component i in phase 2

C_b or C Sufactant concentration in the bulk

C_s Surfactant concentration in the sub-surface region

C_{mix} Critical micelle concentration in the mixed system

C_{DNA} DNA concentration

C_2 Saturation concentration

C_1 Contentration when formation of precipitates begins to occur

C'' Contentration when formation of precipitates begins to redissolve

CMC Critical micelle concentration

CAC Critical aggregation concentration

C_{NaBr} NaBr concentration

$C(Z)_{H_2O}$ Water concentration at height Z

$C_{solution,H_2O}$ Water concentration in the solution phase

C_{vapor,H_2O} Water concentration in the vapor phase

$\Delta C(Z)_{H_2O}$ Difference of water concentration at height Z

n_i Total amount of component i in the system

n_i^{σ} Quantity of component i at the interface

A Surface area

dA Differential of surface area

Γ Surface concentration

Γ_{i} Surface concentration of component i

Γ_0 Initial surface concentration

Γ_{eq} Equilibrium surface concentration

Γ_{∞} Surface concentration at saturation

$\Gamma(\mathrm{H_2O})$ Surface concentration of water

$\Gamma_{\mathrm{critical}}$ Surface concentration at the lag time τ

$\Gamma_{\mathrm{average}}$ Average surface concentration

Γ_{CMC} Surface concentration at CMC

c Fitting constant using the equation $\log(\tau) = -2\log C + c$

k_{a} Adsorption constant

k_{d} Desorption constant

k Effective desorption rate

τ_1 Characteristic time in the kinetically-controlled desorption

τ_{κ} Characteristic time in the kinetically-controlled adsorption

τ Lag time corresponding to the slow decrease of γ

E_{a} Adsorption energy

E_{d} Desorption energy

k_{B} Boltzmann constant

T Temperature

dT Differential of temperature

P Pressure

S Entropy

dS Diffential of the entropy energy in the bulk

S^{σ} Entropy at the interface

dS^{σ} Diffential of the entropy energy at the interface

U Internal energy

dU Diffential of the internal energy in the bulk

U^{σ} Internal energy at the interface

dU^{σ} Diffential of the internal energy at the interface

μ_i Chemical potential of component *i*

$d\mu_i$ Differential of chemical potential

μ_i^{θ} Chemical potential of component *i* at standard conditions

R Molar gas constant

γ Surface tension

γ_0 Initial surface tension

γ_{eq} Equilibrium surface tension

$d\gamma$ Differential of surface tension

dN_i Differential of the quantity of component *i* in the bulk

dN_i^{σ} Differential of the quantity of component *i* at the interface

Z_0 Height between the plane and the bulk bottom where the surface concentration of water is zero

Z Height between the plane and the bulk bottom

RM Molecular formula for the surfactant

XM Molecular formula for the electrolyte

R^{z_+} or R^+ Surfactant ion of the surfactant

M^{z_-}, M^{z_s} or M^- Counter-ion of the surfactant or the electrolyte

$X^{z_+^s}$ or X^+ Co-ion of the electrolyte

v_+ Number of surfactant ion in a surfactant molecule

v_- Number of counter-ions in a surfactant molecule

v^s_+ Number of co-ions in the electrolyte

v^s_- Number of counter-ions in the electrolyte

z_+ Number of charges carried by a surfactant ion

z_- Number of charges carried by a counter-ion

z_+^s Number of charges carried by the co-ion

z_-^s Number of charges carried by the counter-ion

D Diffusion constant of surfactant molecules

b Bubble radius

h Adsorption depth $h=\Gamma_{eq}/C_b$

K Normalized term $K=\frac{C_b}{\Gamma_{eq}}\sqrt{t}$

t_i Time at state i

A_i Area of bubble surface at state i

A_{eq} Area of bubble surface at the equilibrium state

r_0, r_1, r_2 and r_3 Fitting parameters in the $\gamma(C_b)$ plot using the equation

$$\gamma = r_0 + r_1 \times \ln C + r_2 \times (\ln C)^2 + r_3 \times (\ln C)^3$$

a_0, a_1 Fitting parameters in the $\gamma(C_b)$ plot using the equation $\gamma = a_0 + a_1 \ln C$

a_0, a_1, a_2 Fitting parameters in the $\gamma(C_b)$ plot using the equation

$$\gamma = a_0 + a_1 \ln C + a_2 (\ln C)^2$$

a Fitting constant using kinetically limited adsorption model

s Number of carbon atoms of the spacer

ds Stretched length of the spacer

dt Equilibrium distribution of the distance between the headgroups

I_1/I_3 Intensity ratio of the first peak (at wavelength 373 nm) to the third peak (at wavelength 397 nm)

κ Electrical conductivity

T^{450} Transmittance of solutions at the wavelength of 450 nm

I_c Critical ionic strength

X_0 Center point of the S curve with Boltzmann type

Δx calculation steps

r^2 Square of correlation coefficient

m Mass of particle

σ Diameter of particle

r_c Cut-off length for particles

k_s Spring constant $R_0=2\sigma$

L Length of the cubic box

τ_s Integral time step

ε Well depth

λ_B Bjerrum length

e Elementary charge

ζ Product ofrelative dielectric constant of the medium and vacuum permittivity

N_s Adsorption amount of surfactants onto the polyelectrolyte

$\langle R_g^2 \rangle$ Mean-square radius of gyration

λ Wavelength

Z Charge ratio (+/–) of cationic surfactant to polyelectrolyte in the system

Z_c Electric charge ratio (+/–) of polyelectrolyte/surfactant complex

C_0 Preferred curvature of monolayer

Appendix Publication list

1. **Yunfei He**, Yazhuo Shang, Honglai Liu, Dominique Langevin, Anniina Salonen*, Surfactant adsorption onto interfaces: measuring the surface excess in time, *Langmuir* 2012, **28**, 3146-3151.

2. **Yunfei He**, Yazhuo Shang*, Zhenhai Liu, Shuang Shao, Honglai Liu, Ying Hu, Interactions between ionic liquid surfactant [C_{12}mim]Br and DNA in dilute brine, *Colloids and Surfaces B: Biointerfaces* 2013, **101**, 398-404.

3. **Yunfei He**, Yazhuo Shang, Shuang Shao, Honglai Liu, Ying Hu, Micellization of Cationic Gemini Surfactant and Its Interaction with DNA in Dilute Brine, *Journal of Colloid and Interface Science* 2011, **358***,* 513-520.

4. **Yunfei He**, Shouhong Xu, Di Sun, Yazhuo Shang*, Xiaofang Zhao, Honglai Liu, Decompaction of Cationic Gemini Surfactant-Induced DNA Condensates Using Triblock Copolymer $(PEO)_{20}$-$(PPO)_{70}$-$(PEO)_{20}$, *Colloid Polym Sci* 2013, DOI 10.1007/s00396-013-2954-5.

5. **Yunfei He**, Yazhuo Shang, Honglai Liu, Dominique Langevin, Sascha Heitkam, Anniina Salonen*, Desorption Kinetics of Surfactants at the Air/water Interfaces, *in preparation*.

6. Wanxia Wang, **Yunfei He**, Yazhuo Shang*, Honglai Liu, Interaction between the Gemini Surfactant(12-6-12)and DNA, *Acta Physico-Chimica Sinica* 2011, **27**,156-162.

7. Xiaofang Zhao, **Yunfei He**, Yashuo Shang*, Xia Han, Honglai Liu,Effect ofElectrolytes and Ethanol on the Interaction between DNA and the Gemini Surfactant, *Acta Physico-Chimica Sinica* 2009, **25**, 853-858.

Acknowledgements

I would like to extend my gratitude to Prof. Honglai Liu, Prof. Yazhuo Shang, Prof. Dominique Langevin and Dr. Anniina Salonen for their enduring support and patience throughout my thesis. This thesis is finished under the constructive suggestions and inspiring encouragements from them. Their profound understanding in colloid and interface science has greatly helped me in designing both the thoughts and experiments scientifically. Their aspiration for scientific research always encourages me to analyze the problem and conquer the difficulty with appropriate methodology.

Thank Prof. Honglai Liu for giving me the opportunity to further my research abroad. Thank Prof. Dominique Langevin for offering me the impressive experience to perform the research in Laboratoire de Physique des Solides.

I feel lucky that I am surrounded by intelligent and helpful mates in the labs in China and France. I have benefited immensely from Dr. Anniina Salonen for the continous support in the experimental design, instrumental use, data interpretation and for the valuable suggestions on the preparations for conferences, from Prof. Yazhuo Shang and Dr. Xiaofang Zhao for the fundamental knowledge in surfactant science, from Clément Honorez for the continuous help in using Tracker and Thin Film Pressure Balance, from Amélie Lecchi for providing me with the Gemini surfactant 12-2-12·2Br, from Sascha Heitkam for the help in the Matlab simulations for the desorption kinetics, from Prof. Shuang Shao for the support in using ITC.

I would like to thank Réine-Marie Guillermic, Wiebke Drenckhan, Manue Rio, Armando Maestro, Laurie Saulnier, Aouatef Testouri and Steven Levannier for being dedicated lab mates. Gratitude is extended to Dongyan Zhi, Yuli Xu, Na Zhao, Lang Shuai, Di Sun, Yichen He, Zijun Bian, Jing Tang for the support in my daily life.

Finally, I would like to give my best thanks to my father, mother and sister, who have always been supportive throughout my entire five years for the thesis. My boyfriend Dr. Gangwei Sun has given me immense support in my work and daily life, and I am especially grateful for his continuous concern during my stay in France.

This thesis is supported by the NSFC (N20736002, 20706013, 21173079), the creative team development project of Ministry of Education of China (IRT0721), the 111 Project of Ministry of Education of China (No.B08021), the Fundamental Research Funds for the Central Universities and China Scholarship Council.

Author: Yunfei He